Developing Magnetic resonance elastography (MRE) breast actuation system for detecting breast cancer

Quazi T.A. Linda

A thesis submitted for the degree of
Master of Engineering
in
Mechanical Engineering
at the
University of Canterbury,
Christchurch, New Zealand

March 2012

Acknowledgements

First of all I would like to thank my previous supervisor Dr. Elijah Van Houten. He has a lot of expertise in the field of MRE and always had an idea to solve many problems I encountered along the way.

Many thanks to Dr. Geoff Chase, Dr. David Aitchison and Dr. Dean Kirk for their time and support.

I would like to appreciate the help and guidance that I received from Brian Donohue, Bruce Sparks, Ken Brown, Julian Phillips, Kevin Stobs, Mervin Chandrapal, Rajen Fernandez, Dr. Thomas Lotz and Dr. Stefanie Gutschmidt. The other students in the MRE research group, Matt McGarry, David Viviers, Andrew Petrov and Helen Kershaw, thanks for all your input as well.

And finally I would like to say thanks to my family and specially my husband for all his encouragement and support.

Contents

List of Figures

List of Tables

Abstract

It is well known in medicine that changes in tissue elasticity may be related to pathological phenomena such as cancer and other disease. Physicians routinely use palpation as means of inspecting the thyroid, prostate, and breast, where a palpably hard mass can often indicate the presence of a malignant lesion.

Magnetic Resonance Elastography (MRE) has emerged as a relatively new elasticity imaging technique which can be used to spatially map and measure displacement patterns resulting from harmonic shear-wave propagation in soft tissue. Displacement fields are then used in reconstructing the tissue's elastic property distributions.

The feasibility of using MRE as a noninvasive means of characterizing the mechanical properties of silicone phantom mimicking human breast, was investigated though experiments involving MRE acquisitions of four phantoms. To achieve sufficient excitation of the phantom tissue, an acoustic actuator was developed. The results of these studies have shown the MRE acquisition to be successful in capturing sufficient data for elastic parameter reconstruction.

Another different type of actuator has been developed and tested in the laboratory. The results show the potential for future use of this actuator in MRE experiments.

Chapter 1

INTRODUCTION AND BACKGROUND

Introduction

The human body is made up of billions of cells that grow, divide, and then die in a predictable manner. Cancer occurs when there is uncontrolled cell division and growth. Cancer cells lump together and form a mass of extra tissue, also known as a tumor, which continues to grow unchecked by normal regulation. As it grows, it may damage and invade nearby tissue.

In the case of breast cancer, the disease starts in the milk producing cells in the breast, and in the cells lining the small milk-ducts. There is a pre-invasive stage of cancer during which malignant cells are confined within the duct system. This stage is followed by an invasive phase. In this latter phase the cancer invades the surrounding tissues and has the potential for spread to local lymph nodes and to distant sites, such as the bones, liver and brain. These secondary deposits are called metastases. Although breast cancer may disseminate early in its natural history, the rate of growth is variable and in many women it may be years from the development of the disease to the appearance of metastases in other sites. The main aim of breast cancer screening is to detect cancers early enough that they are still localized to the breast, and before secondary spread has occurred [1].

1.1 Breast cancer screening

Breast cancer screening can reduce cancer mortality by detecting the disease at the earliest possible stage while it is still localized. Fast growing cancers spend a relatively short time in the phase when they are detectable by screening and are not yet necessarily evident to the

woman herself. Hence, screening is likely to pick up relatively few of these fast-growing cancers and proportionally more of slow-growing or even non-progressive, non-invasive cancers. Women with these cancers will anyway have a better chance of survival as a result of screening and early detection [1].

1.1.1 Clinical examination

A clinical examination is a form of careful examination of the breast performed by trained medical or nursing personnel. It is done by manual palpation to find a lump or change in the breast. Malignant tumors are stiffer and less mobile than surrounding healthy tissues [2]. The majority of tumors detected using manual palpation are large (> 1 cm in diameter) and thus they are often later stage, metastatic, and treatable only by employing the most aggressive therapies [3]. However some tumors cannot be located by manual palpation due to their size and location.

1.1.2 Mammography

Mammography is an x-ray technique specially developed for taking images of the breast. It has the potential to detect tumors that cannot be detected by a clinical examination. Radiographers using specially designed equipment, take one or more X-ray views of each breast. The women are positioned so that the entire breast tissue is included on the film (mammogram). This method is favored because of its relatively low cost. However mammography has the following limitations,

- Certain types of tumors are undetectable by x-rays.

There is difficulty and variability in interpreting the resulting images due to the low contrast between tumors and the surrounding healthy tissue [4]. This lack of image contrast accounts for 30–50% of all false-negative results [5].

- The radiation exposure associated with mammography is a potential risk of screening. The risk of exposure overtime is thus greatest in younger women. The largest study of radiation risk from mammography concluded that for women 40 years of age or older, the risk of radiation-induced breast cancer was minuscule, particularly compared with the potential benefit of mammographic screening, with a benefit-to-risk ratio of 48.5 lives saved for each life lost due to radiation exposure [6].
- Mammography also includes pain experienced as the breast is compressed to take the image [7]. Using a visual analogue scale, Ashgari et al. found that 92% of patients reported a mammogram as being painful, a similar result to the 88% of painful mammography experiences reported by Kashikar- Zuck et al. [6, 8, and 9]. In general terms, patients report pain during mammography at a low to moderate level, although the pain levels experienced show high variability [9]. Kashikar-Zuck et al. found no significant relationship between breast density and pain levels, a conclusion that conflicts with the findings of Kornguth et al., who observed a connection between breast density and discomfort [10]. Although the percentage of women that reported severe pain levels during mammography is low, a number of patients indicate they would not have further mammography due to the pain they experienced. In addition to reduced compliance from women who have experienced discomfort while having a mammogram, the perceived discomfort amongst those women who have not enrolled in a screening program can be a significant barrier to widespread participation [9].

Hence there are several issues that affect the success of mammography. Specifically, variability form low contrast and dense breast tissue, low compliance due to associated pain and the risk due to x-ray exposure. As a result, mammography is not as effective as it might be due to these issues and many cancers are not detected until later stages.

1.1.3 Ultrasonography

Ultrasonography (US) is a useful diagnostic tool for detecting breast cancer. High frequency sound waves are produced by vibrations of an electronically crystal transducer and passed into the breast. The wave reflects off tissue structure back to transducers, where they are reconverted into electrical signals, creating a cross-sectional image of the structure through which the sound passed. No harmful radiation is used in this process. Limitations of ultrasound systems include a low spatial resolution and a limited ability to detect microcalcifications, which are often an early warning sign of breast cancer [11]. They can also suffer from significant signal noise. Finally, there is no set method for regular screening tests using US, and thus it is primarily used as a confirmatory diagnostic.

1.2 Elastography

A number of articles have appeared in the literature, showing various techniques related to the measurement and visualization of the mechanical properties and motion of soft tissues using ultrasound. These techniques relied upon the use of Doppler Ultrasound velocity measurements, cross-correlation techniques, and visual inspection of M-mode and B-mode images [12]. In 1991, Ophir et al. described a new method named Elastography. This method

involves application of load on the tissue of interest and imaging of local responses of the medium by imaging the longitudinal or shear strain components at different locations of the tissue [13].

Magnetic Resonance Elastography (MRE) is an emerging technique to spatially map and measure displacement patterns resulting from harmonic shear wave propagation. It also has several technical advantages over transient ultrasound elastography. These advantages include: 1) the ability to analyze considerably larger volumes, thereby limiting the problem of sample variability; 2) the applicability in patients who are obese or have ascites; and 3) the ability of make a precise analysis of the viscoelastic parameters by assessing the full three dimensional displacement vector [14]. Furthermore, MRE has proven advantageous since the technique does not require estimation of the local static stress distribution, and has shown great potential as a noninvasive means of quantifying the mechanical properties of a variety of tissues in vivo [15].

1.2.1 Tissue Excitation

In general, MRE uses low frequency, harmonic, transverse acoustic waves (shear waves approximately 10 Hz – 1 kHz) as a means of imparting mechanical stress upon a region of interest [19, 20,21]. Acoustic shear waves in this frequency range are used for two reasons. First, because the attenuation of these signals is much less than that experienced at higher frequencies. Second, these frequencies have wavelengths in biological tissues and tissue-like materials in the useful range of millimeters to tens of millimeters [22] As the acoustic waves

propagate through the medium, small cyclic displacements are induced, the amplitudes of which are on the order of hundreds of nanometers [19].

1.2.2. Data Acquisition

Phase Measurements

Muthupillai et al [19, 20, 21] presented the following basic theory governing motion detection using Nuclear Magnetic Resonance (NMR). The phase shift φ (τ) in an NMR signal resulting from the motion of nuclear spins in the presence of a magnetic field gradient is defined:

$$\Phi(\tau) = \gamma \int_0^{\tau} \boldsymbol{G}_r(t).\, \mathbf{r}(t)\, dt \qquad (1.1)$$

where, γ is the gyromagnetic ratio intrinsic to the material, τ is duration of the applied gradients after excitation, $\boldsymbol{G}_r$ (t) is a time dependent function of the magnetic gradient superimposed on the main magnetic field Bo, and **r**(t) is a time dependent function of the nuclear spin position. Assuming **r**(t) represents linear motion, r(t) can be written:

$$\mathbf{r}(t) = \mathbf{r}_o + \mathbf{v}_o(t) \qquad (1.2)$$

where, $\mathbf{r}_o$ and $\mathbf{v}_o$ are the initial position and initial velocity respectively. If the acceleration of the spins and other higher order terms are neglected, and the appropriate gradient function is used, then Equation (1.1) provides a relation between the phase-shift of the NMR signal and the first gradient moment. The first gradient moment is defined:

$$\int_0^{\tau} \boldsymbol{G}_r(t)\, t\, dt \qquad (1.3)$$

Furthermore, complex motion can be described:

$$\mathbf{r}(t) = \mathbf{r}_0 + \vec{\xi}(\mathbf{r}, t) \tag{1.4}$$

where, $\mathbf{r}_o$ is the mean position of the nuclear spin, and $\vec{\xi}(\mathbf{r}, t)$ is the displacement of the spin about its mean position. Next, considering simple harmonic motion about **r** :

$$\vec{\xi}(\mathbf{r}, \boldsymbol{\theta}) = \vec{\xi}_0 \cos(\mathbf{k} \cdot \mathbf{r} - \omega t + \boldsymbol{\theta}) \tag{1.5}$$

is $\vec{\xi}_0$ the displacement amplitude, **k** is the wave vector, **ω** is the angular frequency of the mechanical excitation, and **θ** is the initial phase offset. At this point, it is useful to consider a basis function gradient $\boldsymbol{G}_r$ (t) that is switched in polarity at the precessional frequency of the nuclear spins. The phase-shift induced in the NMR signal by cyclic motion resulting from a mechanical wave propagating in a given medium at a frequency 1/T, and in the presence of a cyclical motion-encoding gradient is then described by the following equation:

$$\Phi(\mathbf{r}, \boldsymbol{\theta}) = \lambda \int_0^{\tau = \mathrm{NT} < TE} \boldsymbol{G}_r\ (t).\cos(\mathbf{k}.\mathbf{r} - \omega t + \boldsymbol{\theta}) \tag{1.6}$$

$\vec{\xi}_0$

$$\Phi(\mathbf{r}, \boldsymbol{\theta}) = \frac{2\gamma\ \mathrm{NT\ (G\ .\ \ )}}{\pi}\ \sin(\mathbf{k}.\mathbf{r} + \boldsymbol{\theta})$$

where, N is the number of gradient cycles, T is the period of the mechanical excitation, and TE is the time at which the NMR echo is received. Furthermore, the angular frequency is defined $\omega = 2\pi/T$.

Equation (1.6) shows that the phase-shift is proportional to the scalar product of the gradient vector G and the displacement vector $\vec{\xi}_0$. This outcome indicates that the wave motion can

be measured along any direction [16]. Lastly, the proportional relationship between the phase-shift experienced by the NMR signal and the number of gradient cycles, N, allows for increased sensitivity to small-amplitude oscillatory motion by accumulating phase shifts over multiple cycles of mechanical excitation and synchronous gradient waveform [18]. Implementing multiple wave cycles and subsequent gradient readouts, accumulating phase-shifts can allow this technique to accurately convey cyclic motions with amplitudes less than 100 nm [19].

1.2.3 Motion Encoding Gradients (MEGs)

MEGs are sinusoidal gradients applied in one of the three spatial directions during the pulse sequence. A complete MRE acquisition entails measuring motion in all three directions. The frequency of oscillation of the gradient is equal to that of the mechanical actuation. When a sample is being moved with a sinusoidal vibration, and sinusoidal MEGs are used, the phase of the MR signal is a cosine function whose amplitude and phase uniquely determine the amplitude and phase of the harmonic vibration [16]. In addition, the phase of the MEGs relative to the motion is controlled.

To accurately sample the resulting waveform, multiple phase-offsets between the MEGs and the applied vibration are required. Weaver et al. [15] report that eight relative phases are used from which the amplitude and phase of the harmonic motion at each position in the sample is determined using a least squares algorithm. The samples themselves are evenly distributed across one cycle of the cosine function so that the average phase during the sampling is zero. Weaver et al also notes that work is being done to optimize the acquisition process further by reducing the number of required samples [16]. A schematic of the pulse sequence is provided in Figure 1.1.

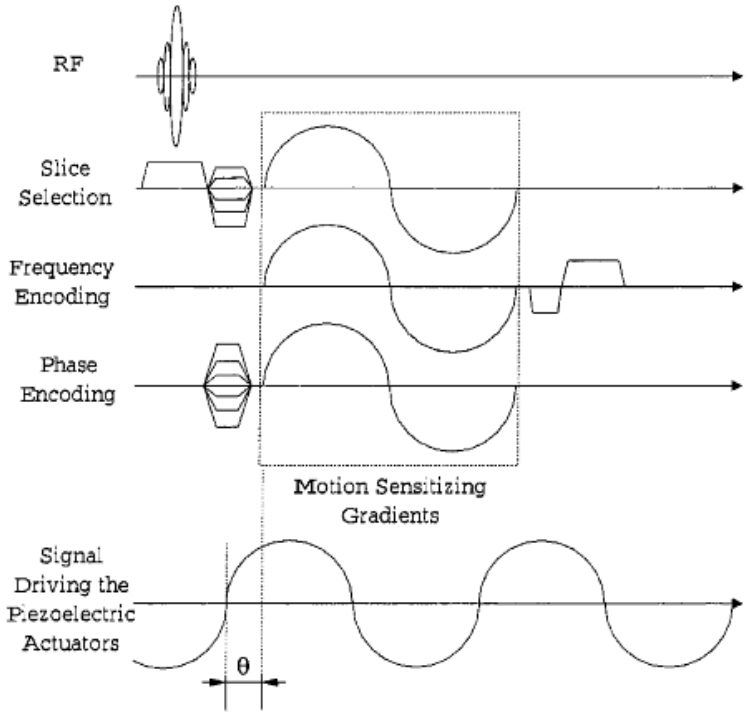

Figure 1.1: MRE pulse sequence including motion sensitizing gradients [19].

The 3D phase-contrast gradient-echo pulse sequence is used to measure the displacement of each pixel within the sample during excitation." The phase angle between the applied harmonic motion and the motion encoding gradients is labeled as θ [16].

1.3 Summary

MRE has already produced promising results as a feasible, noninvasive method for characterizing the mechanical properties of the human breast, prostate, and muscle tissue in vivo [15, 17]. Steady-state dynamic MR elastography requires that the tissues under investigation be excited by an external mechanical stress to produce harmonic

shear waves, which propagate though the tissue as explained in 1.2.1. Most commonly, excitation is provided by one or more actuators coupled to a region of interest. The primary purpose of this thesis is to come up with a noble MRE breast actuator that can us used for both phantoms and patients. The actuator should be compatible with the MRI scanner and it should generate sufficient motion to generate successful reconstruction. For this, two different types of actuator concepts have been developed and explained.

Chapter 2 covers the development of an acoustic actuator and its initial laboratory test results.

Chapter 3 presents another new actuator and its initial laboratory test results.

Chapter 4 presents over view of making the silicone phantoms. A simulations study is shown in Chapter 5 and Chapter 6 shows MR test using acoustic actuator and reconstruction method. Results are discussed in Chapter 7 and future work to conduct in Chapter 8.

Chapter 2

Acoustic Actuator: Design and Analysis

The actuator is an essential part of the MRE process as it creates propagating shear waves in the tissue of interest. Different breast actuators have been used for MRE. They can be categorized as electromagnetic, piezoelectric and pneumatic. Each one has strength and weakness in use for MRE.

Electromagnetic actuators are the most common as they can be used in simple and cheaper designs. However it can cause significant interference with the MR signal producing artefacts in the image. Piezoelectric actuators can provide strong force and are excellent in maintaining proper control of motion frequency and magnitude [23]. However, they may also cause MR image distortion due to susceptibility and eddy current artefacts [23]. Pneumatic actuators donot have these limitations with respect to creating artefact. However, the frequency range at which they operate is limited to 150 *hz* [23].

Acoustic actuators have been used in the past for imaging human brain [23, 24] and liver [25]. McKnight et al. [26] described an electromechanically driven actuator to detect 25 *mm* diameter tumours in phantoms at 100 *hz*. The stiffness contrast ratio between the surrounding and the tumour in this case was approximately 1:2.

To characterize the mechanical properties of silicone phantoms using MRE, an actuation system was developed that could reliably excite breast tissue or phantoms at sufficient amplitude. Preliminary experiments were performed on silicone breast phantoms due to their size and mechanical properties. The following sections describe the design, construction, and characterization processes involved in the creation of the Acoustic actuator for this study.

2.1 System Specifications

The system specification for the acoustic breast actuator is outlined base on specific application requirement. In particular the system must:

- Induce sinusoidal motion in the phantom tissue of at least 100 µm peak-to-peak
- Fit inside the Standard MRI breast coil (Figure 2.1).
- Be easily assembled inside the Standard breast coil
- Be cost effective
- Made of non-magnetic materials to avoid interference with MRI.

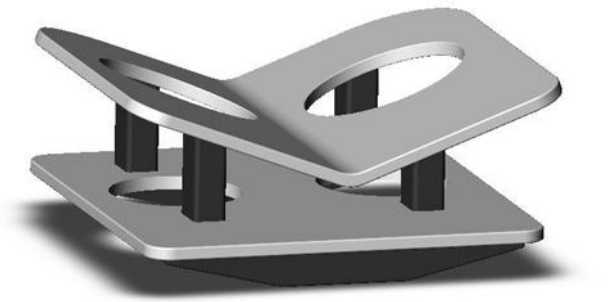

Figure 2.1: Standard MRI Breast coil

Further, the system must not:

- Interfere with the data acquisition. It is imperative for the elastic parameter reconstruction that image artefacts, such as localized signal degradation and overall signal noise, be minimized

2.2 Material Selection

The choice of materials in any MRE system is restricted to only non-magnetic materials. Thus, most of the parts were made of Perspex. Others were made of nylon.

2.3 MR Imaging Requirements

The MR imaging system used for the MRE data acquisition in this research was a 1.5 Tesla GE SIGNA superconducting magnet located in the MRI suite at the Dartmouth Hitchcock Medical Centre in Lebanon, New Hampshire. Due to the intense magnetic field, some guidelines needed to be maintained for the safety of the patient and the technicians, as well as for and preserving image quality. These guidelines include a restriction on the types of materials allowed near the magnet. Magnetic susceptibility describes the extent to which a material becomes magnetized when placed in a magnetic field [27].

Diamagnetic materials are known to have a slightly negative susceptibility, opposing the local magnetic field. Paramagnetic materials are known to have a slightly positive susceptibility, enhancing the local magnetic field, yet they have no measurable self-magnetism. Ferromagnetic materials (also known as “super paramagnetic”) on the other hand, demonstrate large positive susceptibility, are capable of exhibiting self-magnetism, and will significantly augment the existing magnetic field [3.5]. Examples of ferromagnetic materials include iron, nickel, and cobalt.

As a result, common medical devices comprised of these materials are strictly prohibited from entering the imaging room. Instead, alternative materials, such as plastics and low susceptibility metals are used to produce “MR compatible” equipment. Since MRE requires the use of a MR imaging system, all experimental setups are required to be MR compatible. However, an even more important material consideration is their effect on image quality [12].

Though faster than the conventional spin-echo pulse sequence, the gradient-echo pulse sequence used in the MRE data acquisition presented here is vulnerable to susceptibility artefacts caused by paramagnetic and diamagnetic materials, as well as inhomogeneities in the main magnetic field. Local enhancements/oppositions of the magnetic field during the MRE scan will cause "spins" (protons) in the vicinity to experience an increase or decrease in their precessional frequencies. Deviations from the Larmor frequency will inhibit the spins from absorbing energy from RF pulses through resonance. The result is a local degradation in the T2 and T2* signals from the MRI system due to faster decay constants [5].

2.4 Acoustic Actuator Selection

The driving force for the acoustic actuator was generated by a commercial 750 watt subwoofer. The subwoofer can be operated at a frequency range from 50-100 Hz. . The subwoofer was modified as shown in Figure 2.2, where the plate at the back of the subwoofer was removed and the front plate was replaced with a Perspex plate. A tube was inserted in the middle of the plate. The other end of the tube was inserted into an inclined box (Figure 2.3). Thus, acoustic pressure was delivered from the subwoofer to the box. The box was made inclined in order to fit inside the MRI breast coil (Figure 2.1). The box is rigid and one end is opened. Perspex plates of different thickness were used on the open end of the box as membrane. The box was connected to a cup by two links. The cup is designed to be in direct contact with the breast phantom. The cup has curved surface to ensure maximum contact between the actuator and tissue or phantom to transfer motion into largest area. The cup too was also inclined. The cup was made to slide across the breast coil pillar. A schematic diagram of the actuator has been shown in Figure 2.4.

When the subwoofer was turned on, the sound vibration moves the membrane back and forth. That vibration is transmitted to the cup by linkage shown in Figure 2.3. Thus, the motion was finally transmitted to the breast or phantom through the cup, as in Figure 2.4.

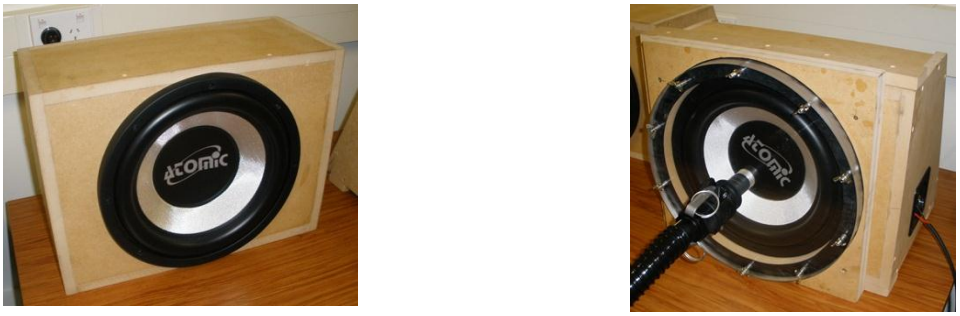

(a) (b)

Figure 2.2 (a) initial subwoofer (b) Modified subwoofer

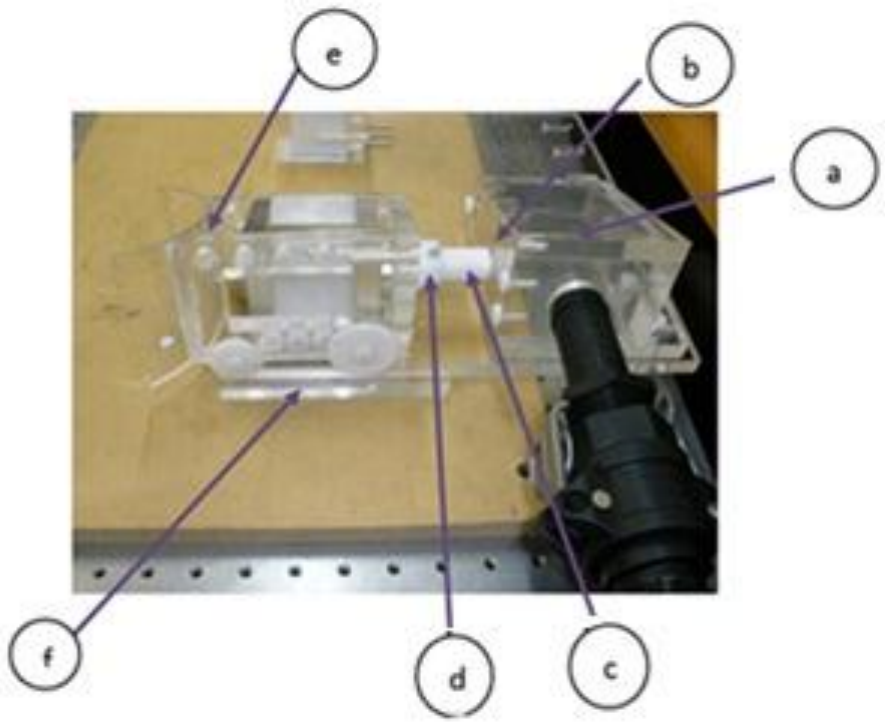

Figure 2.3: Acoustic actuator assembly. Where, (a) inclined box; (b) Membrane in front of the box; (c) Connector from the box (link 1); (d) connector to the breast cup (link 2); (e) Breast cup and (f) Rail system on which the cup can slide.

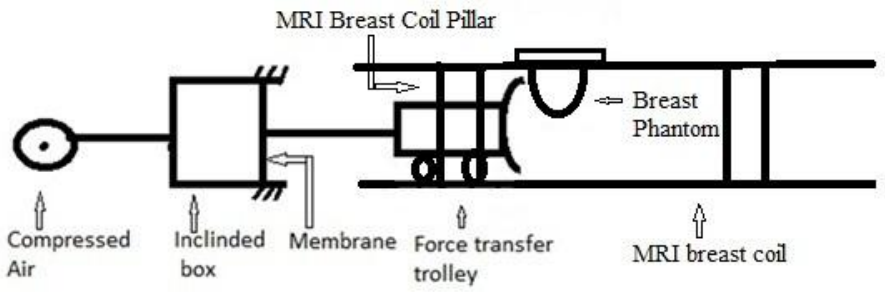

Figure 2.4: Schematic diagram of the actuator.

2.5 Acoustic actuator testing

Initially, the actuator was tested in the laboratory outside the MR environment to validate its design performance. Displacement was measured at the cup surface using a laser interferometer at different frequencies ranging from 50-100 Hz at no load. This system can be considered as a single degree of freedom system with sinusoidal excitation, where the diaphragm is the spring. Its vibration modes vary as $(t/L)^3$, where t is the thickness of the membrane and L is the length of its longest side. Thus, small changes in thickness (t) can affect the modal frequencies significantly. Similarly, the choice of material is important since the modal frequencies vary as $(1/\rho)^{1/2}$ where ρ is the material density.

Several different thickness diaphragms were tried. Their responses are plotted (Figure 2.5). The 1.2*mm* thick membrane produced the maximum displacement of 450 μm in the frequency range of 60-90 Hz. A 2 *mm* thick membrane produced 200 μm at 100 Hz. However, the 1.2 *mm* membrane resonated in a 60-90 Hz frequency range that is most useful in this application.

While in most mechanical systems it is wise to avoid operation in a resonant condition, in some applications it is an advantage. Such cases include ultrasonic welding and cutting, where the tool is designed to operate using a horn that resonates. The resonant condition means that less energy is required to produce a given displacement. For this particular application, maximum vibration input motion was desired. By choosing a diaphragm such that its displacement peaked in the desired frequency range, the amount of acoustic energy required to drive it was minimized.

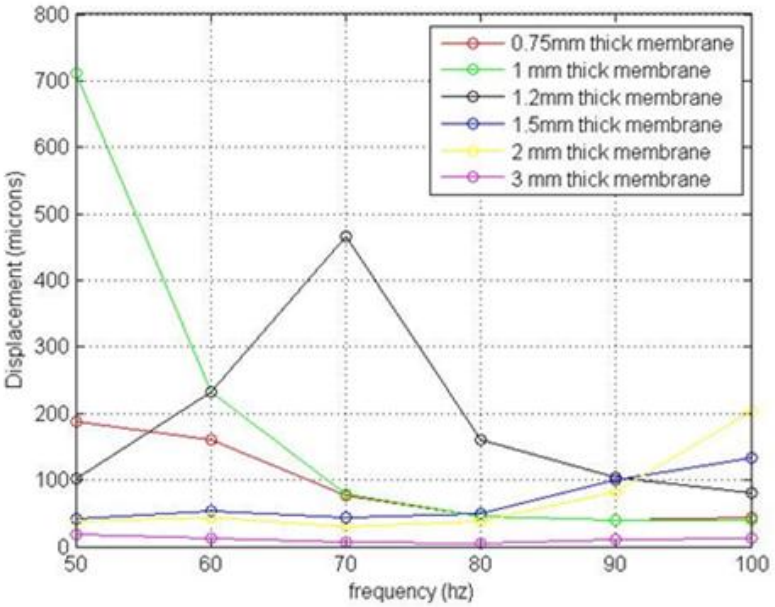

Figure 2.5: Frequency vs Displacement plot for membranes of different thickness

2.6 Summary

The acoustic actuator described in this chapter is simple, cost effective and capable of producing sufficient motion at the desired frequency range. The laboratory test results are satisfactory and lay the foundation for testing it in the MRI scanner, described in Chapter 6.

Chapter 3

Piezo-Electric Actuator: Design and Analysis

An alternative actuation system was also developed to reliably excite the breast phantom tissue at sufficient amplitude. Initially, the actuator was developed to be tested in MR environment. The following sections describe the design, construction, and characterization processes involved in the creation of the Piezo-electric driven actuator.

3.1 System Specifications

The system specification for the Piezo-electric breast actuator prototype is given below. It **Must**:

- Induce sinusoidal motion in the phantom tissue of at least 80μm peak-to-peak. Eighty microns is the maximum attainable displacement for most piezoelectric actuators, as quoted from manufacturers, although the actual tissue displacement will vary as a result of constructive and destructive interference of the propagating waves
- Fit inside the standard MRI breast coil of Figure 2.1
- Be easily assembled inside the Standard breast coil
- Be cost effective

These specifications are the guide to the design created.

3.2 Piezoelectric Actuator Selection

The Piezo-electric actuator used for this project was a non-magnetic preloaded Piezo-electric actuator (P-842K022, Physik Instrumente, GmbH Co. KG) as shown in Figure 3.1. The specifications of the actuator give a 90 µm travel range and a push/pull force capacity of 800/300N. Electronics were also developed in the previous project to deliver a sinusoidal signal of variable amplitude. The maximum output was −2 to 12V to match the specification of the amplifier unit (E505.00, Physik Instrumente, GmbH Co. KG). The amplifier drives the actuator at 10 times the input voltage provided, resulting in a maximum peak-to-peak output of 140V. The actuator was driven at 100Hz and 85 Hz , and with an input voltage of 9V. For further information on the technical data of the actuator, check the appendix A.

Figure 3.1: Linear Piezo-electric actuator PI 842.60

3.3 Actuation System Design

3.3.1. First generation Piezo-electric breast actuator

Initially, the actuator was intended to be used in the MR environment. So all the parts were made of non-magnetic materials, mostly plastic A major design consideration for the actuator base module was the need to have it fit seamlessly into the Standard MR breast-coil shown in

Figure 3.1. To achieve this goal, it was necessary to have a portion of the base module match the dimensions of the breast coil. This section was called the base plate and the dimensions of the base plate were made equal to the available space on the coil. All other parts were positioned around this plate and were made with proportions to fit inside the MR coil .

The linear Piezo-electric actuator was supported at the back by a solid block attached to the base plate and shown in Figure 3.2. The motion from the actuator was amplified using a wooden lever arm, which was pivoted on the base plate. Wood is used because it is not magnetic and this will not interfere with the MRI scanner. This amplified motion from the lever arm is transmitted to a silicone phantom through a cup. The cup has a curved surface to touch the phantom. The restoring force for the phantom is provided by a spring.

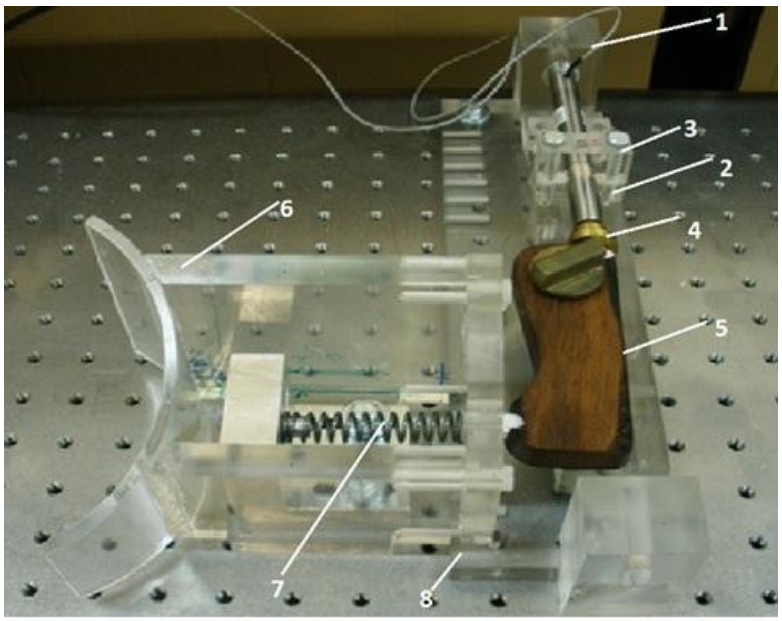

Figure 3.2: Initial piezo-electric actuator setup (1)Solid block supporting the piezo actuator (2) and (3) Clamps holding the actuator (4) Piezo actuator tip (5) Wooden lever arm (6) Breast cupl (7) Coil spring (8) Base plate

3.3.1.1 Lever arm

The motion of the piezo-electric actuator was increasd by a lever arm. The lever was made of Jarrah wood. Modal analysis has been done on this lever arm to calculate its natural frequency using FEA and assure it is dynamically stiff enough as shown in Figure 3.3. The natural frequencies of the wooden lever are found to be 893.95 Hz, 2459.3 Hz, and 3435.2 Hz as shown in Figure 3.4. These frequncies are above the applied frequency of 100 Hz and 85 Hz. Hence, Jarrah wood is safe to use as a lever material. Since these frequencies are well above the actuation frequency of 100 Hz so there is not going to be any affect from resonance.

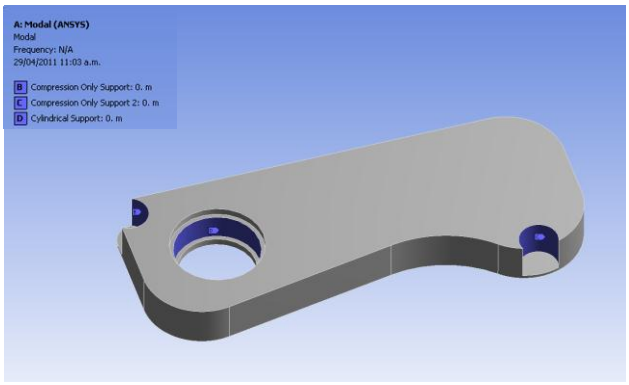

Figure 3.3: Modal analysis of the lever arm

Figure 3.4: Modal frequencies of the lever arm

3.3.1.2 System Characterization

Preliminary Calculations

It was desired to produce around 400 µm displacement at the phantom surface so that even after damping there would be sufficient motion in tissue. Thus, a lever arm was designed to magnify the available piezo displacement of 90 µm. The lever design is shown in Figure 3.5. Its main characterestics and design verification include:

Piezo-electric actuator pushing force,f1 = 800 N

Pulling force, f2 = 300 N

d1=16.38mm, d2=77mm (chosen to amplify the motion)

Maximum displacement provided by the Piezo-electric actuator, x1=0.09 mm or 90 microns (Table 1)

Let, the force we can get on other end is f_3

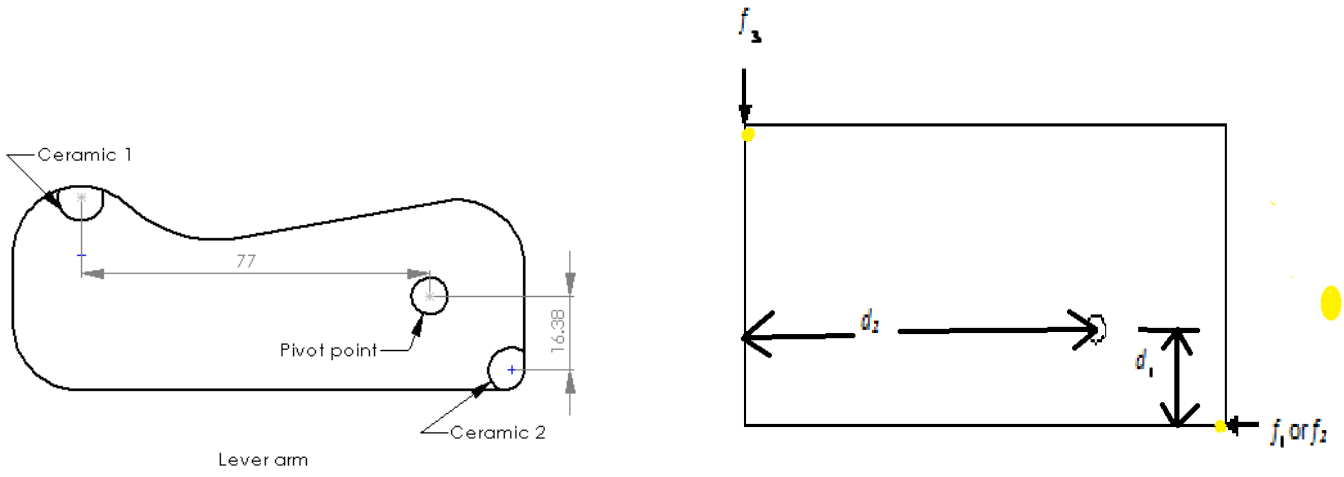

Figure 3.5: Schematic Diagram of lever arm

Let, the displacement at the other end is x3

$$f_1 d_1 = f_3 d_3 \qquad (1)$$

Or, 800 x 16.38 = f_3 x 77

$\therefore\ f_3 =$ 170.2 N

Then, $f_1 x_1 = f_3 x_3$ (2)

Or, 800 x 0.09 = 170.2 x x_3

$\therefore x_3 = 0.423$ mm

So theoretically the maximum displacement that can be obtained from the lever arm is 423 microns at no load.

3.3.1.3 Experimental Measurements

The setup shown in Figure 3.3 was tested in the Laboratory at no load. All the parts were assembled and the measurements were done using a Laser interferometer at the surface of the cup. The spring was compressed by different amounts starting from 1 mm to 5mm. From the plot in Figure 3.6, it was found that the maximum displacement was achieved when the spring was compressed by 1mm. The displacement reduced gradually with the increase of spring compression. In other words, displacement decreased with the increase in spring stiffness showing some nonlinearity in the spring. These results were found to be repeatable and consistent.

However, the maximum displacement obtained through the lab test was a lot smaller than the maximum theoretical displacement. This difference could be associated with the frictional loss of different parts of the system, in particular the friction between the cup and the table. The mass of the cup was also significantly higher than what was required. Reducing the mass of the cup and the friction between the cup and the table could increase the displacement

significantly and make the design more compact. These changes were made in a subsequent design.

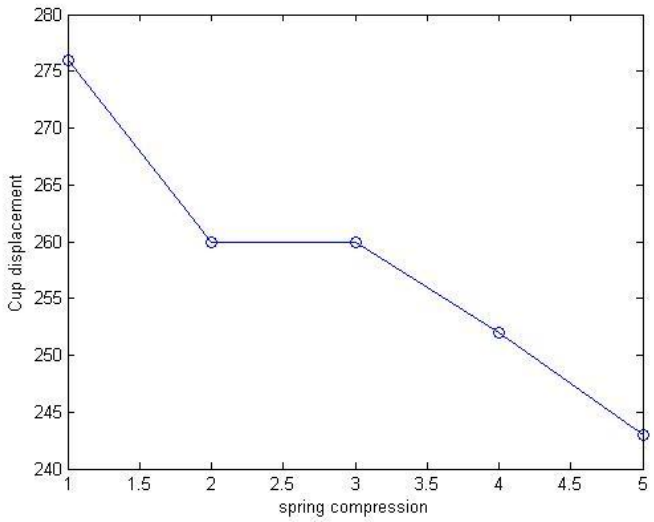

Figure 3.6: Spring compression vs. cup Displacement

3.3.2 Second generation Piezo-electric breast actuator

In the second generation piezo-electric breast actuator, the actuator was modified as Figure 3.8. The principal of the actuator was the same as the first design. Only the positioning of the actuator was changed and it was placed sideways. In this case, a tension spring was used instead of a compression spring to reduce complexity. In addition, the entire actuator was made more compact. In this design, the spring stiffness could be changed easily without opening the whole assembly. The cup was made lighter and some degrees of freedom were kept in the system to be able to shake phantoms/breasts of various sizes. Since MR testing at MR was not available at this stage, the setup was tested at the laboratory on phantoms to check its efficiency and ability to meet the design specifications.

3.3.2.1 Preliminary Calculations

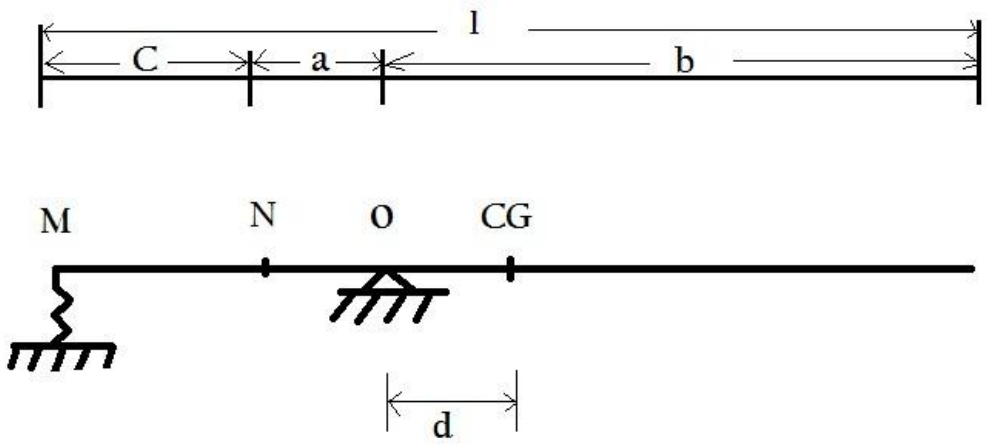

Figure 3.7 : Long lever arm

In this design analysis

a=34 mm

b=153 mm

c=52 mm

d=33.5 mm

l= a+b+c = 239 mm

CG= l/2=119.5 mm

$M_{rod=}$ 80 gm

M_{cup} = 30 gm

The mass moment of inertia of the rod, (in terms of CG) is defined:

$$(Irod)_{CG} = M_{rod}/12(h^2+l^2)$$

In terms of pivot point o, $(Irod)_o$ = Mass moment of inertia of the rod along CG+ mass* (distance between the CG and pivot point)^2

Or, $I_{rod} = M_{rod}/12(h2+l2) + M_{rod} \cdot d^2$

Or, ,$I_{rod=}$ 3.73×10^{-4} Kgm^2

Mass moment of inertia due to added mass m kg at the end of the rod , $I_{mass} = mb^2$

Or, $I_{mass} = 7.0 \times 10\text{-}^4$ kgm^2

Total moment of inertia including the rod & the mass is, $I_{total} = I_{rod} + I_{mass}$

Or, $I_{total} = 11.73 \times 10\text{-}^4$ kgm^2

At point p the displacement is defined : $X = - A \cos(2\pi f) t + A$ [A= 40 μm = 40 e-^{6} m]

Again, $v_p = \omega_o \times a$

Or, $\omega_o = v_p/a = A/a\ (2\pi f) \sin(2\pi f)t$

Therefore, $\alpha = d\omega_o/dt = -A/a\ (2\pi f)^2 . \cos(2\pi f)\ t$ where $-A/a\ (2\pi f)^2$

$\alpha_{max} = A/a\ (2\pi f)^2$

Here f= 85 hz, so $\alpha_{max} = 335.4$ $rads^{-2}$

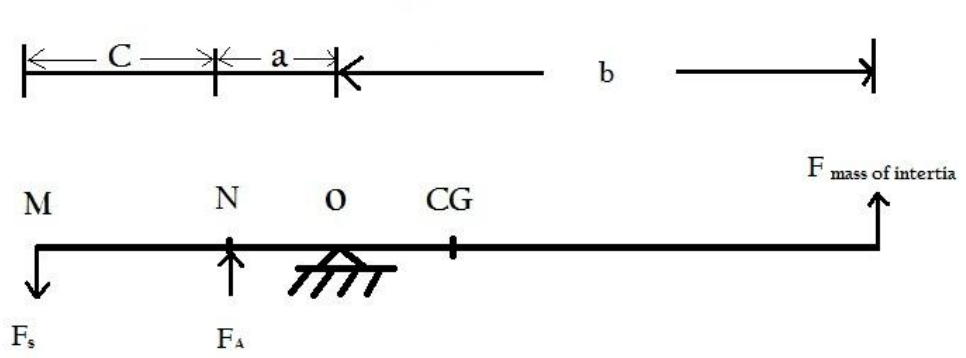

Figure 3.8 : Free body diagram of long lever arm showing forces at different points

$F_{inertia} \times b = I_{total} \times \alpha$ [3.1]

Or, $F_{inertia} = (I_{total} \times \alpha)/ b = 2.5$ N

Moment Balance,

$F_A \times a = F_s \times (a+c) + F_{inertia} \times b$ [3.2]

If F_A is considered to be zero, than from equation 3.2

$F_s \times (a+c) = - F_{inertia} \times b$

So, $F_s = -3.4$ N

However if $F_A = 300$ N, $F_s = 113.15$ N

The current tension spring stiffness is 8.1 N/mm (measured)

Therefore 8.1 N is required to move 1 mm

So, 3.4 N is required to move 3.4/ 8.1 = 0.543 mm

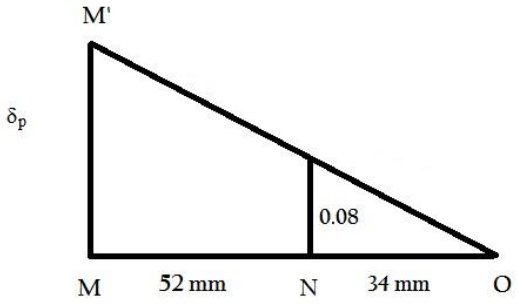

Figure 3.9: Triangle created on the pivot point o

From traiangle OMM' in Figure 3.9,

δ_p / (52+34) =0.08/34

Or, δ_p = 0.2 mm

So, δ_{start} = 0.543-0.2

=.343 mm

So, the spring needs to be stretched by 0.343 mm at the beginning. This is called preload. During operations the spring stretches by 0.2 mm more.

3.3.2.1 Experiemental results

Since this actuator was going to be tested in the laboratory only, all the parts were made of aluminium. The modified actuator was tested in the laboratory. The actuator was driven at 99 hz and displacmenet was measured at the extended lever arm tip as seen in Figure 3.10. The displacement was sufficient and the results were found to be repetable. Figure 3.11 shows the voltage vs displacement plot for the actuator. Thus it shows that our desired displacemtn can be achieved within the safe voltage limit of 10 v of the linear piezo-electric actuator or LVPZT.

The advantage of this actuator is that it can be used as one piece and inserted into the MR breast coil easily. It is light compared to the previous version discussed in section 3.3.1. Again the lever arm tip is adjustable to rotate it at various angle to get into a suitable position to touch the pahntom or breast tissue.

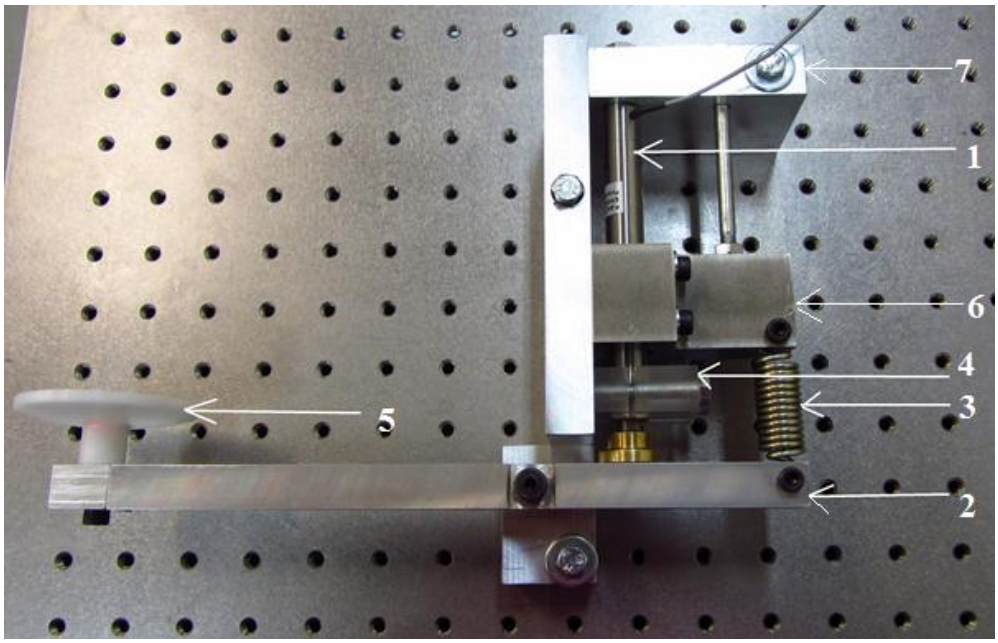

Figure 3.10: Second generation piezo-electric breast actuator (1) Linear piezo-electric actuator or LVPZT (2) Long lever arm (3)Tension spring (4) Clamps for actuator (5) Extended lever arm tip which is a circular nylon disk (6)Movable part for elongating the spring (7) Aluminium frame for holding the LVPZT

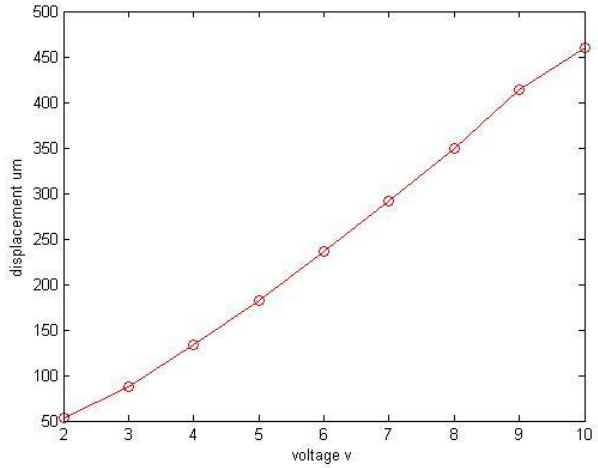

Figure 3.11: Voltage vs Displacement plot for the second generation Piezo-electric actuator

3.4 Summary

The actuator looks promising for future use in MRE for shaking both phantom and human breast tissue.

Chapter 4

Methods for testing phantoms

4.1 Silicone Phantom

Breast shaped silicone phantoms are made using a symmetric, approximately breast shaped core and cavity mold (Figures 4.1 and 4.2). Different types of silicone materials, such as LSR 05, A 341 and a softening agent are mixed in different quantities to form the phantom. Each phantom has four parts, the soft interior, a stiff tumor, a perspex plate and skin at the back of the Perspex plate. Sometimes, an external skin may also be added.

Figure 4.1: Breast shaped cavity

Figure 4.2: Breast shaped mold

4.1.1 Phantom Skin

The stiffness of the skin lies between the soft interior and the hard tumor. It affects the damping properties of the phantom by applying surface tension around the phantom. For

phantom skin, a combination of 80% of A341 and 20% of LSR05 or silicone elastomer is mixed together. These ingredients are shown in Figures 4.3 and 4.4. The total amount of silicone mixture used is 50 gm.

After mixing the silicone, it is taken into a vacuum chamber (Figure 4.5) to remove air bubbles from the mixture. The mixture is poured into the breast shaped cavity and the mold is placed on top of it. This produces a thin but uniform skin of 1 mm thickness. The skin is cured at room temperature in 18 to 20 hours or at an elevated temperature of 60 degree C it cures within two hours.

Figure 4.3: Silicone Elastomer LSR05

Figure 4.4: Silicone A341, part A and part B.

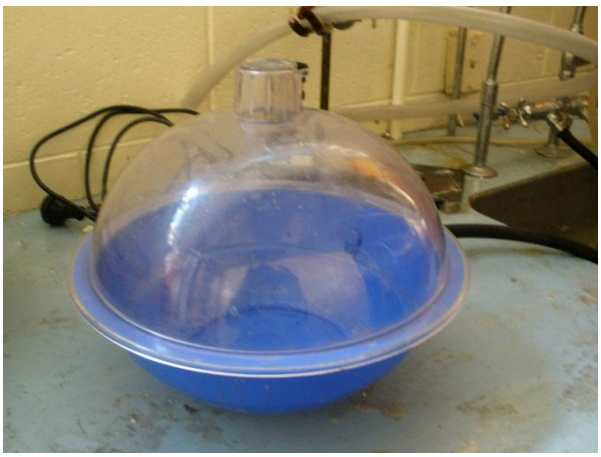

Figure 4.5: Vacuum pump

4.1.2 Phantom tumor

Each phantom had a stiffer silicone inclusion to replicate a tumor placed within the phantom. The tumor is made of equal amounts of LSR 05 parts A and B to create a stiffer silicone material by approximately a factor of two. This mixture is also made bubble free using a vacuum pump, and it is then cured.

4.1.3 Phantom interior

The interior is the most compliant (lowest stiffness) part of the phantom. For making this portion of the breast phantom, 60% of Dow Corning 200 Fluid or softening liquid is mixed with 40% of A341. The total amount of this mixture is 300 gm. The mixture is then placed inside the vacuum pump to make it bubble free and then poured into the cavity mold of Figure 4.2.

Figure 4.6 shows a tumor suspended from a support in by a wire. Silicone mixture for the interior is poured from the side and the cavity is filled up to approximately ¾ th of its total depth. It takes half a day at room temperature or one and a half hours at 60 degree C to cure. The remaining ¼ th depth of the cavity is filled by another mixture discussed in section 4.1.4.

Once the interior silicone is cured, the wire is removed and a perforated plastic plate (Figure 4.7) is placed on top of the silicone phantom. The plate is used to hold the phantom. It has two different sized holes in it. The larger holes of the plate help to bind the silicone with the plate, while the smaller holes are used to attach nylon bolts for ease of handling and clamping during later test using the phantom. The nylon bolt and perspex plate assembly is placed on top of the cured interior silicone in the cavity.

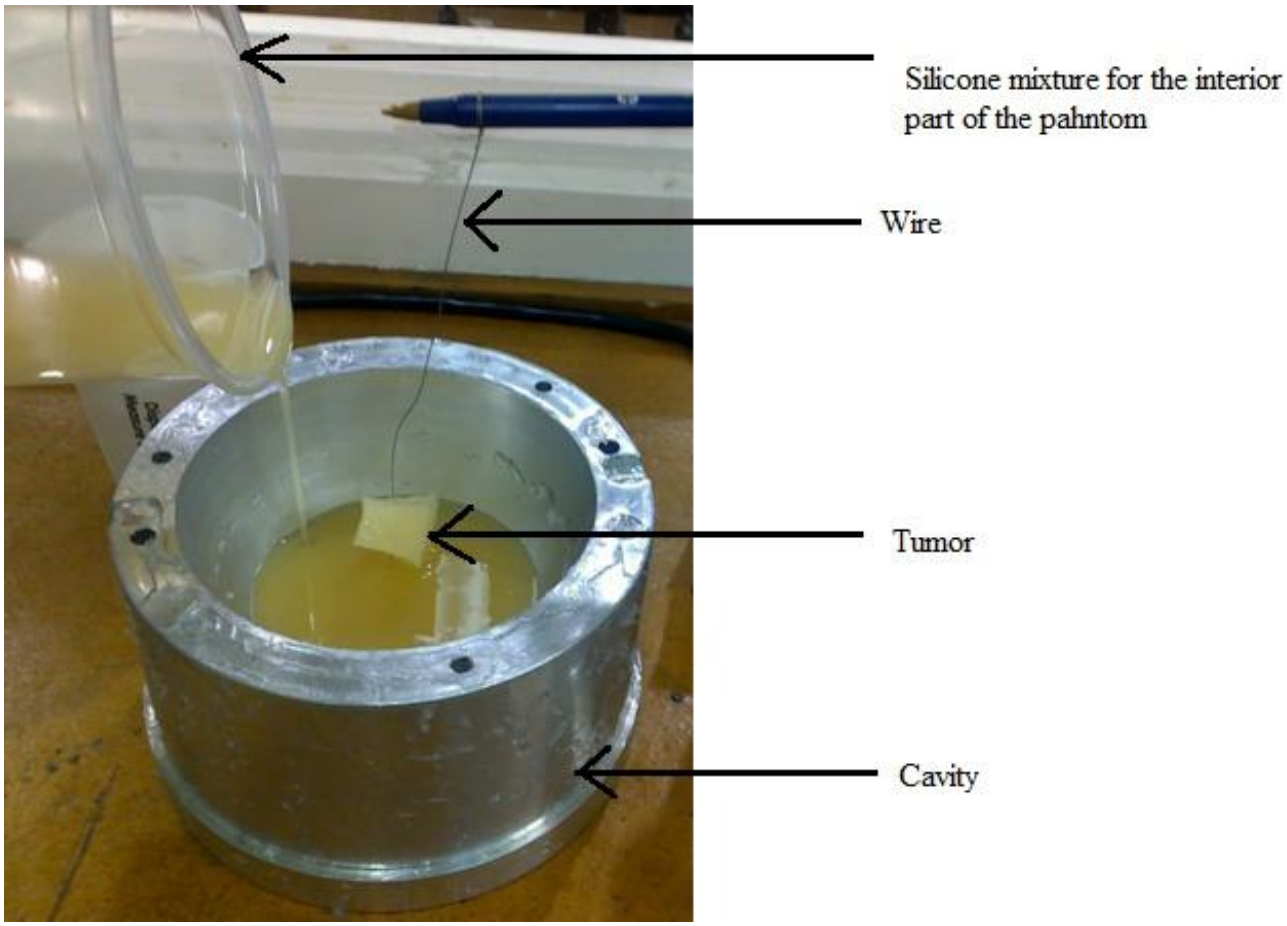

Figure 4.6: Silicone mixture poured into the cavity

Figure 4.7(a): Perforated plate

Figure 4.7(b): Perforated plate and nylon bolt assembly on the cavity

4.1.4 Back skin

The silicone composition and the cure time for creating the back skin of the phantom is the same as described in section 4.1.1. Here the total amount of silicone mixture is 80 gm. This higher amount of silicone (80 gm) compared to the outer skin (50 gm) is required because this mixture fills out the remaining $1/4^{th}$ depth of the cavity mold as seen in Figures 4.8 (a) and (b). It is poured on top of the perforated plate and nylon bolt assembly. The silicone composition and the cure time are the same as in section 4.3.1.

When this back skin was cured, the whole phantom is taken out of the cavity and the final product looks as shown in Figure 4.9.

Figure 4.7 a

Figure 4.7 b

Figure 4.8(a) Perspex plate assembly in the cavity (b) silicone mixture filling the entire cavity

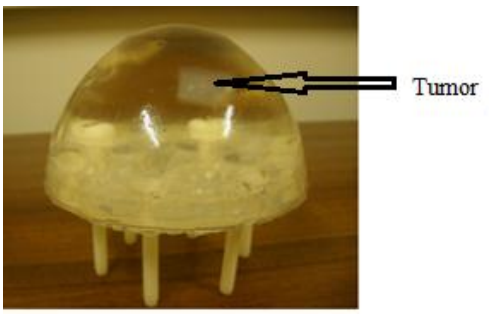

Figure 4.9: Clear breast phantom with a white inclusion at the top right hand corner

4.1.5 Category of Phantoms

Four different types of phantoms were made in the lab with tumors placed at different locations. Figure 4.10 shows a schematic slice of a phantom to define these locations. Table 4.1 shows the description of these phantoms. Each of them had a mean diameter of 55 mm at the back.

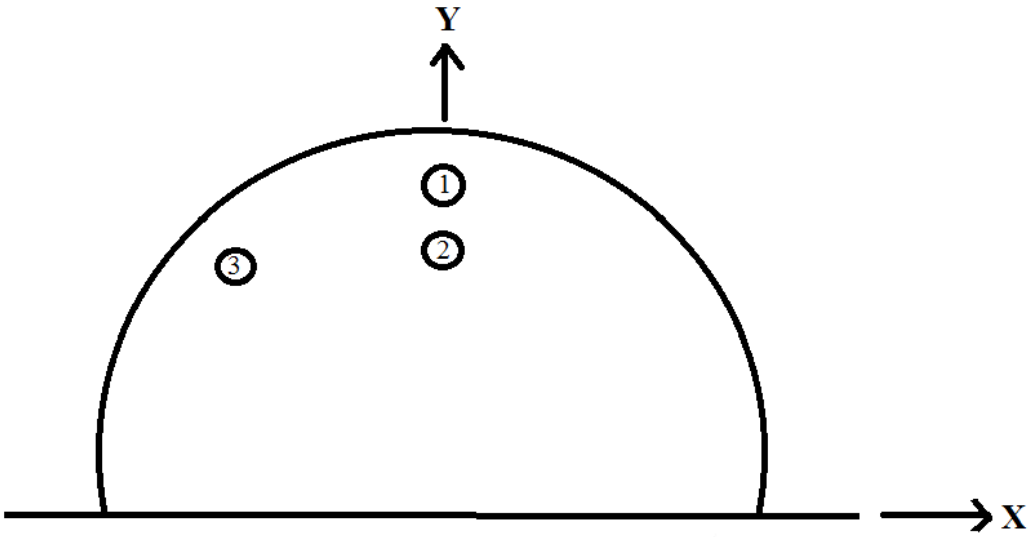

Figure 4.10: Schematic slice of phantom showing different tumor locations

Table 4.1: Silicone Breast phantoms

Description	Name
A 7.5 mm tumor located 50 mm from the back of the back of the phantom	Case 1
A 7.5 mm tumor located 40 mm from the back of the phantom	Case 2
A 12 mm tumor located 50 mm from the back of the back of the phantom	Case 3
Homogeneous phantom with no tumor	Case 4

4.2 Summary

The silicone phantoms are a good approximation of human breast. The acoustic actuator is thus tested on these phantoms in the laboratory initially as discussed in Chapter 2 and later in the MRI scanner as discussed in Chapter 6.

Chapter 5

Phantom simulation study

5.1 Phantom Simulation

In this chapter, a phantom simulation case study is presented. The study was conducted to examine how the proposed external actuator of chapter 2 would, effect the mechanical properties of the phantom. In particular, the idea was to examine how the sideways or shear inputs would highlight the phantom's mechanical properties with respect to inverse problem solutions.

This study is thus based on forward simulation problem, where the boundary forcing and approximate mechanical properties are given to a simulated phantom and the resulting tissue displacement are obtained. This simulated displacement data is converted to a mesh and file format suitable for the MRE reconstruction and an initial estimate for the material properties is generated based on the mechanical testing of biological tissue [13]. Tumor stiffness is assumed twice the surrounding stiffness. Finally the shear modulus of the phantom is calculated corresponding using inverse solution method described later the next chapter. Hence, it simulates a complete test and inverse problem solution in silicone prior to experimental testing.

First, a mesh was generated on the breast model as shown in Figure 5.1 (b) using Gambit^{TM}. Initially, the mesh had 5715 nodes with a tumor (<18 mm) inside the mesh (Figure 5.9b). The phantom is given an initial displacement of 50 microns on one side and constrained on the other side**.** The phantom is also constrained at the back. In particular in Figure 5.9(c) the black nodes denote the fixed edge, yellow nodes shows displacement, red nodes denote tumor and green nodes at the back indicate fixed support. This simulated phantom is similar to

case1 in Table 4.2 except the tumor size which is slightly bigger here in the simulated phantom .

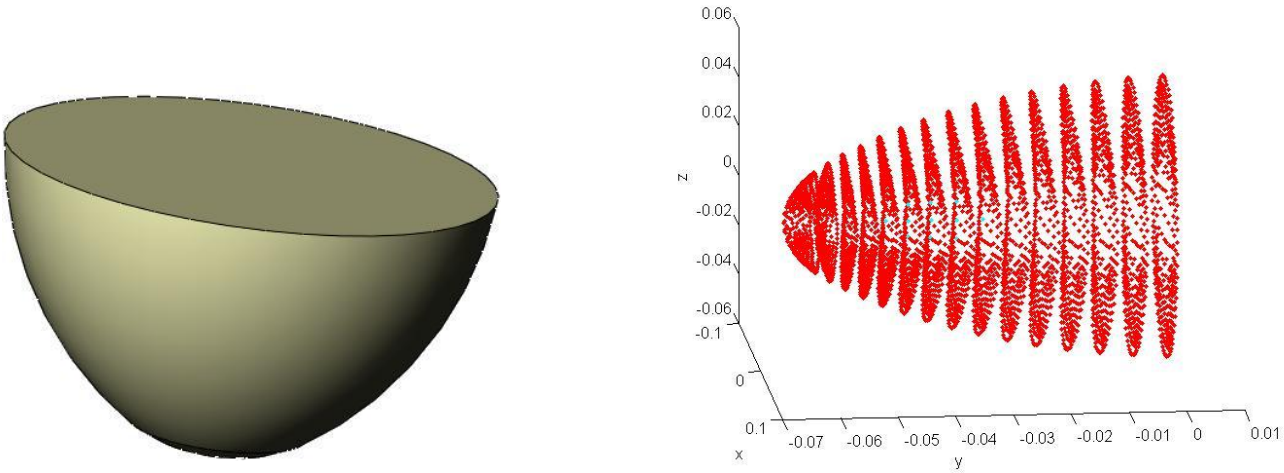

(a) (b)

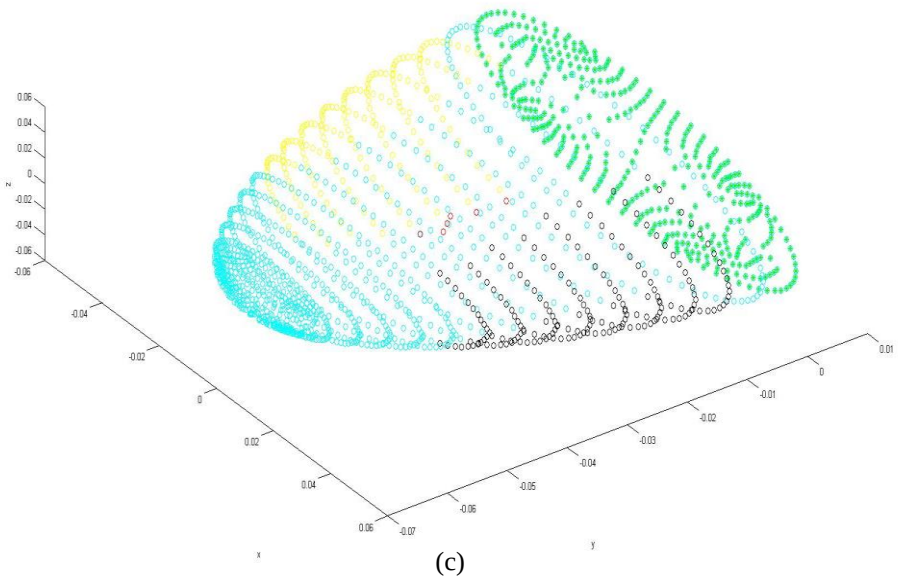

(c)

Figure 5.1: (a) Cad model of the simulated breast phantom (b) initial breast mesh slice view, blue nodes in the middle denote the tumor (c) Mesh colored by different boundary condition

5.2 Summary

The simulation study is a way to predict the outcome without the real testing of the actuator and the phantom. The results of this study are in Chapter 7.

Chapter 6

MR Test and Data Reconstruction Method

6.1 Phantom test in MR (Data acquisition)

Each phantom was placed in a prone position as shown in Figure 6.1(c) on the breast coil during testing using the acoustic actuator described in Chapter 2 for actuation. The actuator was placed on one side of the phantom as shown schematically in Figure 6.2. The goal was to fix the other end of the phantom, as was the case of simulation as in Chapter 5 using a fixed cup. However, due to space constraints, this option was not possible. Hence, the phantom was excited from one side and the other side was left free for MR experiments.

The MR imaging is done using a 3T Philips Achieva scanner. A 1.2 *mm* thick Perspex membrane is used as a membrane in the actuator box (Chapter 2). The subwoofer unit of the acoustic actuator is placed outside the MR scanner room. The actuator was driven at 85 Hz for input to the phantom.

Twenty-five 2 *mm* thick slices of data are collected for each silicone phantom, with in-plane resolution 1.97×1.97*mm*, using a modified EPI sequence with added motion sensitizing gradients (Weaver et al. [16]). All three motion components were measured,

The sinusoidal motion amplitudes were calculated using measurements from 8 phase offsets, equispaced across the harmonic cycle. A 3D phase unwrapping algorithm was used to correct phase wrapping where required (Wang et al [34]). The echo time, TE, was 47.05*ms*, and the repetition time, TR, was 1764*ms*. Total scan time for all three motion directions was 14 minutes.

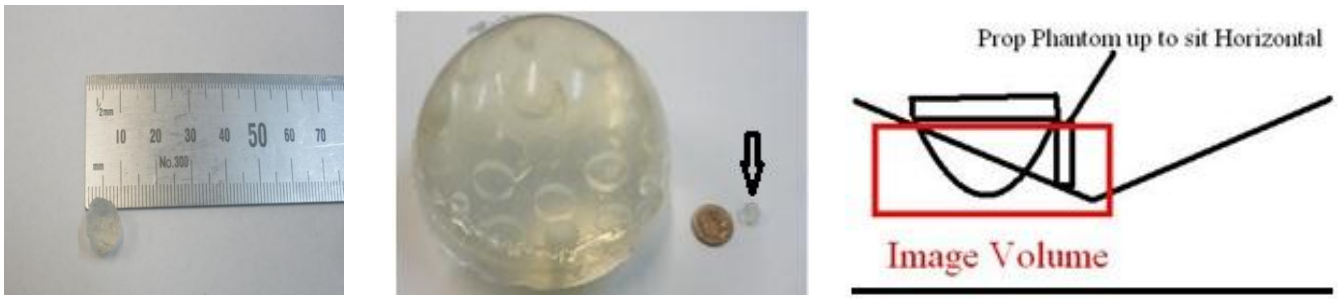

(a) (b) (c)

Figure 6.1: (a) 7.5 *mm* tumor used in silicone phantom; (b) Average size of the breast phantom and the 7.5 *mm* tumor (marked by an arrow); (c) Phantom arrangement on the Standard clinical MR breast coil

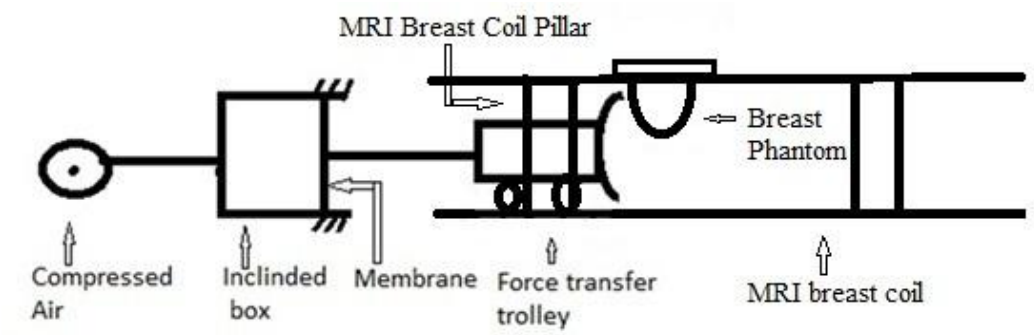

Figure 6.2: Schematic diagram of the actuator

6.2 MRE imaging technique

Figure 6.3 shows the three steps in generating an elastogram using MRE or any other motion data. First, the tissue under investigation is stimulated mechanically by an external actuator. The spatial distribution of the internal displacement field is dependent not only on the mechanical properties of the underlying tissue structures, but also on external and internal boundary conditions and on the nature of mechanical simulation (i.e. quasistatic or harmonic)

[28]. Second, the amplitude and phase of the induced tissue motion is measured by processing relative phase images, which are acquired using a phase contrast MR imaging sequence [16, 29, 30]. Third, the spatial distribution of the shear modulus distribution is estimated by applying a model-based inversion technique to MR measured motion images [31, 32, 33].

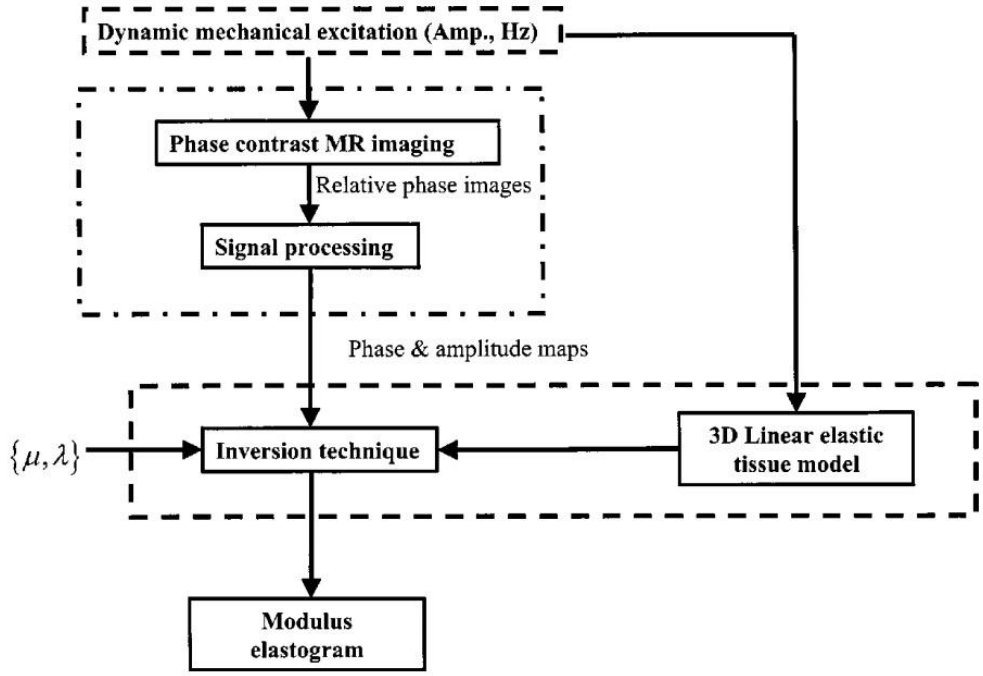

Figure 6.3 Flowchart describing the 3 step process used to generate a harmonic elastogram in the MRE process [31,32 ,33]

6.3 Inverse Method

When the material property distribution θ and boundary condition data are known, and mechanical response **u** is calculated, the solution is known as forward solution. In contrast, finding the mechanical properties of an object given the mechanical response is known as the

inverse problem. Thus, if the mechanical response **u**, and boundary condition data is known, than the material property distribution θ can be calculated.

The size of inverse problems are defined by the number of observed measurements, NO and the number of parameters being reconstructed, NP. For MRE, NO is the number of measured displacements, and NP is the number of parameters required to define the material property distribution. It is assumed that the displacement field is described by Navier's equation, a partial differential equation governing time-harmonic, isotropic, linearly elastic motion,

$$\nabla . G\, \nabla \mathbf{u} + \nabla (\lambda + G)\, \nabla . \mathbf{u} = -\rho\, \omega^2\, \mathbf{u} \qquad [6.1]$$

where **u** is the displacement vector, ρ is the tissue density and G and λ are Lame′'s constants:

$$G = \frac{E}{(2+2\upsilon)} \qquad [6.2]$$

$$\lambda = \frac{\upsilon E}{(1+\upsilon)(1-2\upsilon)} \qquad [6.3]$$

Where υ is Poisson's Ratio, and E is Young's modulus. For simplicity ρ and υ are considered to be known constants, leaving G or, equivalently, E as the elastic property parameter distribution to be estimated from the displacement field.

The inverse problem can be solved by direct inversion of the elasticity equation of Equation 6.1, provided there are at least as many measurements as parameters to be identified NO ≥ NP. However, the iterative nature of optimization techniques results in extremely computationally intensive problems.

To mitigate that issue, a subzone inversion technique was developed and described in detail by Van Houten et al [32, 33]. The complete problem domain is divided into small subzone partitions and the parameter was updated for each of them. This approach allows a high degree of spatial discretization, while maintaining computational tractability.

Subzones are generated in a random order and property reconstruction is made from a given initial elasticity distribution. The isotropic shear modulus and damping ratio are thus found for each node in the sample (breast phantom). Figure 6.4 shows the overall inversion algorithm based on [32, 33].

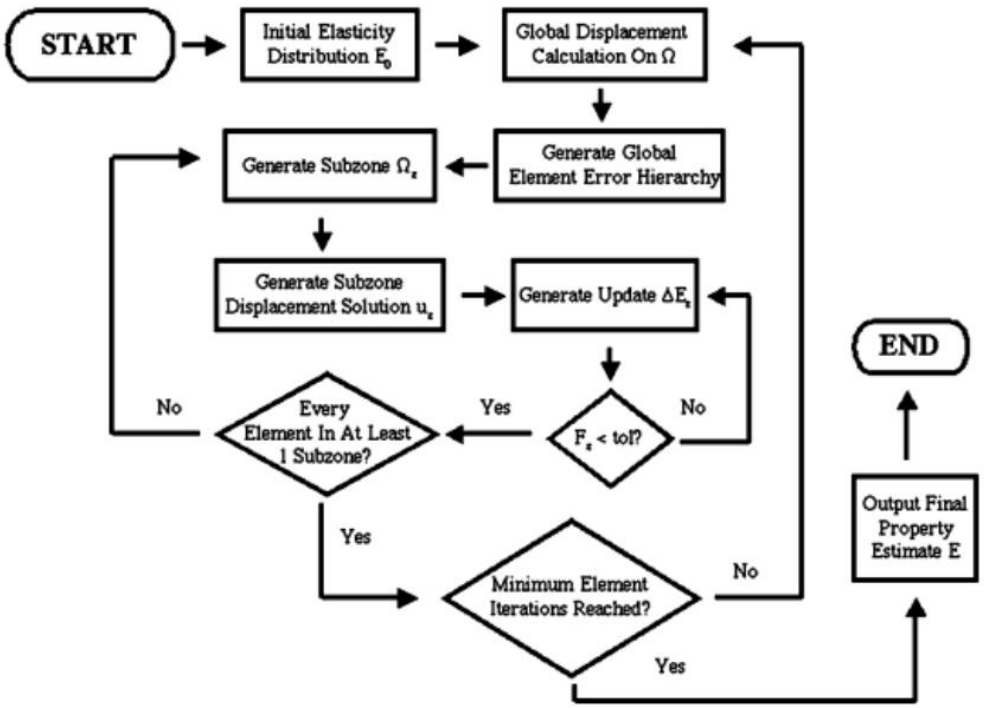

Figure 6.4: Flow diagram of the 3D subzone inversion process based on [32, 33]

Convergence is tested by the size of the minimized subzone functional, F_z, in equation [6.4] relative to a tolerance, tol, defined

$$F(E) = \sum F_z \, E_z \qquad [6.4]$$

Where:

$$Fz\,(Ez) = \sum_{l=1}^{N_z} (u_1^m - u_1^c)^2 + (v_1^m - v_1^c)^2 + (w_1^m - w_1^c)^2 \qquad [6.5]$$

Equation 6.5 compares the measured displacement data, u_1^m to the calculated displacement data, u_1^c. The minimization of this error is carried out by setting its derivatives with respect to Young's modulus, E, to zero and solving the resulting nonlinear system by use of Newton's method [33].

6.4 Summary

The data obtained by imaging the phantoms as shown in section 6.2, is reconstructed using the inverse method. The results are presented in the next chapter.

Chapter 7

MR Test Results

7.1 Displacement pattern in Silicone Phantom

The tissue displacement near the acoustic actuator surface was approximately 120 μm. This motion was satisfactory as our goal is to produce at least 100 μm in the phantom. However the displacement reduced gradually as the wave travelled inside the phantom.

Figure 6.3 shows the displacement pattern of slice 12 of case 2. The steady state harmonic wave patterns in the measured displacement images in Figure 7.1 shows larger wave amplitudes close to the actuator (top of the phantom), with smaller amplitudes further from actuation surface due to the effects of attenuation and dispersion. This behavior is expected in a viscoelastic material.

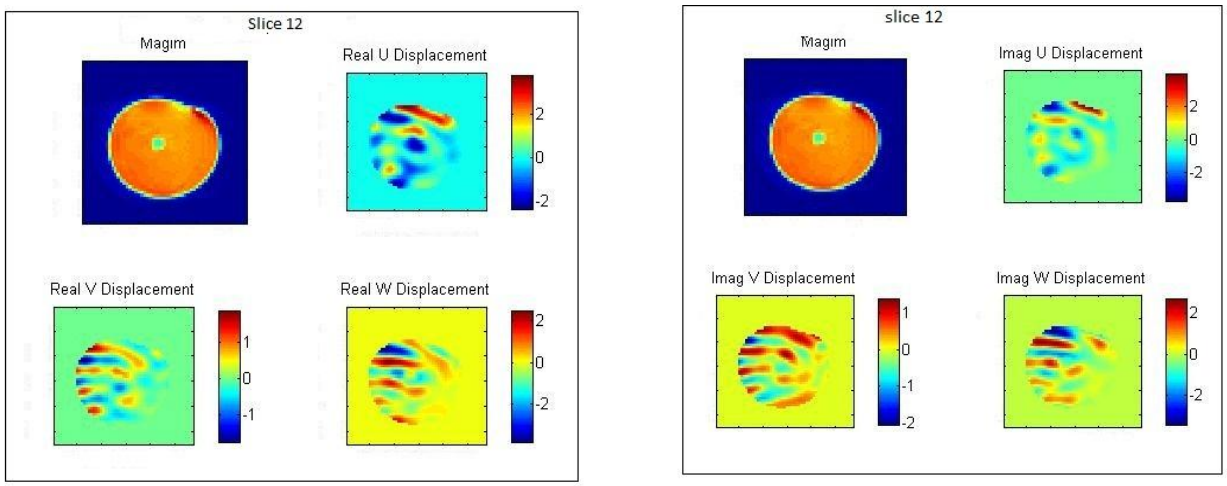

Figure 7.1: Displacement pattern inside silicone phantom, where (a) Real displacement, (b) Imaginary displacement. The color scale indicated the magnitude of travelling wave in a chronological order. From the Figure, the wave amplitude is higher in the area which is in contact with the actuator and attenuated gradually as it travelled, due to the viscous nature of the phantom tiss

7.2 Case 1

In Case 1, a 7.5 mm tumor was embedded on one side of a silicone phantom. The tumor was located 50 mm from the back surface (Perspex plate mimicking the chest wall) and was approximately twice as stiff as the surrounding phantom silicone. Figure 7.2 shows the greyscale MR images from Case 1 and Table 7.1 shows the initial guess used for reconstruction of the displacement data for Case 1. There was an indication of a suspicious solid region on the top left side (slices 5 to 10) as seen in row 2 of this matrix of images.

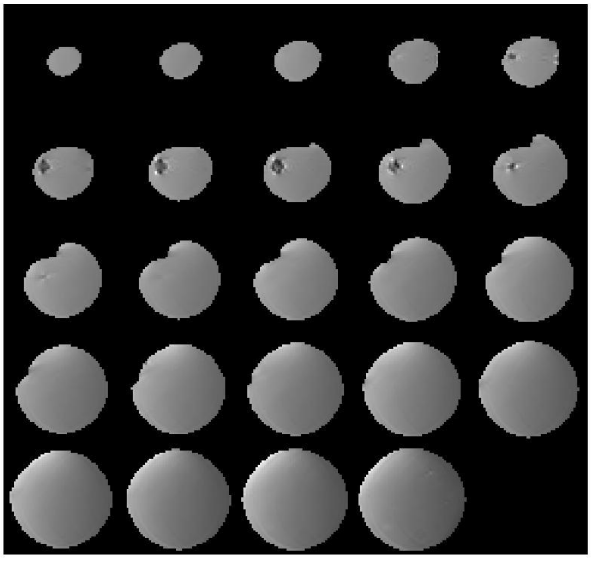

Figure 7.2: MR grayscale image of Case 1, all slices are shown from bottom (near the nipple) to top (near the perspex plate)

Figure 7.3 shows the T2* MR magnitude image of the Case 1 (slice 8). The blue region on the left identifies a suspicious region of higher stiffness. Shear modulus reconstruction (Figure 7.3b) shows the stiffness of that region to be very high. The mean stiffness of the phantom from the inverse problem is approximately 1.7 *Kpa* (Table 7.2). However that specific region was approximately 3.8 *Kpa*, matching expectation for the stiffness of the inclusion.

Signal to noise ratio (SNR) compares the level of a desired signal to the level of background noise. A high SNR indicates receiving "useful" information as opposed to a low SNR, which refers to not getting much useful information. In MRE, motion based SNR are commonly used. The shear strain, Υ is directly related to the shear modulus, μ, through the definition of shear stress, $\tau = \mu\Upsilon$. Therefore noise in the strain is the important factor in determining the quality of motion data rather than the noise in the motion [35]. McGarry et al. [35] showed that the reconstructed modulus values stabilizing at a strain SNR above 3. From Figure 7.4, the strain SNR for Case 1, was 3 inside the phantom. Thus, the tumor was identified correctly.

In Case 1, the SNR at the boundary was very poor (SNR < 2). Hence there was much greater noise in the data near the boundary. However, the SNR in the inside of the phantom is greater than 3, which means the overall reconstruction is reliable.

Some blending effects can be observed in Fig 7.3(b), especially near the boundary. This result is potentially due to two reasons. One cause may be the presence of noise at the boundary as explained previously. A second reason may be due to partial volume reconstruction error. Partial volume effect usually refers to an MRI measurement artifact. Basically, MR measurements are taken over a voxel (2x1.97x1.97mm in this Case). If part of this voxel is outside of the tissue, the measurement will be affected (e.g. if 1/4 of the volume of the voxel is air, the signal measured for that voxel will only be 3/4 of the signal coming from the tissue. Partial volume effects can also be generalized to any situation where discrete measurements are taken of a continuous field. Thus the stiffness value right on the edge of an inclusion for MRE could be considered a partial volume effect. So the reconstruction near the edge of the phantom is sometimes not very reliable.

For the damped elastic system model, the damping ratio ζ can be written:

$$\zeta = \frac{1}{2}\left(\frac{\mu_I}{\mu_R} - \frac{\rho_I}{\rho_R}\right) \qquad [7.6]$$

where μ_R is real shear modulus, μ_I is imaginary shear modulus, ρ_R is real density and ρ_I is imaginary density. This value provides the relative level of attenuation within the material [36].

Usually, the damping ratio is lower in less stiff materials. As the silicone phantom is compliant in general, the overall damping ratio reconstruction as shown in Figure 7.3(c), shows very low damping, as expected. The mechanical properties chosen as initial guesses for reconstruction in this case are shown in Table 7.4 such that ζ <0.2.

Table 7.1: Initial guess for mechanical Properties of Case 1

	μR (*Kpa*)	μI (*Kpa*)	ρR (*kg/m3*)	ρI (*kg/m3*)	*ζ*
Background & tumor	3	0.05	1000	-150	0.166

Rayleigh Damping, also referred to as proportional damping, is a damping model that attributes attenuation to both elastic and inertial forces [37, 38]. For Rayleigh Damped materials, an additional Rayleigh Composition (RC) measure can be defined:

$$RC = (2\,\zeta)^{-1}\left(\frac{\mu_I}{\mu_R}\right) \qquad [7.7]$$

The Rayleigh composition is poorly defined in the relatively homogeneous substance, but well or better defined at the boundary of the stiff region [36]. However, Figure 7.3(d) did not show any such trend, which could be due to partial volume reconstruction error or other errors.

For the reconstruction of all four Cases, the total number of global iterations was 120 and zone iterations was one. In the past, enough iteration was run on different data sets to be confident that the parameter estimates stabilized by 120 global iterations. Again, the convergence plot shown in Figure 7.5 also indicates that the solution has converged. One zone iteration was used because the computation time for one global iteration with two iterations per zone is about the same as two global iterations with one iteration per zone, and the second option converges faster most of the time, based on experience.

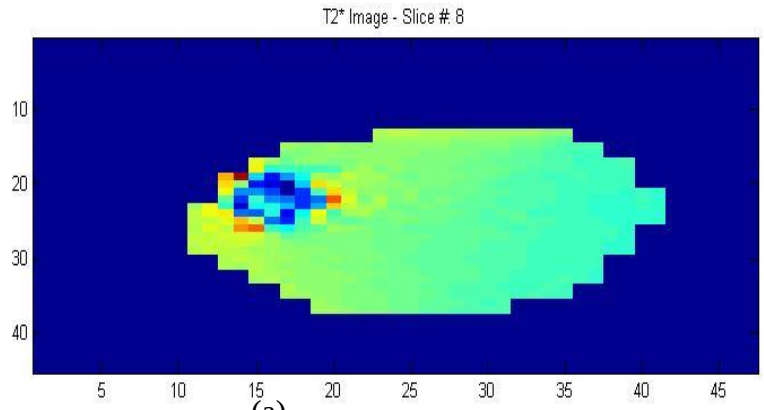

(a)

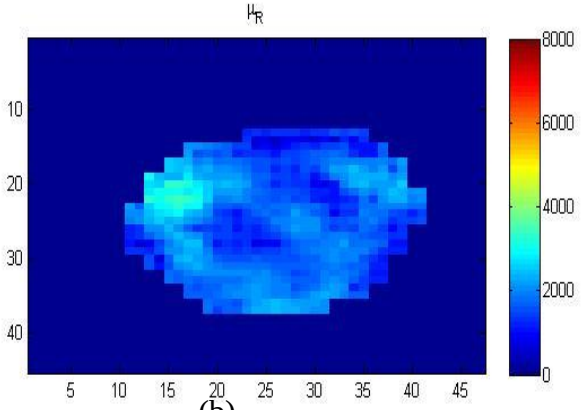

(b)

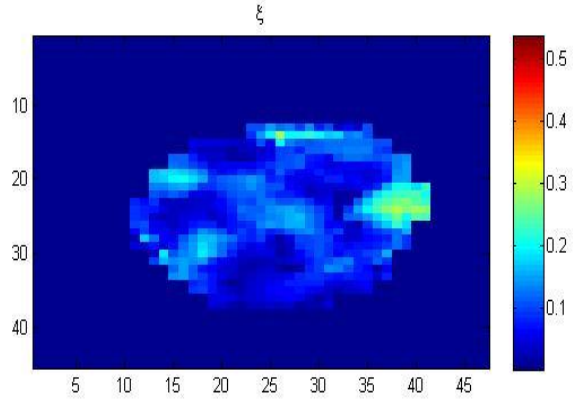

(c)

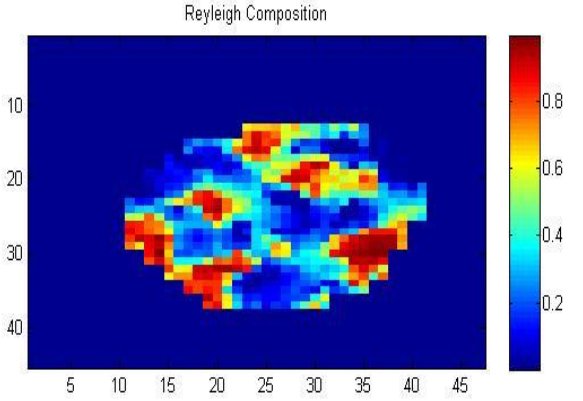

(d)

Figure 7.3: Reconstruction of Case 1(slice 8) (a) MR image, (b) Shear modulus reconstruction, (c) Damping ratio reconstruction and (d) Rayleigh composition.

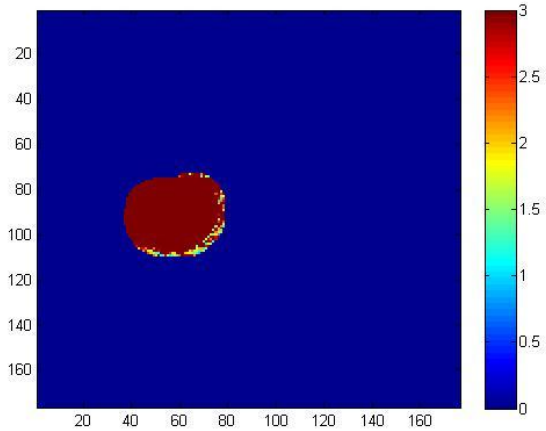

Figure 7.4: Strain SNR image of Case 1 (slice 8)

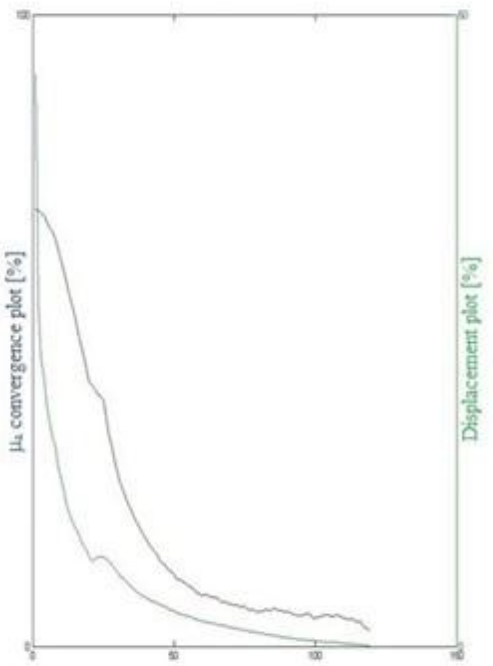

Figure 7.5: Convergence plot for Case 1 for shear modulus μ_R and displacement

Table 7.2: Mechanical Properties of Case 1 after reconstruction

	Shear modulus (*pa*)	Damping ratio	Rayleigh Composition
Mean	1738.4	0.09	0.358
Standard deviation	367.12	0.06	0.275

7.3 Case 2

In Case 2, a 7.5 mm tumor was embedded in the middle of the phantom. The tumor was located 40 mm from the back surface and was approximately twice as stiff as the surrounding phantom silicone. The mechanical properties used as initial guess for reconstruction of Case 2 are the same as Table 7.1.

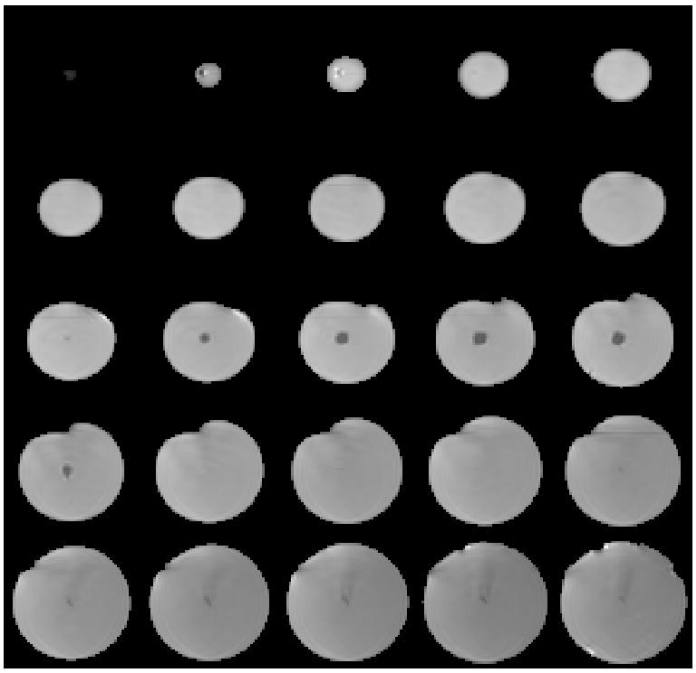

Figure 7.6: MR grey scale image of Case 2

Figure 7.6 shows the greyscale MR image of Case 2. Slices 10 to 15 indicate the presence of a suspicious high stiffness region in the middle of the phantom. That area corresponds to a high stiffness in Figure 7.7(a). From Figure 7.8(a), the signal inside the phantom is strong and Figure 7.8(b) indicates the convergence of the solution, confirming that stiff region to be a tumor. Some

blending effects can be seen on the boundary of the shear modulus diagram that could be due to partial volume error and noise. Damping ratio reconstruction as shown in Figure 7.7(b) is unclear as it is full of blending effects. However, the Rayleigh composition in Figure 7.7(c) shows the defined boundary around the tumor. Table 7.3 lists the final reconstruction results of Case 2.

Table 7.3: Mechanical properties of the Case 2 after reconstruction

	Shear modulus (*pa*)	Damping ratio	Rayleigh Composition
Mean	1997.4	0.064	0.4152
Standard deviation	371.4	0.04	0.2851

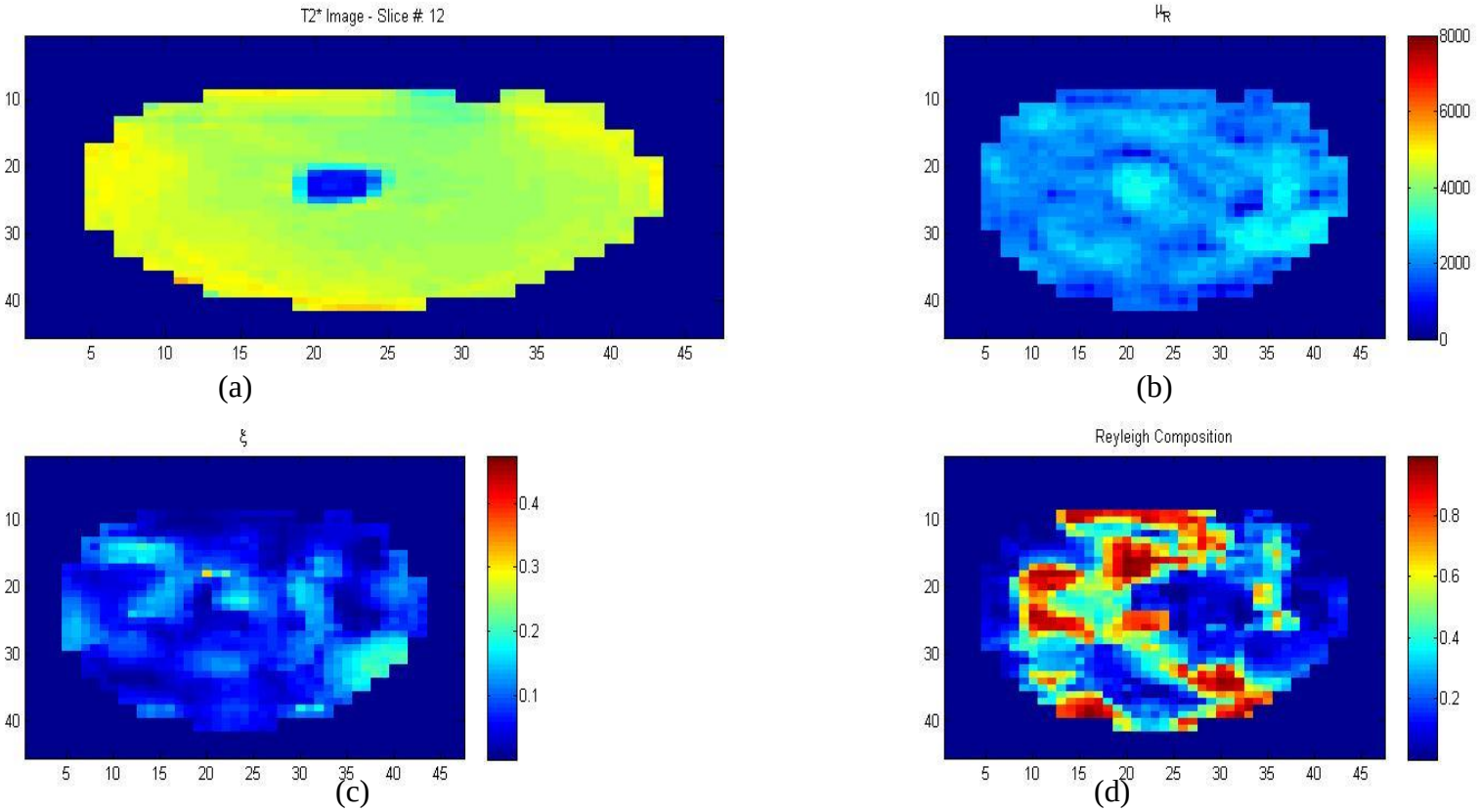

Figure 7.7: Reconstruction of Case 2 for slice 12 (a) MR image, (b) Shear modulus reconstruction, (c) Damping ratio reconstruction and (d) Rayleigh composition

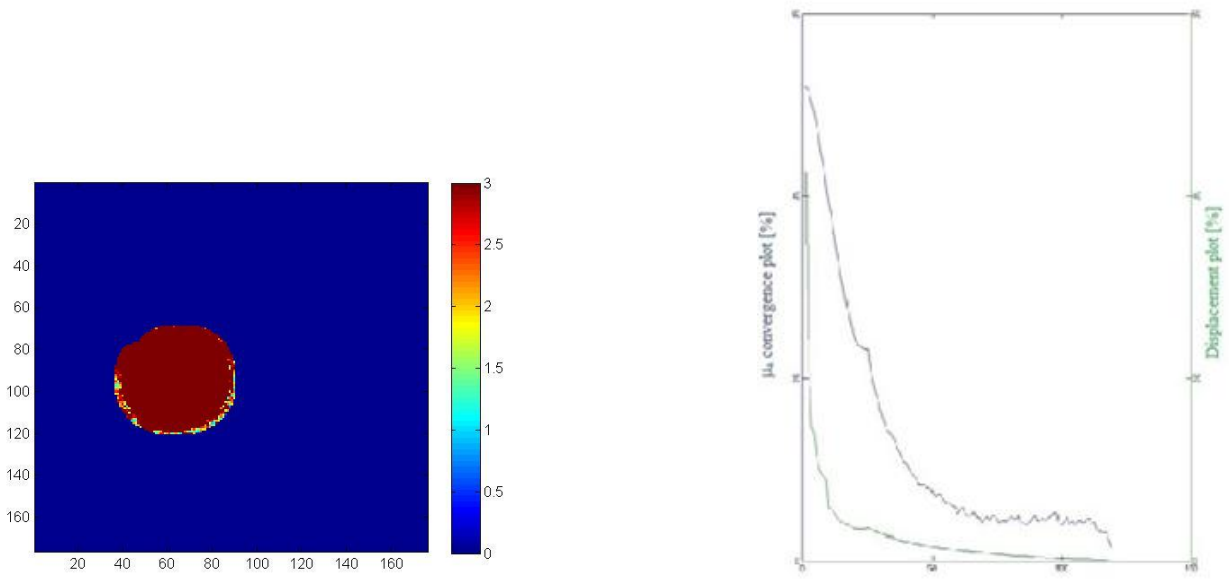

(a) (b)

Figure 7.8 (a) Strain SNR image of Case 2 (slice 12) (b) Convergence plot of Case 2

7.4 Case 3

In Case 3, a 12 mm tumor was embedded on one side of a silicone phantom. The tumor was located 40 mm from the back surface (Perspex plate) and was approximately twice as stiff as the surrounding silicone phantom. The mechanical properties used as initial guess for reconstruction of are the same as Table 7.1.

Figure 7.9 displays the grey scale MR image of the Case 3. A suspicious region can be seen on the slices of the last two rows of the matrix of images. The stiffness of that specific area is higher compared to the background, as seen in Figure 7.10(b). The signal inside the phantom is strong, as seen in Figure 7.11(a), and the solution has also converged as shown in Figure 7.11(b). These

results ensure that the stiff region in Figure 7.10 is an inclusion. Damping ratio reconstruction in Figure 7.10(c) is unclear which is probably due to blending effects. However the Rayleigh composition in Figure 7.10(d) shows the defined boundary around the tumor. Table 7.4 lists the final reconstruction results.

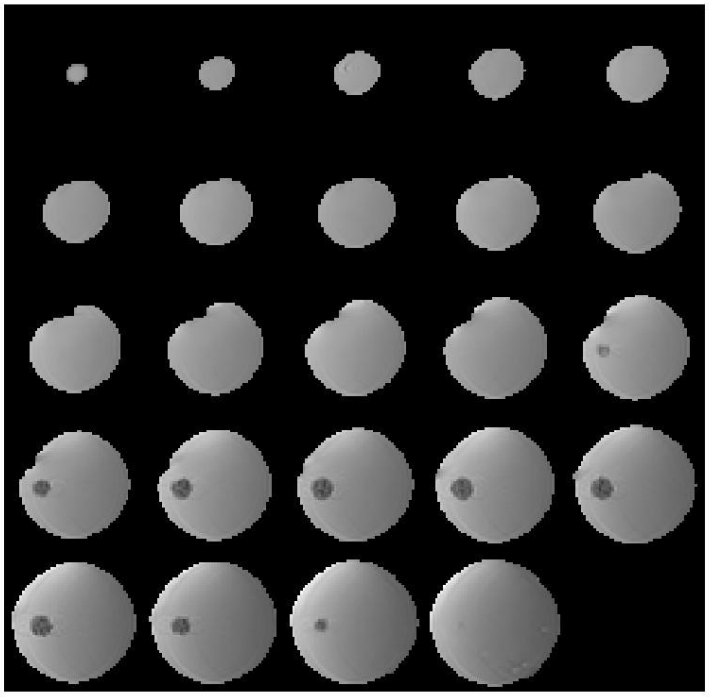

Figure 7.9: MR grayscale image of Case 3

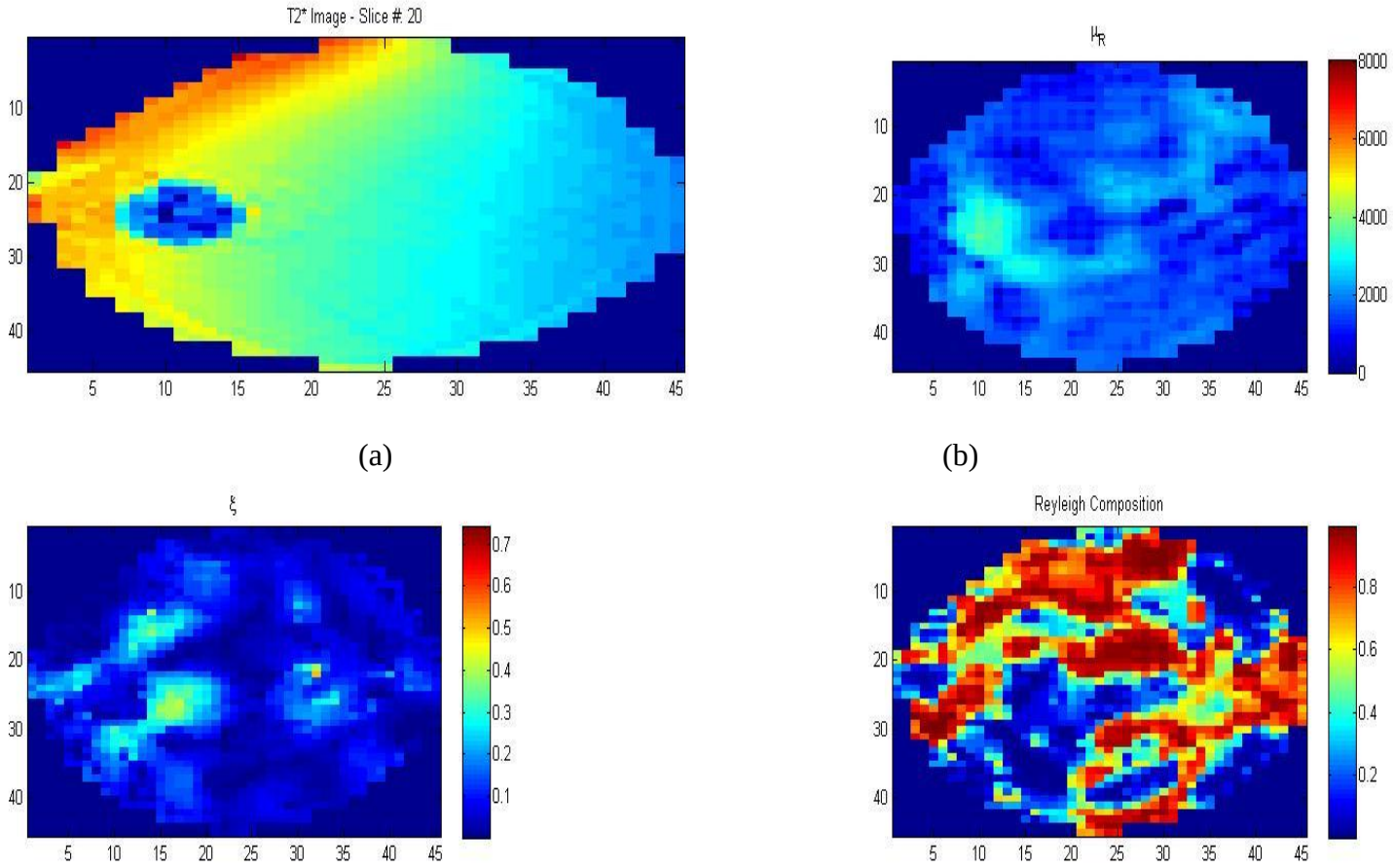

Figure 7.10: Reconstruction of Case 3 (slice 20) (a) MR image (b) Real shear modulus, (c) damping ratio (d) Rayleigh composition of Phantom blue (slice 20)

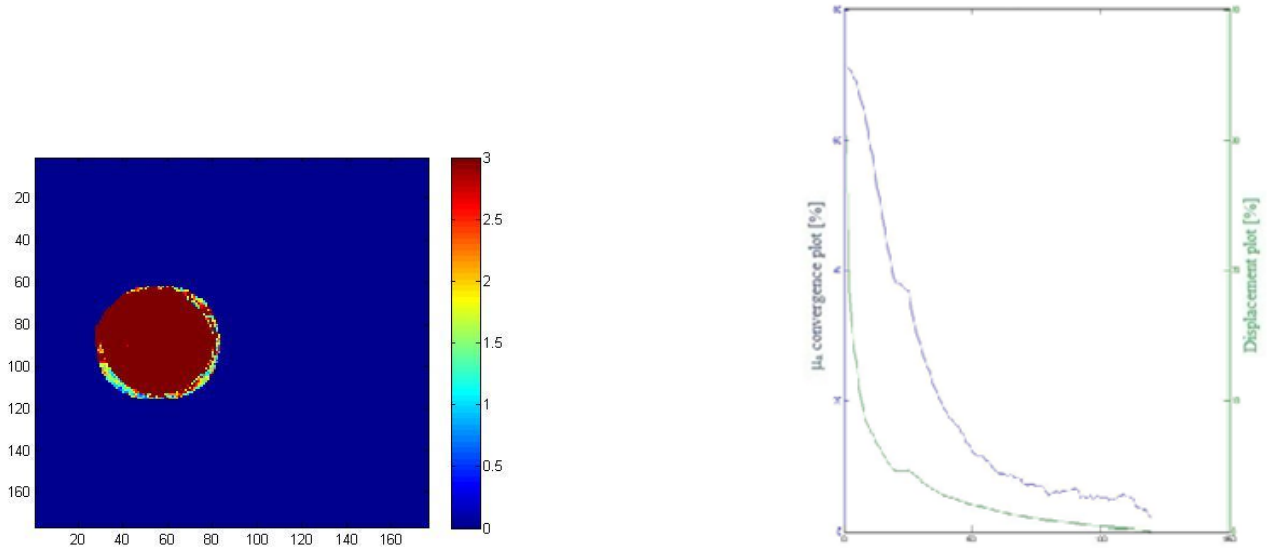

(a) (b)

Figure 7.11: (a) Strain SNR image of Case 3 (slice 20) (b) Convergence plot of Case 3

Table 7.4: Mechanical Properties of Case 3 after reconstruction

	Shear modulus (*pa*)	Damping ratio	Rayleigh Composition
Mean	1767.66	0.1	0.4
Standard deviation	407.3	0.08	0.294

7.5 Case 4

Case 4 was a homogenous silicone phantom. Figure7.12 shows the grey scale MR image of the phantom. This is a homogeneous phantom so the shear modulus should be uniform everywhere.

However, the shear modulus diagram in Figure 7.13(b) shows an artifact. This artifact can be associated with poor SNR values at the boundary as seen in Figure 7.14(a). For similar reasons, some blending effects can be noticed in the damping ratio reconstruction in Figure 7.13(c). However, the Rayleigh composition in Figure 7.13(d) shows a trend of definitive boundary around the regions, which appears stiff in the shear modulus diagram. Table 7.5 lists the final mechanical values after reconstruction and Figure 7.13(b) shows the convergence of displacement and shear modulus for Case 4.

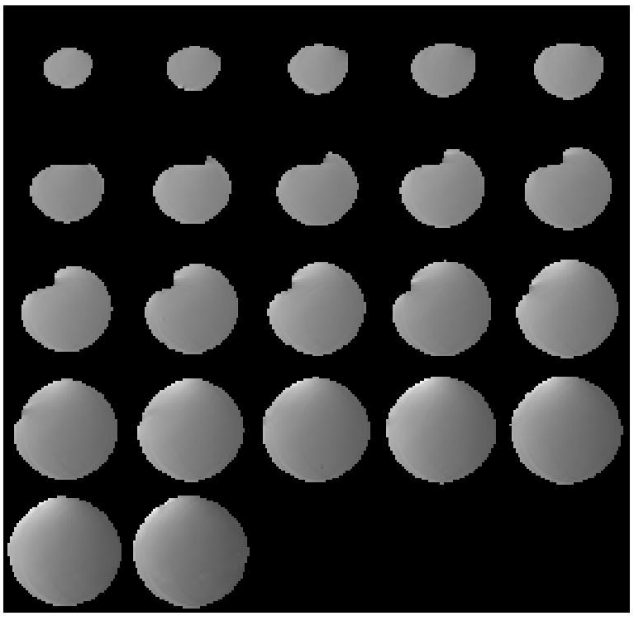

Figure 7.12: MR grey scale image of Case 4

Table 7.5: Mechanical Properties of Case 4 after reconstruction

	Shear modulus (*pa*)	Damping ratio	Rayleigh Composition
Mean	1745	0.11	0.36
Standard deviation	393.5	0.07	0.27

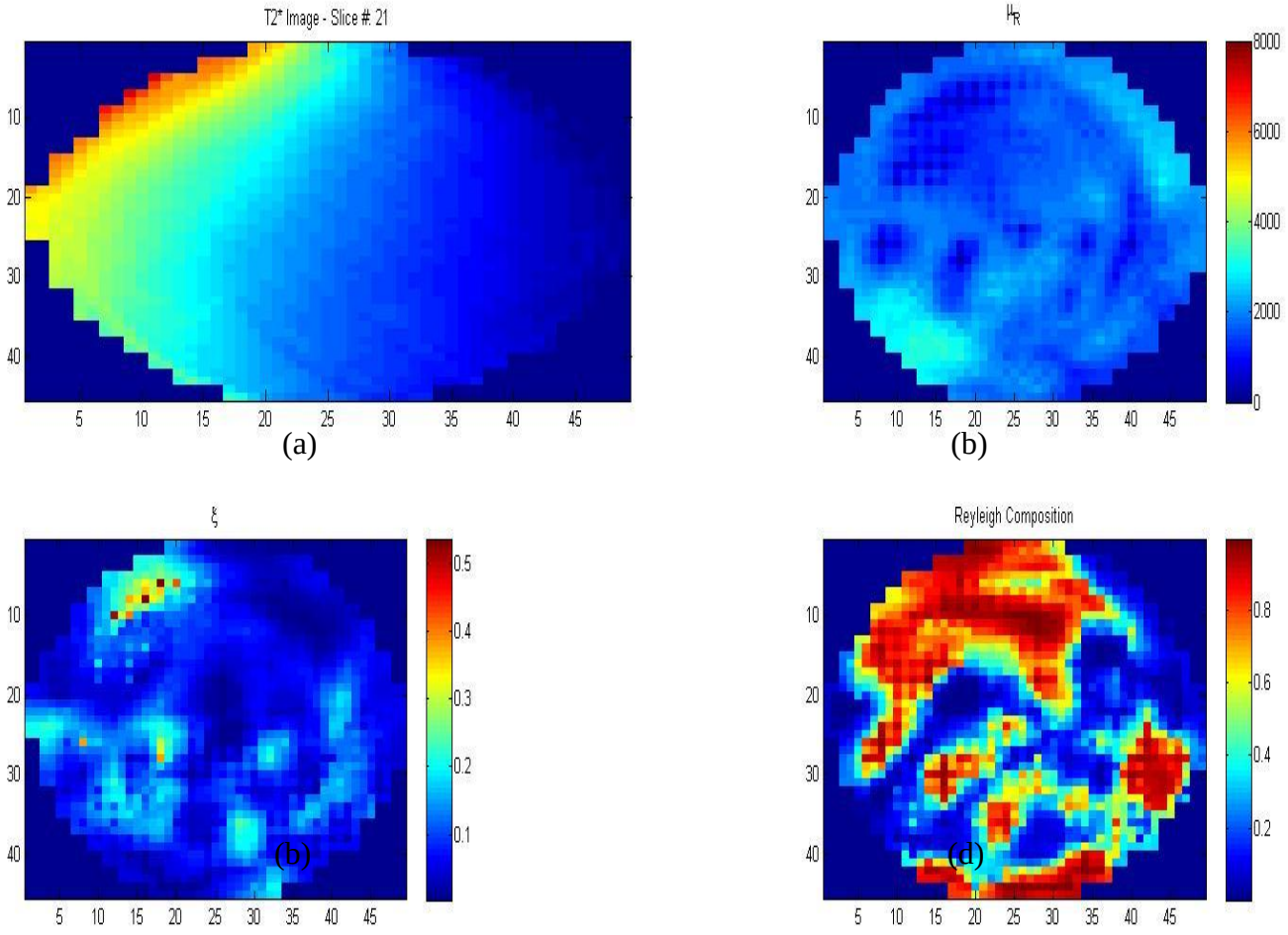

Figure 7.13 Reconstruction of Case 4 (slice 21) (a) MR image (b) Real shear modulus, (c) damping ratio (d) Rayleigh composition of Phantom blue (slice 20)

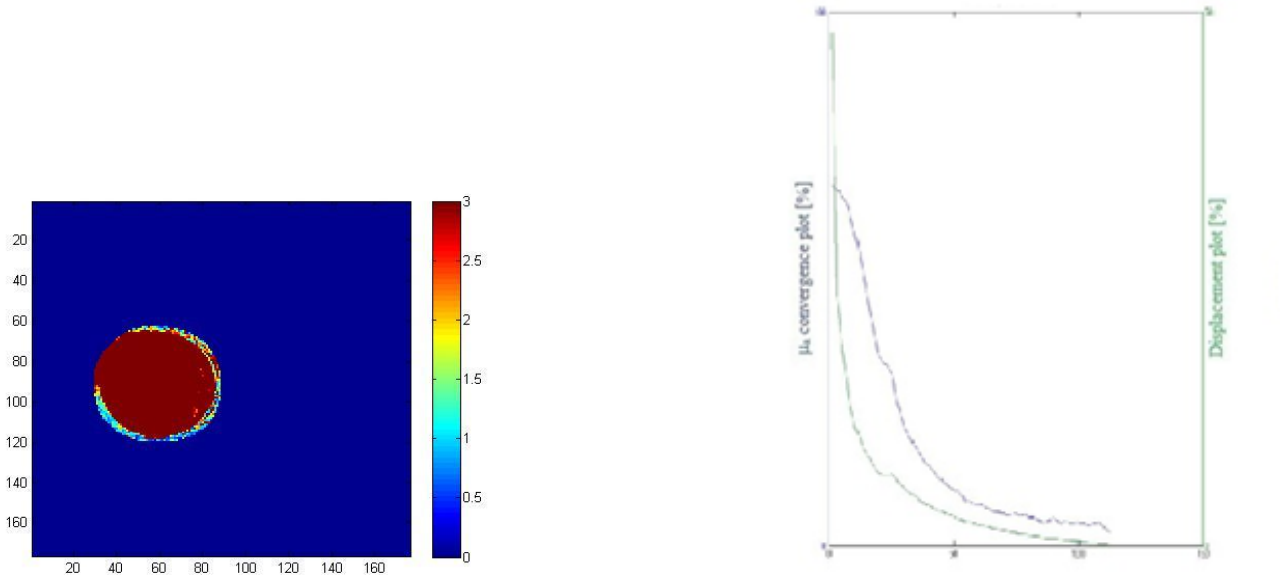

(a) (b)

Figure 7.14: Strain SNR image of Case 4 (slice 21) (a) Convergence plot of Case 4

7.6 Displacement pattern in simulated phantom

First the applied displacement produces a transverse wave in all there directions inside the simulated phantom, as seen for one example in Figure 7.15. These values are then used as data, in the reconstruction process to test the method. The initial guess used for reconstruction is given in Table 7.6.

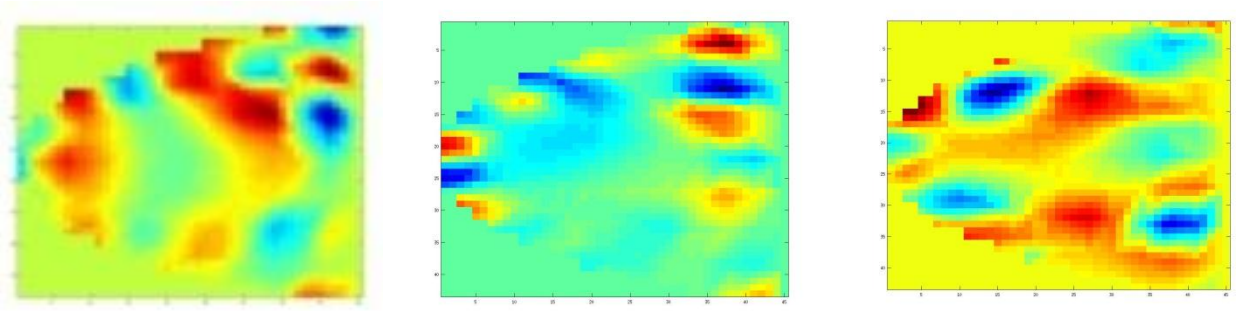

(a) Motion in X direction (b) Motion in Y direction (c) Motion in Z direction

Figure 7.15: Motion produced inside the simulated breast phantom due to the applied displacement on the surface

Table 7.6: Initial guess for mechanical properties for simulated phantom

	μR (Real shear modulus)	**μI(Imaginary shear modulus)**	**ρR (Real density)**	**ρI (Imaginary density)**	**ζ (Damping ratio)**
Background	3 Kpa	0.05 Kpa	1000 kg/m3	-150	0.166

7.7 Simulation Results

Figure 7.15 shows the shear modulus diagram of all the slices of the simulated phantom of Case 1, as shown in Chapter 5. The background stiffness is approximately 4100 Pa, whereas the red region in the middle shows a very high stiffness value of approximately 6000 Pa. The location of this red region corresponds to the location of simulated tumor in Figure 5.9(a) and Case 1. Figure 7.16 also shows a higher damping value in the corresponding region. The significantly higher stiffness and damping shows that if the actuator excites the phantom at 50 μm on one side, than the tumor location can be identified

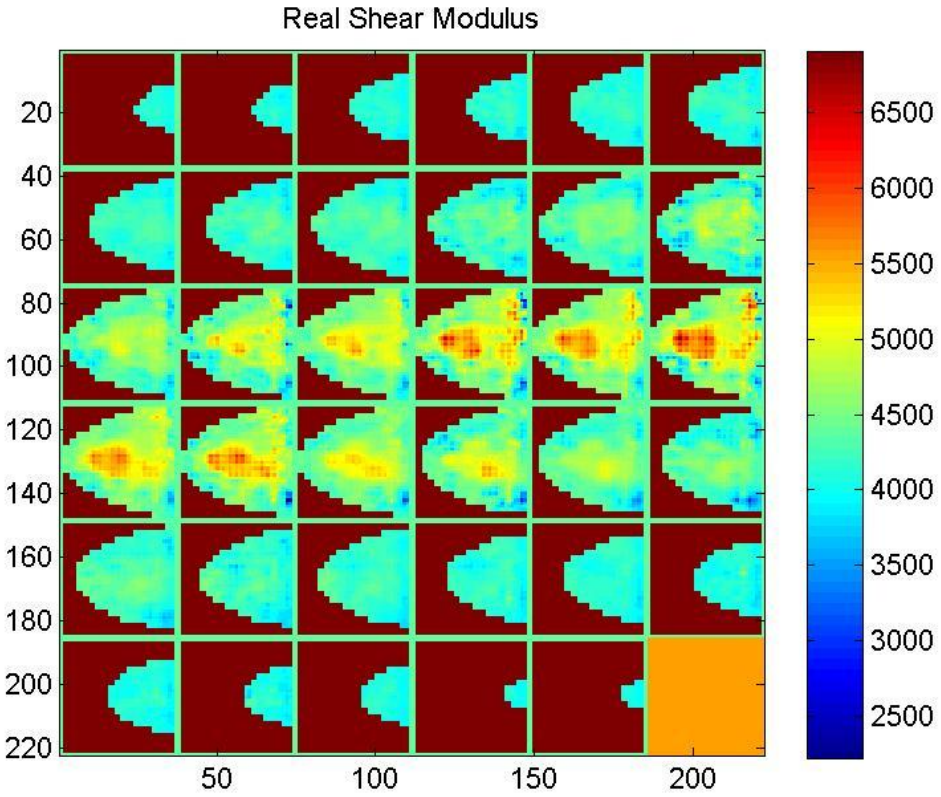

Figure 7.16: Shear modulus reconstruction of the simulated phantom of Case 2

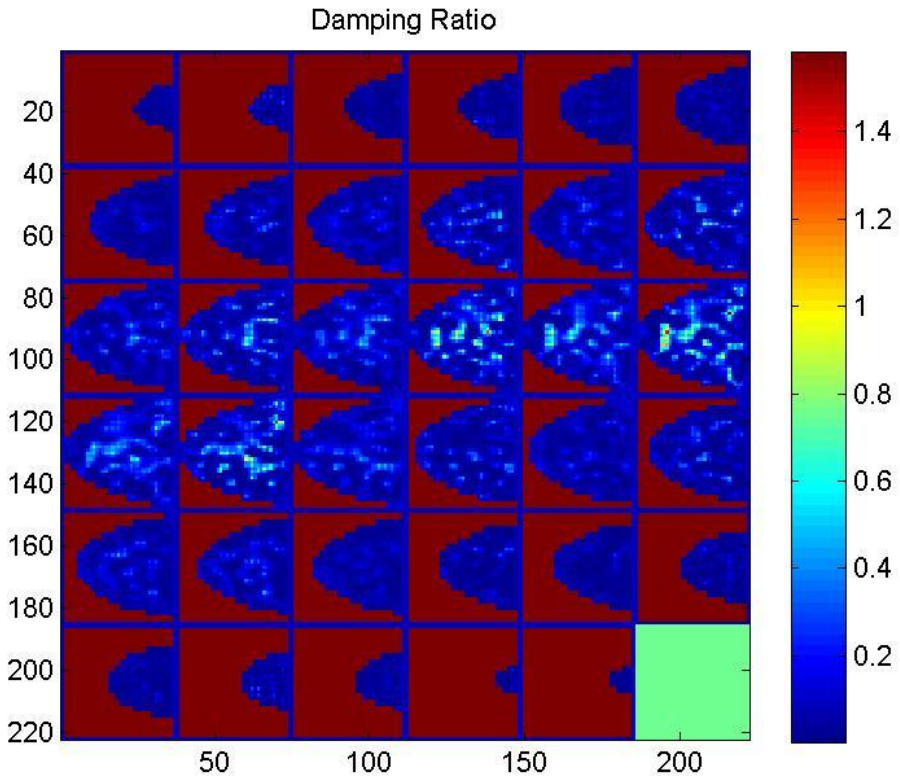

Figure 7.17: Damping ratio reconstruction of the simulated phantom of Case 2

7.8 Summary

The reconstruction results show that the inclusions have been identified correctly in all three cases. This proves that the proposed acoustic actuator generated sufficient motion which is required for successful MRE reconstruction.

Chapter 8

Conclusion

Although the MRE acquisition and reconstruction methods are a long term work in progress, it is evident from the results presented that the main objective posed for the work involved in this thesis can be achieved.

The acoustic actuation system has proven useful in producing measurable harmonic excitation in silicone phantoms mimicking the human breast. This actuation was accomplished by coupling the motion of a plastic membrane to a cup in contact with the phantom and driven by an acoustic subwoofer. MRE acquisitions made during steady-state operation of this actuator allowed meaningful shear modulus maps to be obtained using a 3D phase contrast pulse sequence and an iterative finite element based reconstruction algorithm.

The Piezo actuation system also shows good potential for future use in MR testing of phantom and patient. It is capable of producing measurable harmonic excitation in silicone phantoms. This actuation was accomplished by magnifying the motion of a linear Piezo electric actuator using a long lever arm. The assembly is simple and can fit into the MR coil.

Overall, MRE has emerged as a useful technique in characterizing mechanical properties of tissue both *ex vivo* and *in vivo.* Over the past twenty years, some results have shown good agreement with values found in the literature. However, while others have shown variations from these values as large as several orders of magnitude. While variations in procedure and

environmental conditions related to the mechanical testing of biological tissues may account for part of the discrepancy, it should be clear that the reconstruction techniques have not yet been optimized.

Furthermore, the reconstructive nature of these methods renders them sensitive to the accuracy with which they can account for the behavior observed in the imaged data. More specifically, that is, the final elastographic image produced by such indirect imaging algorithms can only be as good as the fundamental assumptions that underlie the model used and the reconstruction approach.

In short, promising results in MRE's ability to demarcate and yield quantitative measures of elasticity, with specific regard to its clinical potential to detect and differentiate regions of stiffness associated with breast cancers indicates its great potential as a diagnostic tool. Thus, it is clear that imaging techniques, such as MRE, demonstrate the continued growth and development of the synergistic relationship between engineering and medicine.

Chapter 9

Future work

8. 1 Acoustic Actuator

With the current acoustic actuator, satisfactory results have been obtained for silicone phantoms. However, the actuator cup that touches the phantom is heavy and can affect results. It is recommended that in future designs the cup should be made lighter so that it can produce higher displacement.

In particular, a curved surface in front of the cup is fixed. That surface is not suitable for making contact with human breasts, which are diverse versatile in size and shape. In future, the curved surface should be made adjustable. This goal can be achieved by allowing the curved surface to rotate vertically and horizontally until it touches the breast and then lock it in that position. Equally a deformable cup might be used.

Tissue displacement can be increased by using two sets of actuators. For example, two cups shaking a breast from two sides with a phase difference. Such an approach might provide the inverse problem a better data.

For the current acoustic actuator, perspex membrane has been used. Alternative membranes should be investigated to improve the performance of the actuator. For long term stability and reliability it will be necessary to also consider the fatigue characteristics of the diaphragm material.

8.2 Piezo Actuator

For MR test, the whole Piezo actuator setup needs to be made of non-magnetic material. It needs to have a mechanism for clamping it down to the MR breast coil. It is also desirable to have more adjustability in the actuator as described for the acoustic actuator in section 8.1.

P-842 · P-843 · P-844 · P-845

Preloaded Piezo Actuators (LVPZT) with Sensor Option

P-844 piezo actuators (battery for size comparison)

- **Travel Range to 90 µm**
- **Pushing Forces to 3000 N**
- **Preloaded for Pulling Forces to 700 N**
- **Sub-ms Response**
- **Sub-nm Resolution**
- **Options: Vacuum Versions, Water-Resistant Case**

P-842, P-843, P-844 and P-845 series piezo translators are high-resolution linear actuators for static and dynamic applications. They provide sub-millisecond response and sub-nanometer resolution.

Design

These actuators consist of a friction-free, preloaded, monolithic multilayer piezoceramic stack protected by a stainless steel case.

The high preload gives these actuators outstanding properties for dynamic applications (e.g. precision machining, active damping, etc.) and push-pull applications.

Mounting

Mounting is at the foot, although with push/pull forces of less than 100 N, the actuator can be held by clamping the case. The P-176.50 / P-176.60 flexible tips can be installed to decouple the ceramic from bending forces (see page 1-45). For more mounting guidelines, see page 1-48.

High Accuracy in Closed-Loop Operation

The P-842 and P-844 are designed for open-loop positioning tasks. The P-843 and P-845 versions are equipped with integrated high-resolution SGS position sensors and offer high-accuracy, closed-loop operation (for more information, see the "Tutorial: Piezoelectrics in Positioning," Section 4).

Options:

P-703.20

High-vacuum option, p. 1-44.

Application Examples

- Static and dynamic precision positioning
- Disk drive testing equipment
- Optics
- Metrology / interferometry
- Active structures (Adaptronics)
- Precision engineering / micromechanisms
- Adaptive mechanics
- Active vibration control
- Switching applications
- Laser tuning

For more examples, see page 1-5

Technical Data and Product Order Numbers

Order number	Travel range (open-loop) for 0 to 100 V [µm] ±20%	Travel range (closed-loop) [µm]	Integrated position sensor*	Resolution closed-loop / open-loop [nm]**	Static large-signal stiffness [N/µm] ±20%***
P-842.10	15	-	-	- / 0.15	57
P-842.20	30	-	-	- / 0.3	27
P-842.30	45	-	-	- / 0.45	19
P-842.40	60	-	-	- / 0.6	15
P-842.60	90	-	-	- / 0.9	10
P-843.10	15	15	SGS	0.3 / 0.15	57
P-843.20	30	30	SGS	0.6 / 0.3	27
P-843.30	45	45	SGS	0.9 / 0.45	19
P-843.40	60	60	SGS	1.2 / 0.6	15
P-843.60	90	90	SGS	1.8 / 0.9	10
P-844.10	15	-	-	- / 0.15	225
P-844.20	30	-	-	- / 0.3	107
P-844.30	45	-	-	- / 0.45	75
P-844.40	60	-	-	- / 0.6	57
P-844.60	90	-	-	- / 0.9	38
P-845.10	15	15	SGS	0.3 / 0.15	225
P-845.20	30	30	SGS	0.6 / 0.3	107
P-845.30	45	45	SGS	0.9 / 0.45	75
P-845.40	60	60	SGS	1.2 / 0.6	57
P-845.60	90	90	SGS	1.8 / 0.9	38
Notes see page 1-46	A2	A5	B	C1	D1

Accessories

P-176.50

Flexible tip for P-842 / P-843, see p. 1-45

P-176.60

Flexible tip for P-844 / P-845, see p. 1-45
Extension cables with connectors: see pp. 6-55 *ff.*

Note

High-resolution amplifiers and servo-control electronics, both digital and analog, are described in the "Piezo Drivers & Nanopositioning Controllers" section, page 6-8 *ff.*

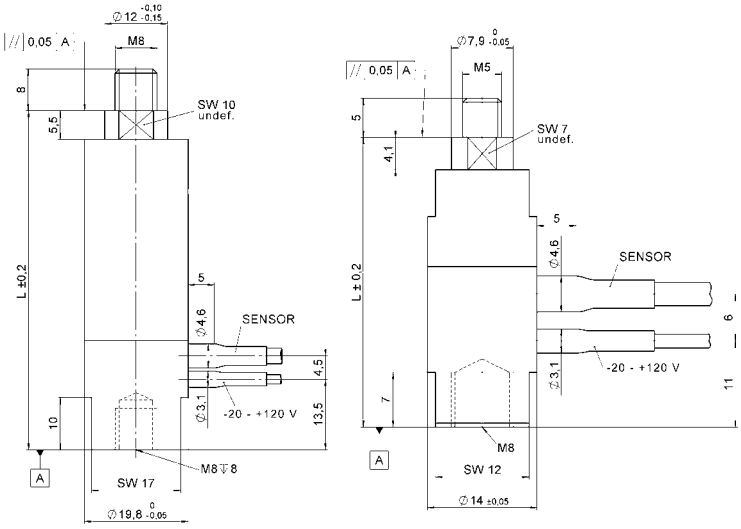

P-844, P-845 dimensions in mm; length = L, see table for value; max. torque at tip: 1 Nm.

P-842, P-843 dimensions in mm; length = L, see table for value; max. torque at tip: 0.35 Nm.

Push/pull force capacity [N]	Electrical capacitance [µF] ±20%	Dynamic operating current coefficient [µA / (Hz x µm)]	Resonant frequency (unloaded) [kHz] ±20%	Weight without cable [g] ±5%	Length L [mm]	Recommended amplifier/controller (codes explained p. 1-3)
800 / 300	1.5	12.5	18	31	37	C, G
800 / 300	3.0	12.5	14	42	55	C, G
800 / 300	4.5	12.5	10	53	73	C, G
800 / 300	6.0	12.5	8.5	64	91	C, G
800 / 300	9.0	12.5	6	86	127	C, G
800 / 300	1.5	12.5	18	31	37	D, H
800 / 300	3.0	12.5	14	42	55	D, H
800 / 300	4.5	12.5	10	53	73	D, H
800 / 300	6.0	12.5	8.5	64	91	D, H
800 / 300	9.0	12.5	6	86	127	D, H
3000 / 700	6.0	50	16	84	47	C, G
3000 / 700	12.0	50	12	108	65	C, G
3000 / 700	18.0	50	9	132	83	C, G
3000 / 700	24.0	50	7.5	156	101	C, G
3000 / 700	36.0	50	5.5	204	137	C, G
3000 / 700	6.0	50	16	84	47	D, H
3000 / 700	12.0	50	12	108	65	D, H
3000 / 700	18.0	50	9	132	83	D, H
3000 / 700	24.0	50	7.5	156	101	D, H
3000 / 700	36.0	50	5.5	204	137	D, H
D3	F1	F2	G2	K		

Voltage connection: LEMO FFA.00.250; 1 m coaxial cable, RG 178, teflon insulation.
Sensor connection: LEMO FFA.0S.304; 1 m coaxial cable with PUR insulation.
Temperature range: -40 to 80 °C.
Case / end pieces: non-magnetic steel

* SGS versions can attain closed-loop linearity up to 0.15% and are shipped with performance reports.
** The resolution of piezo actuators is not limited by stiction or friction. Value given is noise equivalent motion with E-503 amplifier.
*** Dynamic smallsignal stiffness is ~30% higher.

Products

Tips

Services

Maxillofacial

Special Effects

R & D

Training Courses

Consulting

Online Ordering

PRODUCT INFORMATION
A-341
Soft Gel

PRODUCT DESCRIPTION:

A-341 is a unique two component **platinum** RTV silicone gel, and has a wide variety of uses, from prosthetics, special effects and GFA's (gel filled appliances) to various manufacturing applications. This gel will develop much of the same dimensional stability and non flowing characteristics of a solid silicone elastomer.

- **Translucent**
- **Low Viscosity**
- **RTV** very fast setting at room temperature
- **Simple** 10:1 by weight ratio

- **Viscosity** @77°F (room temp) 8 to 12,000cps
- **Pot life** @ 77°F (room temp) 30 minutes

A-341 can be heat accelerated and will cure in 20 minutes @150°F.

MIXING

A-341 should be mixed at 100gms base A to 10gms catalyst B by weight. Thoroughly mix in a clean polypropylene container or equivalent. Care should be taken to minimize air entrapment during mixing. **Vacuum deairation** at 28 inches Hg is recommended. Apply vacuum to a container at least four times the volume of the material to avoid overflow of the bubbles. Allow the material to reach its maximum capacity, and fall to the bottom of the container. Continue to hold the vacuum for 3-5 minutes. This will eliminate the smaller bubbles. When packing the material into a mold, car should be taken to minimize trapping air bubbles.

SUBSTRATE CONSIDERATIONS:

A-341 will cure in contact with most materials. Exceptions include butyl and chlorinated rubbers, some RTV silicones and unreacted residues of some curing agents. Cure inhibition can usually be prevented by washing all containers with solvent, followed by a thorough rinsing with isopropyl alcohol

WARNINGS ABOUT PRODUCT SAFETY:

Factor II technology believes that the information and data contained herein is accurate and reliable; however, it is the user's responsibility to determine suitability and safety of use for these materials.
Factor II cannot know the specific requirements of each application and hereby makes the user aware that it has not tested or determined that these materials are suitable or safe for any application. It is the user's responsibility to adequately test and determine the safety and suitability for their application. Factor II makes no warranty concerning fitness for any use or purpose. There has been no testing done by Factor II to establish safety of use in any medical application. Factor II has tested this material only to determine if the product meets the applicable specification.

(Please contact Factor II for assistance and recommendations when establishing specifications.) When considering the use of a Factor II product in a particular application, you should review the latest Material Safety Data Sheets and contact Factor II for any questions about product safety information you may have.

WARRANTY INFORMATION:

Factor II's warranty period is 6 months from date of shipment when stored below 40°C in original unopened container.

PATENT WARNING:

Factor II Technology disclaims any expressed or implied warranty against the infringement of any patent. Factor II does not warrant that the use or sale of the products described herein will not infringe the claims of any U.S. patents or other country's patents covering the product itself or the use in combination with other products or in the operation of any process.

Revised 11/02

Factor II, Incorporated

P.O. Box 1339
Lakeside, AZ 85929

Phone:(928) 537-8387
Fax: (928) 537-0893

MATERIAL SAFETY DATA SHEET
A-341 Part A
Soft Gel

In Case of Emergency Contact Factor II, Inc. 928-537-8387

Factor II Technology urges each customer or recipient of this MSDS to study it carefully to become aware of and understand the hazards associated with the product. The reader should consider consulting reference works or individuals who are experts in ventilation, toxicology, and fire prevention, as necessary or appropriate to the use and understanding of the data contained in this MSDS.

To promote safe handling each customer or recipient should: (1) notify and furnish its employees, agents, contractors, customers, and others whom it knows or believes will use this material of the information regarding hazards or safety; (2) request its customers to notify their employees, customers and other users of the product of this information.

1. CHEMICAL PRODUCT

PRODUCT NAME: RTV Heat Cure Silicone
CHEMICAL NAME: Organopolysiloxane Mixture

2. PRODUCT COMPOSITION

MATERIAL	CAS#	
POLYMER-ORGANOPOLYSILOXANE	68083192	<60
MIXTURE	13983170/131	<20
MINERAL FILLERS	4234	<20
SILICA FILLER	67762907	

3. HAZARDS and PROTECTION IDENTIFICATION

Personal Protection Recommended: Use local exhaust. Ventilation is required. Use a NIOSH approved respirator to prevent overexposure. Reference 29CFR 1910.134 for Federal standards concerning respiratory protection. Wear impervious gloves and protective clothing as required to prevent skin contact. Wear protective goggles to prevent eye contact. An eyewash and safety shower should be nearby and ready for use.

4. FIRST AID MEASURES

EMERGENCY AND FIRST AID PROCEDURES:

SWALLOWING:

Induce Vomiting

SKIN:

Wash with soap and water.

INHALATION:

Remove to fresh air..

EYES:

Immediately flush eyes with water and continue washing for at least 15 minutes. If irritation persists seek medical attention.

NOTES TO PHYSICIAN:

There is no specific antidote. Treatment of overexposure should be directed at the control of symptoms and the clinical condition of the patient.

P.O. Box 1339
Lakeside, AZ 85929

Phone:(928) 537-8387
Fax: (928) 537-0893

5. FIRE FIGHTING MEASURES

FLASH POINT: (TCC) N/A

FLAMMABLE LIMITS IN AIR (by volume): Not Applicable N/A

EXTINGUISHING MEDIA: Dry Chemical ,Foam or Carbon Dioxide

SPECIAL FIREFIGHTING PROCEDURES: None known.

UNUSUAL FIRE AND EXPLOXION HAZARDS: None Known

6. ACCIDENTAL RELEASE MEASURES

STEPS TO BE TAKEN IF MATERIAL IS RELEASED OR SPILLED:
Contain the spill or leak, scrape up with cardboard or a ra and place in a container.
WASTE DISPOSAL METHOD: Dispose of in accordance with all Federal, State, and local regulations.

7. HANDLING AND STORAGE

PRECAUTIONS TO BE TAKEN IN HANDLING AND STORAGE:
Keep container tightly closed. Store in cool place and keep away from Heat or Flame.
Don't lay container on its side.

8. PHYSICAL AND CHEMICAL PROPERTIES (based on typical material)

APPEARANCE & ODOR: Clear odorless paste
BOILING POINT: 500°F
VAPOR PRESSURE at 77°Fmm Hg
VAPOR DENSITY (air=1) N/A
SOLUBILITY IN WATER (By wt): Insoluble
SPECIFIC GRAVITY (water=1) 1.23

Note: The above information is not intended for use in preparing product specifications.

9. STABILITY AND REACTIVITY DATA

STABILITY: Stable. Hazardous polymerization will not occur.
INCOMPATIBILITY: None known
HAZARDOUS COMBUSTION OR DECOMPOSITION PRODUCTS: Carbon Monoxide, Carbon Dioxide, Silicon Dioxide

10. TOXICOLOGICAL INFORMATION

Not available

11. ECOLOGICAL INFORMATION

ECOTOXICOLOGICAL INFORMATION: Keep out of sewage system.

12. DISPOSAL CONSIDERATIONS

Use proper landfill disposal or incineration.

Dispose of in accordance with all Federal, State, and local regulations.

C H I P REGULATIONS

Chemicals (Hazards Information and Packaging) Regulations 1993 requires physico-chemical and health hazard determination of all substances and preparations manufactured, transported, stored, modified, or consumed within the EEC. Components present in this product at a level which could require reporting under the statute are:

****NONE ****

FEDERAL EPA

Comprehensive Environniental Response Compensation and Liability Act of 1980 (CERCLA) requires notification of the National Response Center of release of quantities of Hazardous Substances equal to or greater than the reportable quantities (RQ's) in 40 CFR 302.4. Components present in this product at a level which could require reporting under the statute are: ****NONE ****

Superfund Amendments and Reauthorization Act of 1986 (SARA) Title III requires emergency planning based on Threshold Planning Quantities (TPQ's) and release reporting based on Reportable Quantities (RQ's) in 40 CFR 355 (used for SARA 302, 304, 3 1, and 312). Components present in this product at a level which could require reporting under the statute are: **** NONE ****

Superfund Amendments and Reauthorization Act of 1986 (SARA) Title III requires submission of annual reports of release of toxic chemicals that appear in 40 CFR 372 (for SARA 3 ~ 3). This information must be included in all MSD S's that are copied and distributed for this material. Components present in this product at a level which could require reporting under this statute are: *** NONE****

INVENTORY STATUS
The ingredients of this product are listed on, or are exempt from listing on, the TSCA inventory.

13. OTHER INFORMATION

HMIS FORMAT:

Health: 0 Flammability: 0 Reactivity: 0

We believe that the information contained herein is current as of the date of this Material Safety Data Sheet, and is offered in good faith. Since the use of this information and of these opinions and the conditions of the use of the product are not within the control of Factor II Technology, it is the user's obligation to determine the conditions of safe use of the product.
Factor II Technology Regulatory Compliance Department

Factor II, Incorporated

P.O. Box 1339
Lakeside, AZ 85929

Phone:(928) 537-8387
Fax: (928) 537-0893

MATERIAL SAFETY DATA SHEET
A-341 Part B
Soft Gel

Factor II Technology urges each customer or recipient of this MSDS to study it carefully to become aware of and understand the hazards associated with the product. The reader should consider consulting reference works or individuals who are experts in ventilation, toxicology, and fire prevention, as necessary or appropriate to the use and understanding of the data contained in this MSDS.

To promote safe handling each customer or recipient should: (1) notify and furnish its employees, agents, contractors, customers, and others whom it knows or believes will use this material of the information regarding hazards or safety; (2) request its customers to notify their employees, customers and other users of the product of this information.

1. CHEMICAL PRODUCT

PRODUCT NAME: Catalyst for RTV Heat Cure Silicone
CHEMICAL NAME: Organopolysiloxane Mixture

2. PRODUCT COMPOSITION

MATERIAL	CAS#	
PROPRITARY-ORGANOPOLYSILOXANE	63148607/471	>90
MIXTURE	341	<10
METHYL HYDROGEN SILOXANE	68037592	

3. HAZARDS and PROTECTION IDENTIFICATION

Personal Protection Recommended: Use local exhaust. Ventilation is required. Use a NIOSH approved respirator to prevent overexposure. Reference 29CFR 1910.134 for Federal standards concerning respiratory protection. Wear impervious gloves and protective clothing as required to prevent skin contact. Wear protective goggles to prevent eye contact. An eyewash and safety shower should be nearby and ready for use.

4. FIRST AID MEASURES

EMERGENCY AND FIRST AID PROCEDURES:

SKIN:

Wash with soap and water.

INHALATION:

Remove to fresh air.

EYES:

Immediately flush eyes with water and continue washing for at least 15 minutes. If irritation persists seek medical attention.

NOTES TO PHYSICIAN:

There is no specific antidote. Treatment of overexposure should be directed at the control of symptoms and the clinical condition of the patient.

P.O. Box 1339
Lakeside, AZ 85929

Phone:(928) 537-8387
Fax: (928) 537-0893

5. FIRE FIGHTING MEASURES

FLASH POINT: (TCC) N/A

FLAMMABLE LIMITS IN AIR (by volume): Not Applicable N/A

EXTINGUISHING MEDIA: Dry Chemical ,Foam or Carbon Dioxide

SPECIAL FIREFIGHTING PROCEDURES: None known.

UNUSUAL FIRE AND EXPLOXION HAZARDS: None Known

6. ACCIDENTAL RELEASE MEASURES

STEPS TO BE TAKEN IF MATERIAL IS RELEASED OR SPILLED:
Contain the spill or leak, scrape up with cardboard or a ra and place in a container.
WASTE DISPOSAL METHOD: Dispose of in accordance with all Federal, State, and local regulations.

7. HANDLING AND STORAGE

PRECAUTIONS TO BE TAKEN IN HANDLING AND STORAGE:
Keep container tightly closed. Store in cool place and keep away from Heat or Flame.

8. PHYSICAL AND CHEMICAL PROPERTIES (based on typical material)

APPEARANCE & ODOR: Slight solvent odor
BOILING POINT: 500°F
VAPOR PRESSURE at 77°Fmm Hg
VAPOR DENSITY (air=1) N/A
SOLUBILITY IN WATER (By wt): Insoluble
SPECIFIC GRAVITY (water=1) 1.00

Note: The above information is not intended for use in preparing product specifications.

9. STABILITY AND REACTIVITY DATA

STABILITY: Stable. Hazardous polymerization will not occur.
INCOMPATIBILITY: None known
HAZARDOUS COMBUSTION OR DECOMPOSITION PRODUCTS: Carbon Monoxide, Carbon Dioxide, Silicon Dioxide, hYDROGEN
INCOMPATIBILITY: avoid contact with acidic bases and oxidizing agents
CONDITIONS TO AVOID: product generates flammable gas on contact with acidic, basic and oxidizing material.

10. TOXICOLOGICAL INFORMATION

Not available

11. ECOLOGICAL INFORMATION

ECOTOXICOLOGICAL INFORMATION: Keep out of sewage system.

12. DISPOSAL CONSIDERATIONS

Use proper landfill disposal or incineration.
Dispose of in accordance with all Federal, State, and local regulations.

C H I P REGULATIONS

Chemicals (Hazards Information and Packaging) Regulations 1993 requires physico-chemical and health hazard determination of all substances and preparations manufactured, transported, stored, modified, or consumed within the EEC. Components present in this product at a level which could require reporting under the statute are:

****NONE ****

FEDERAL EPA

Comprehensive Environniental Response Compensation and Liability Act of 1980 (CERCLA) requires notification of the National Response Center of release of quantities of Hazardous Substances equal to or greater than the reportable quantities (RQ's) in 40 CFR 302.4. Components present in this product at a level which could require reporting under the statute are: ****NONE ****

Superfund Amendments and Reauthorization Act of 1986 (SARA) Title III requires emergency planning based on Threshold Planning Quantities (TPQ's) and release reporting based on Reportable Quantities (RQ's) in 40 CFR 355 (used for SARA 302, 304, 3 1, and 312). Components present in this product at a level which could require reporting under the statute are: **** NONE ****

Superfund Amendments and Reauthorization Act of 1986 (SARA) Title III requires submission of annual reports of release of toxic chemicals that appear in 40 CFR 372 (for SARA 3 ~ 3). This information must be included in all MSD S's that are copied and distributed for this material. Components present in this product at a level which could require reporting under this statute are: *** NONE****

INVENTORY STATUS

The ingredients of this product are listed on, or are exempt from listing on, the TSCA inventory.

13. OTHER INFORMATION

HMIS FORMAT:

Health: 0 Flammability: 0 Reactivity: 0

We believe that the information contained herein is current as of the date of this Material Safety Data Sheet, and is offered in good faith. Since the use of this information and of these opinions and the conditions of the use of the product are not within the control of Factor II Technology, it is the user's obligation to determine the conditions of safe use of the product.

Factor II Technology Regulatory Compliance Department

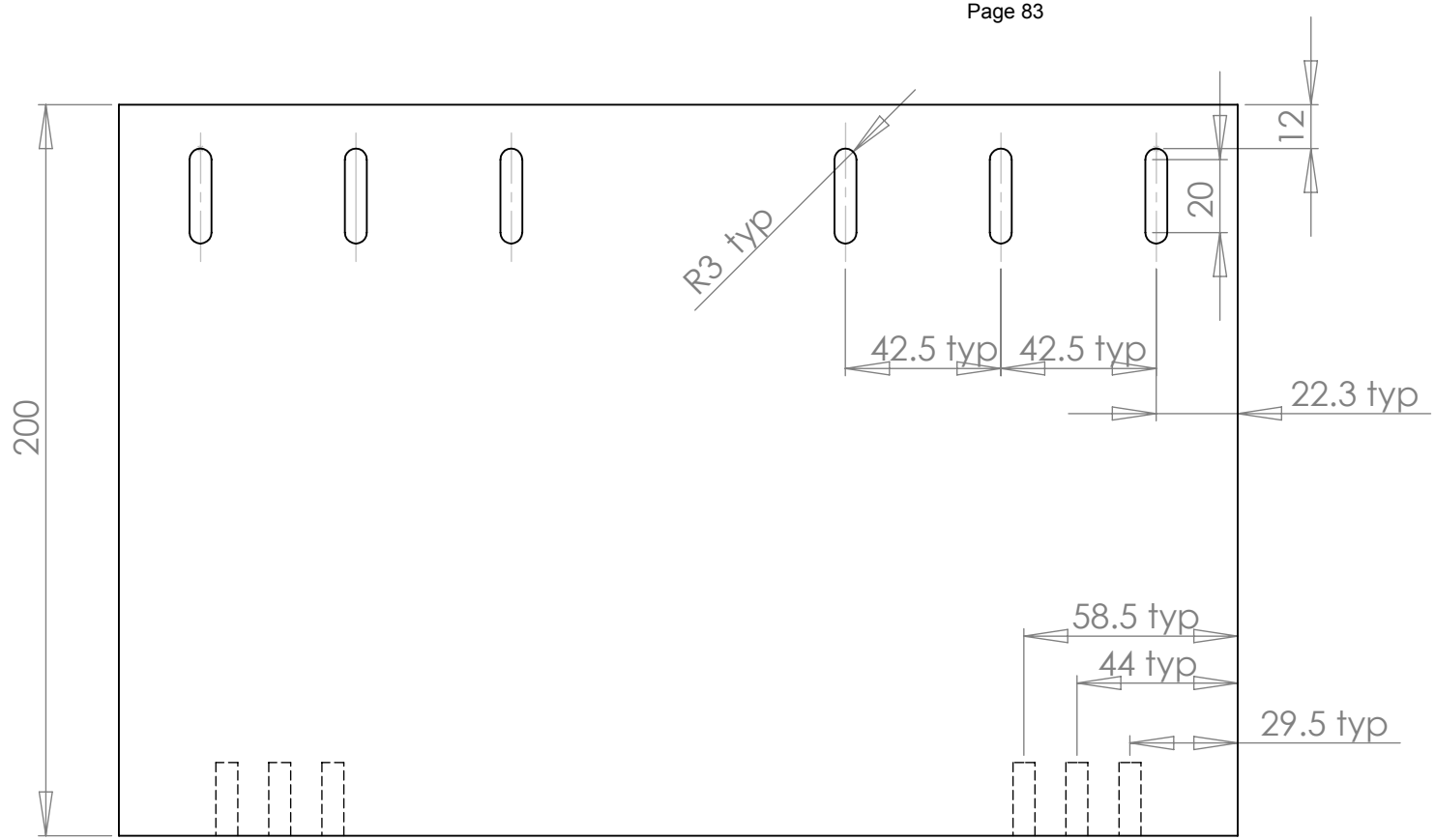

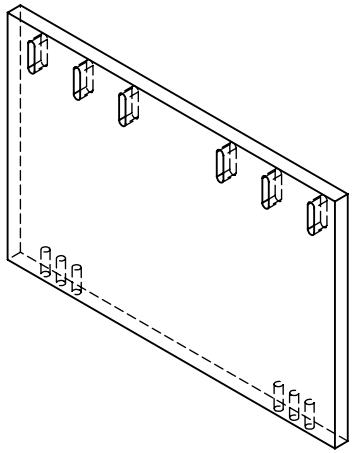

Pneumatic

MRE Breast Coil Actuator **DRG. TITLE**		**UNIVERSITY OF CANTERBURY** **MECHANICAL ENGINEERING DEPT.** CH.CH. N. Z.	
Part name:Base plate_2 Material: wood/plastic	Grant: E5155 Grade:	DRAWN : Quazi Linda	DATE : 15/9/2010
		CHECKED :	DRG. No : 046
SCALE : 1:2	ALL DIMENSIONS IN mm	APPROVED :	Qty: 1

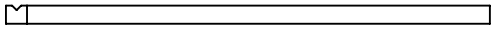

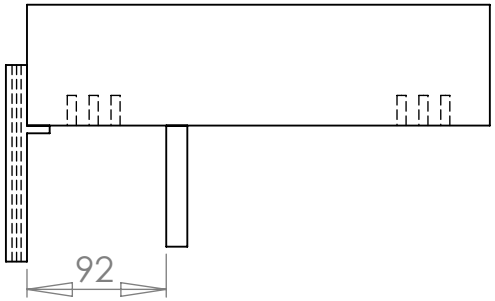

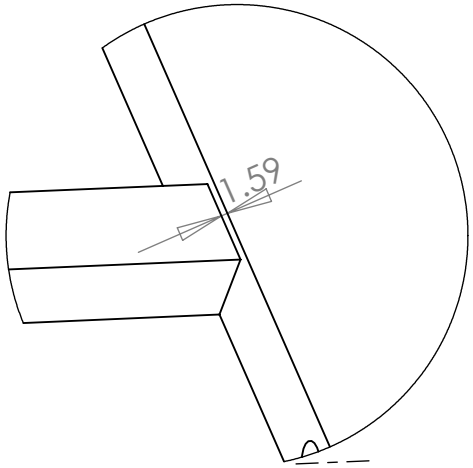

DETAIL F
SCALE 1 : 1

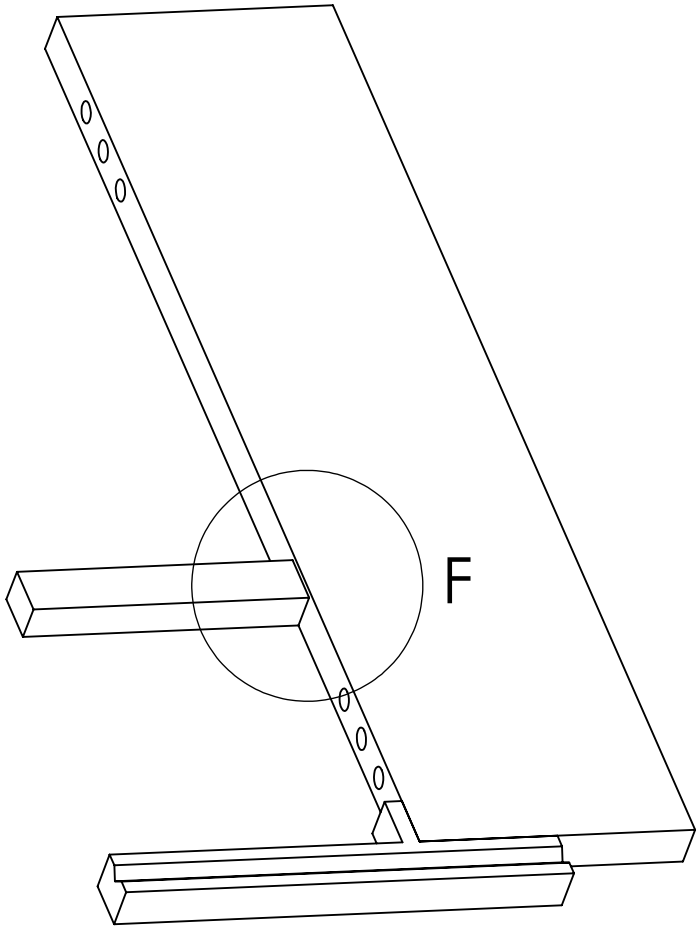

MRE Breast Coil Actuator **DRG. TITLE**		**UNIVERSITY OF CANTERBURY** **MECHANICAL ENGINEERING DEPT.** CH.CH. N.Z.	
Assembly name:Base_assembly Material:Plexiglass	Grant: E 5155 Tolarence:	DRAWN : Quazi Linda	DATE : 16/7/2010
		CHECKED :	DRG. No :
SCALE :	ALL DIMENSIONS IN mm	APPROVED :	**Qty:**

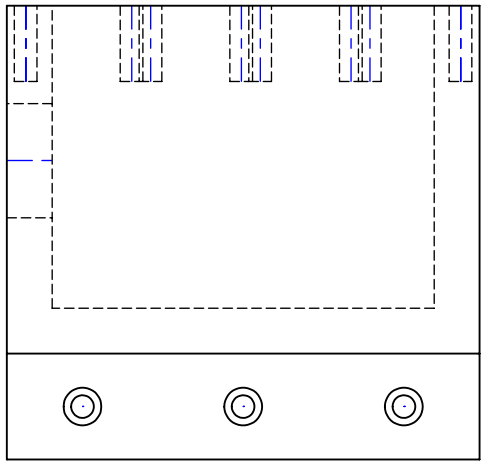

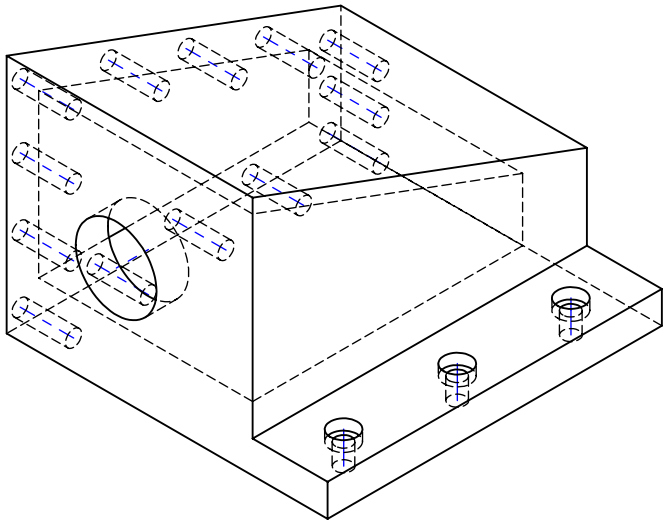

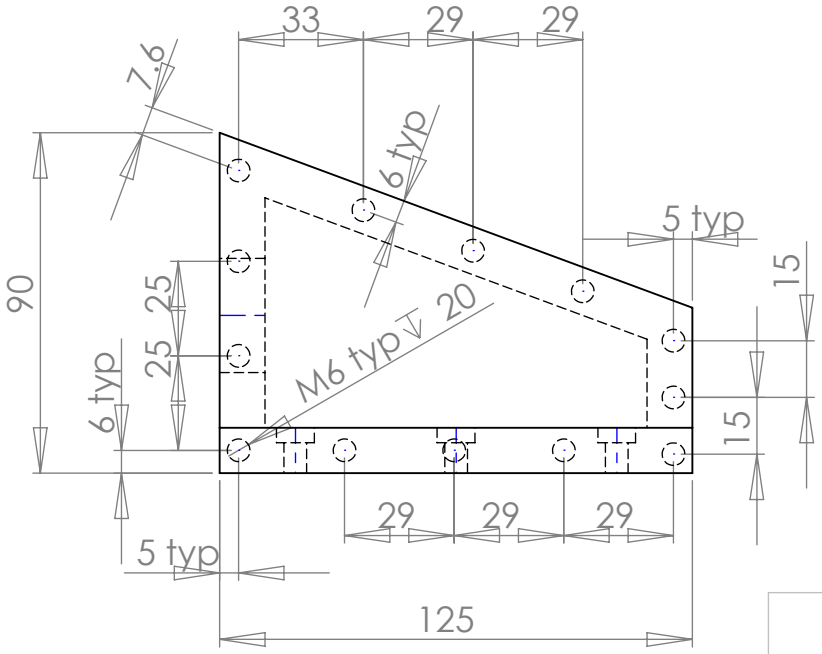

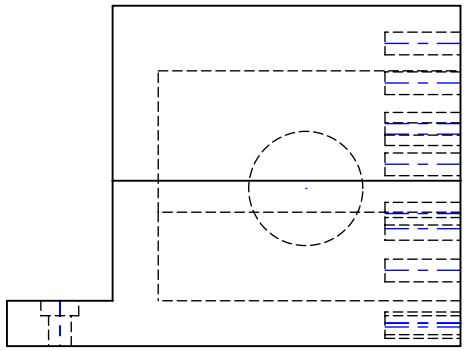

Pneumatic

DRG. TITLE	**UNIVERSITY OF CANTERBURY** **MECHANICAL ENGINEERING DEPT.** CH.CH. N.Z.	
	DRAWN :	DATE : 15/9/2010
	CHECKED :	DRG. No : 048
SCALE : ALL DIMENSIONS IN mm	APPROVED :	Qty: 1

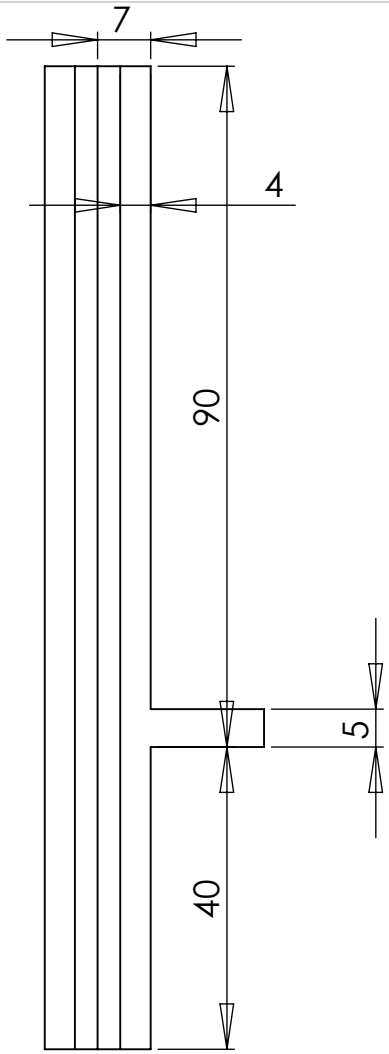

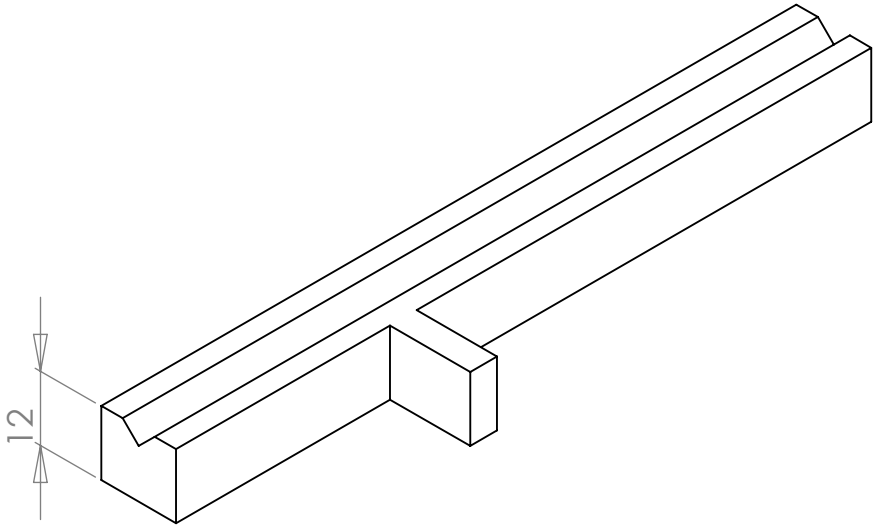

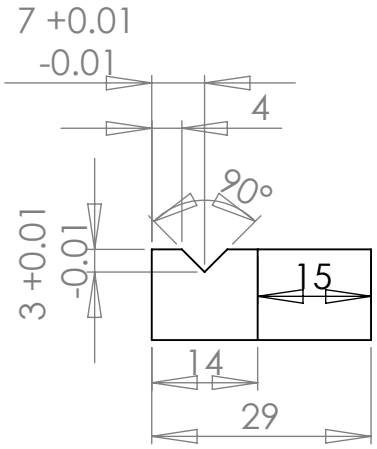

MRE Breast Coil Actuator

DRG. TITLE

Material: Acetal	Grant: E 5155	**UNIVERSITY OF CANTERBURY**	
Part name: Channel	Tolarence: +/-0.1	**MECHANICAL ENGINEERING DEPT.** CH.CH. N.Z.	
SCALE : 1:1	ALL DIMENSIONS IN mm	DRAWN : Quazi Linda	DATE : 26/7/2010
		CHECKED :	DRG. No :
		APPROVED :	**Qty:1**

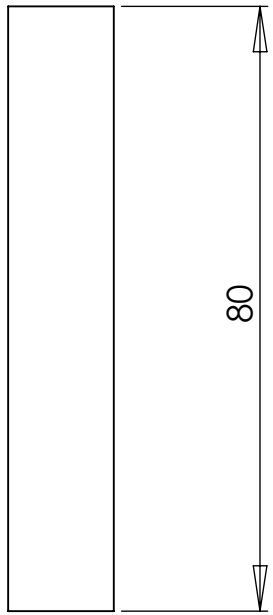

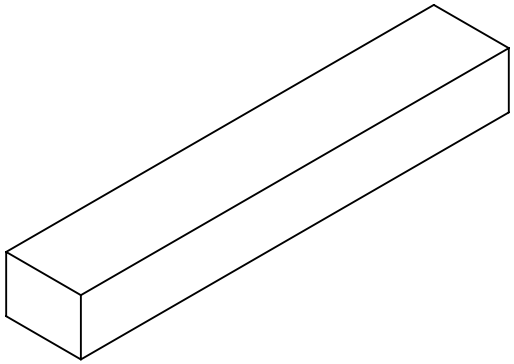

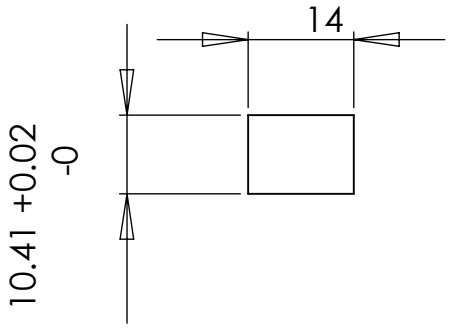

MRE Breast Coil Actuator **DRG. TITLE**		**UNIVERSITY OF CANTERBURY** **MECHANICAL ENGINEERING DEPT.** CH.CH. N.Z.	
Material: Acetal Part name:Plain path	Grant: E 5155 Tolarence:	DRAWN : Quazi Linda	DATE : 16/7/2010
		CHECKED :	DRG. No : 9
SCALE : 1:1	ALL DIMENSIONS IN mm	APPROVED :	**Qty:1**

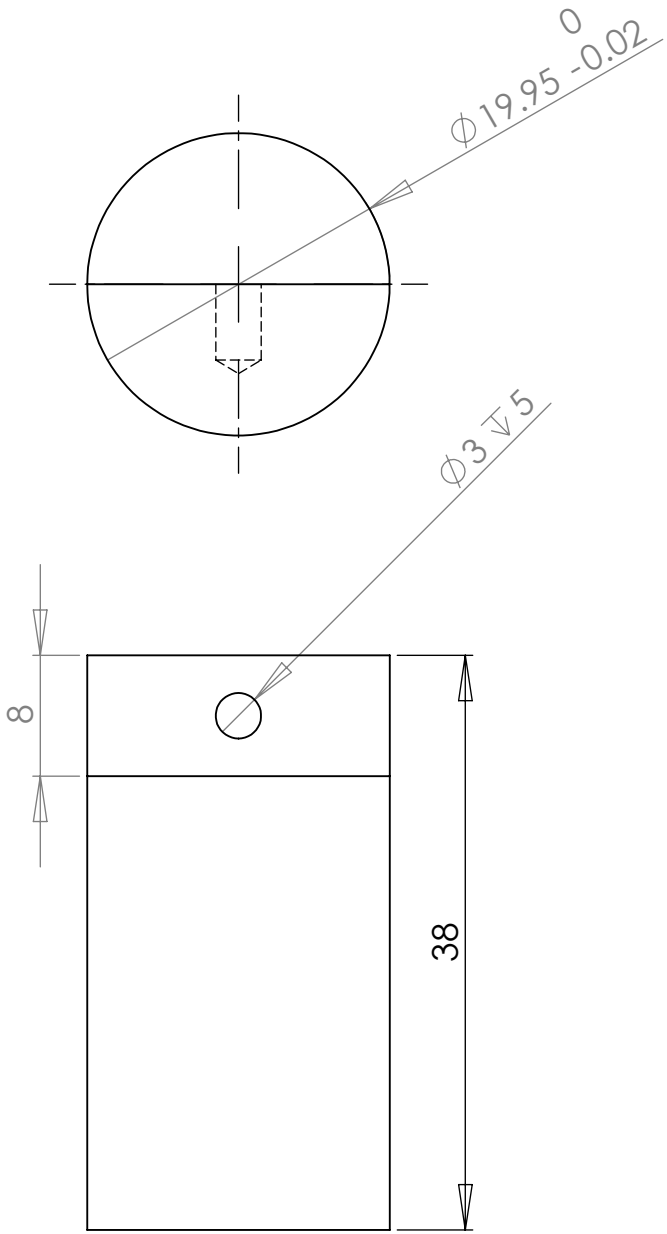

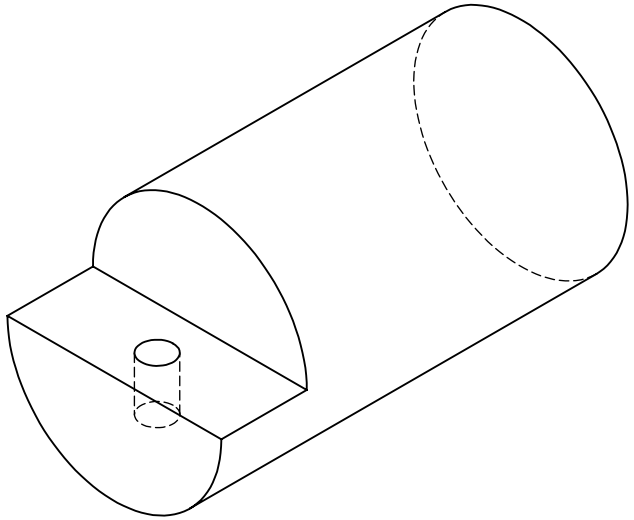

Pneumatic

MRE Breast Coil Actuator **DRG. TITLE**		**UNIVERSITY OF CANTERBURY** **MECHANICAL ENGINEERING DEPT.** CH.CH. N.Z.
Part name: rod2 Material: wood/plastic	Grant: E5155 Grade:	DRAWN : Quazi Linda CHECKED :
SCALE : 2:1 ALL DIMENSIONS IN mm		APPROVED :
		DATE : 15/9/2010 DRG. No : 048 Qty: 1

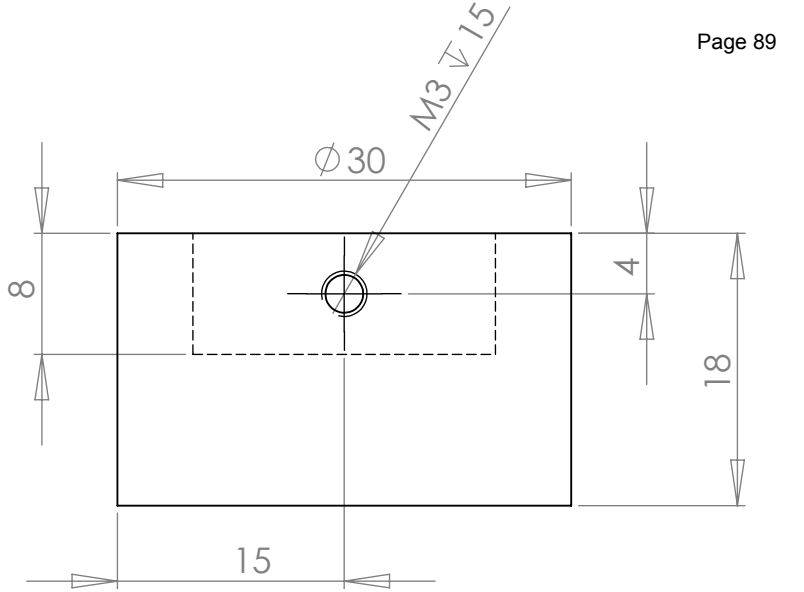

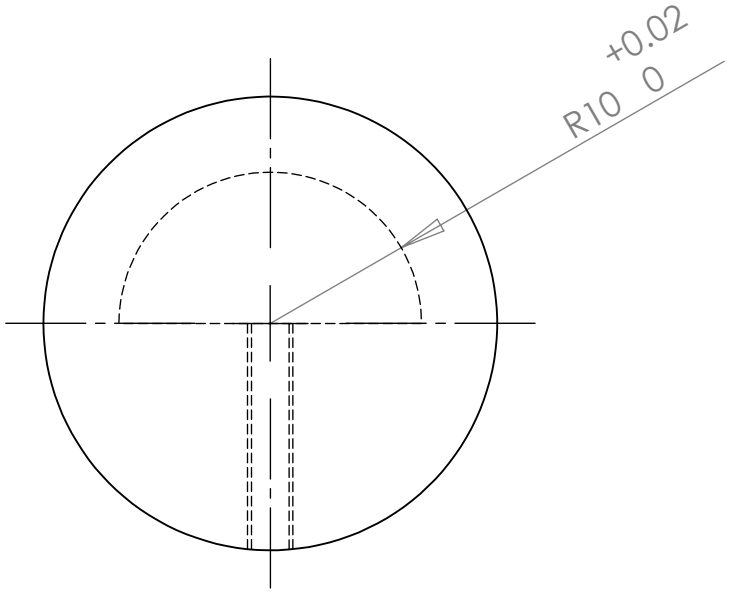

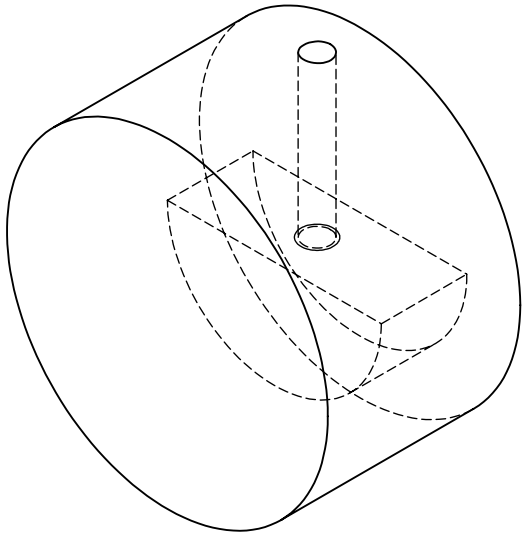

Pneumatic

MRE Breast Coil Actuator **DRG. TITLE**		**UNIVERSITY OF CANTERBURY** **MECHANICAL ENGINEERING DEPT.** CH.CH. N.Z.	
Part name: rod3 Material: wood/plastic	Grant: E5155 Grade:	DRAWN : Quazi Linda	DATE : 15/9/2010
		CHECKED :	DRG. No : 048
SCALE : 2:1	ALL DIMENSIONS IN mm	APPROVED :	Qty: 1

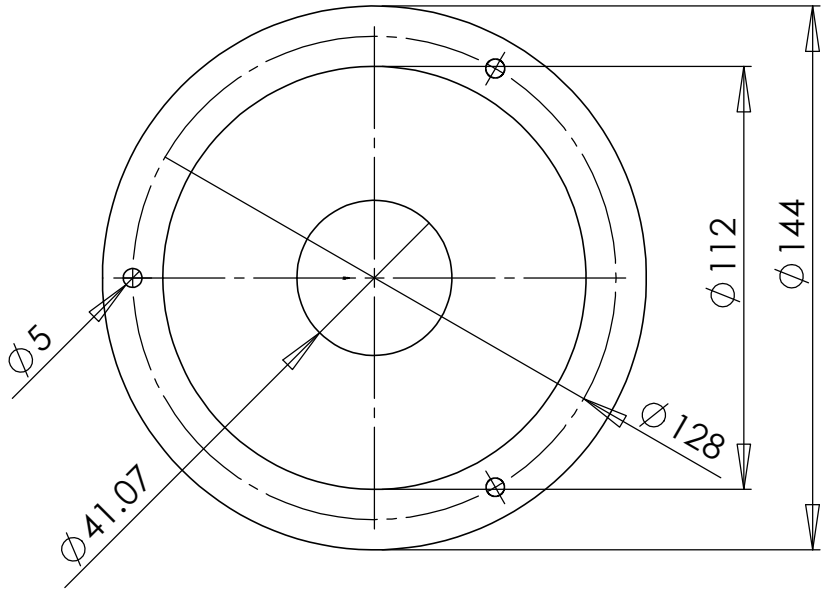

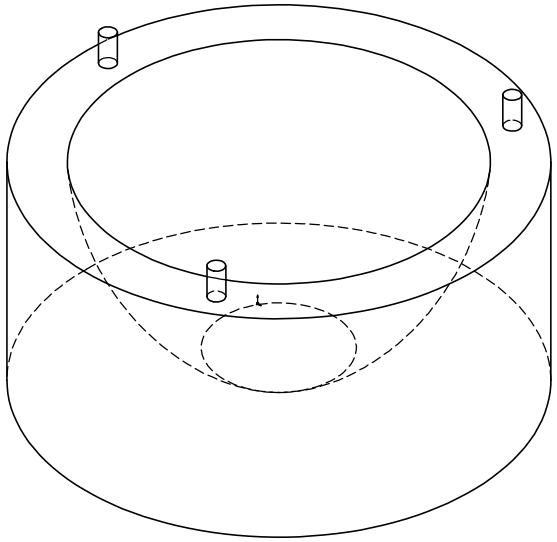

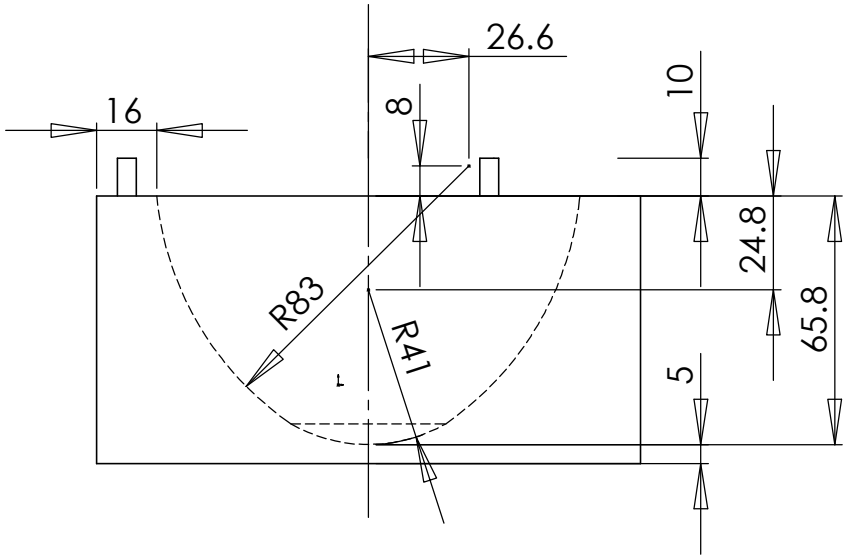

MRE Breast Coil Actuator **DRG. TITLE**	Grant: E5155 Tolarance:+/-0.1	**UNIVERSITY OF CANTERBURY** **MECHANICAL ENGINEERING DEPT.** CH.CH. N.Z.	
Material: Aluminium Grade:7075 Part Name: Cavity		DRAWN : Quazi Linda	DATE : 11/11/2009
		CHECKED :	DRG. No : 022
SCALE : 1:1	ALL DIMENSIONS IN mm	APPROVED :	Qty: 2

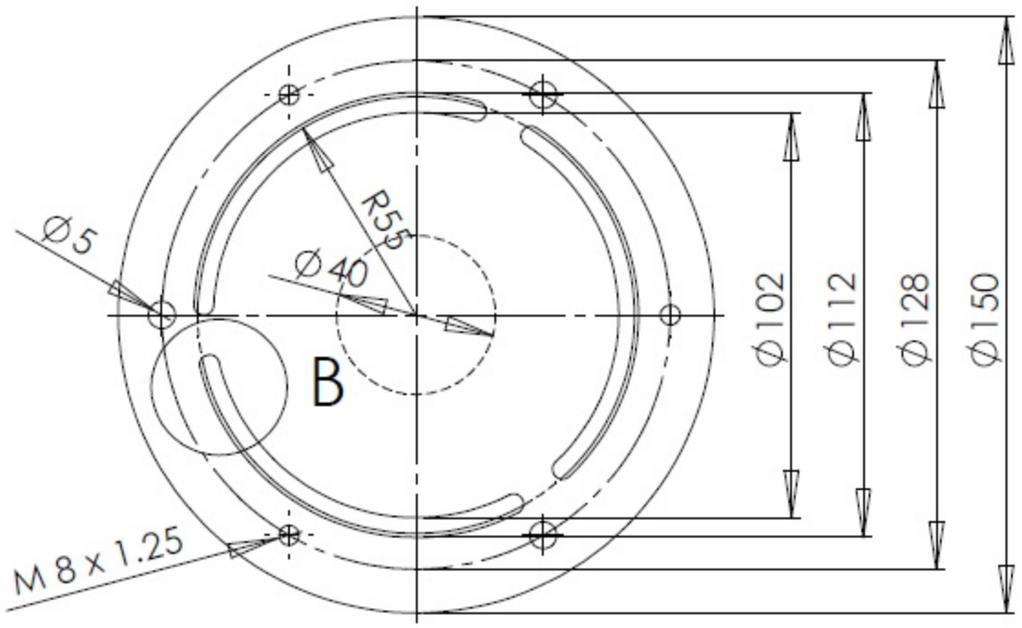

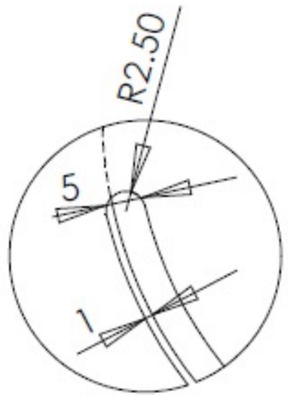

DETAIL B
SCALE 1 : 1

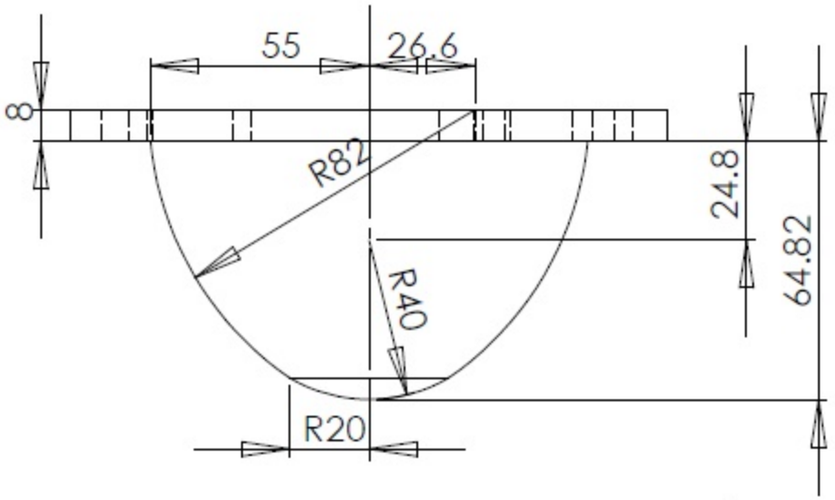

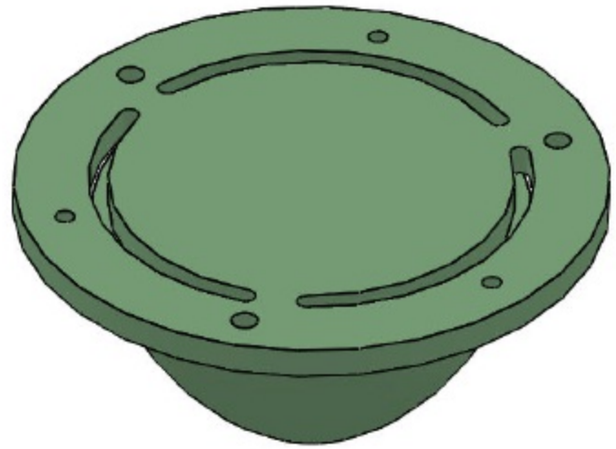

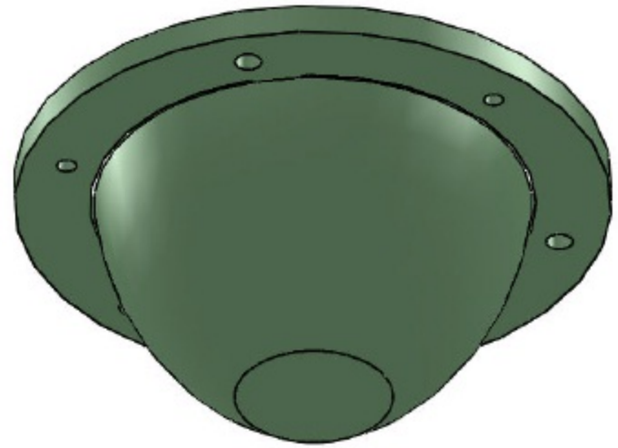

MRE Breast Coil Actuator **DRG. TITLE**	Grant: E5155 Tolerance: +/-0.1	**UNIVERSITY OF CANTERBURY** **MECHANICAL ENGINEERING DEPT.** CH.CH. N.Z.	
Material: Aluminium	Grade: 7075	DRAWN : Quazi Linda	DATE : 11/11/2009
Assembly name: Core and Cavity Assembly		CHECKED :	DRG. No : 023

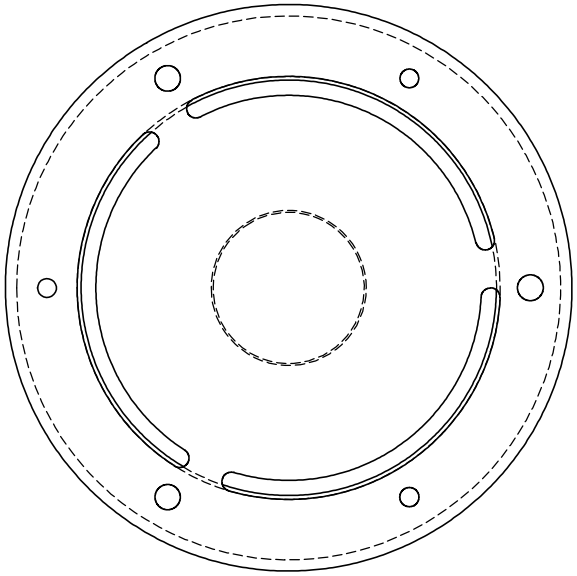

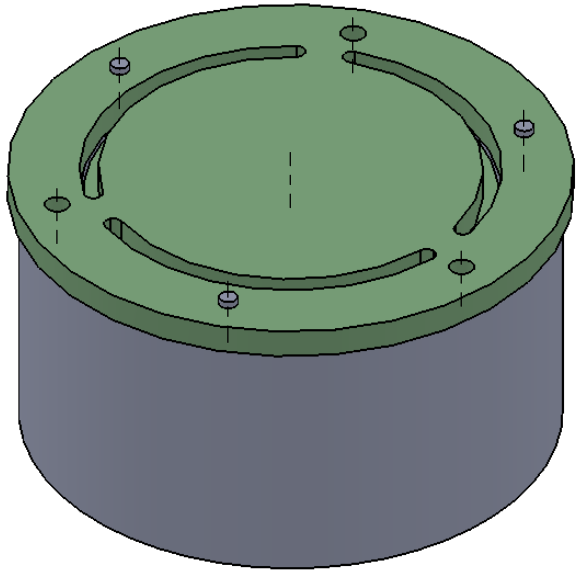

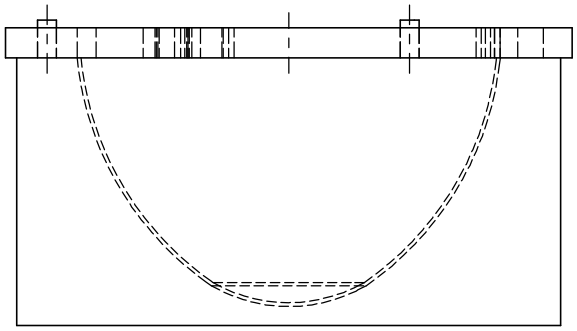

MRE Breast Coil Actuator **DRG. TITLE**	Grant: E5155	**UNIVERSITY OF CANTERBURY** **MECHANICAL ENGINEERING DEPT.** CH.CH. N.Z.	
Material: Aluminium Assembly name: Core and Cavity Assembly		DRAWN : Quazi Linda	DATE : 11/11/2009
		CHECKED :	DRG. No : 023
SCALE : 1:1	ALL DIMENSIONS IN mm	APPROVED :	Qty: 2

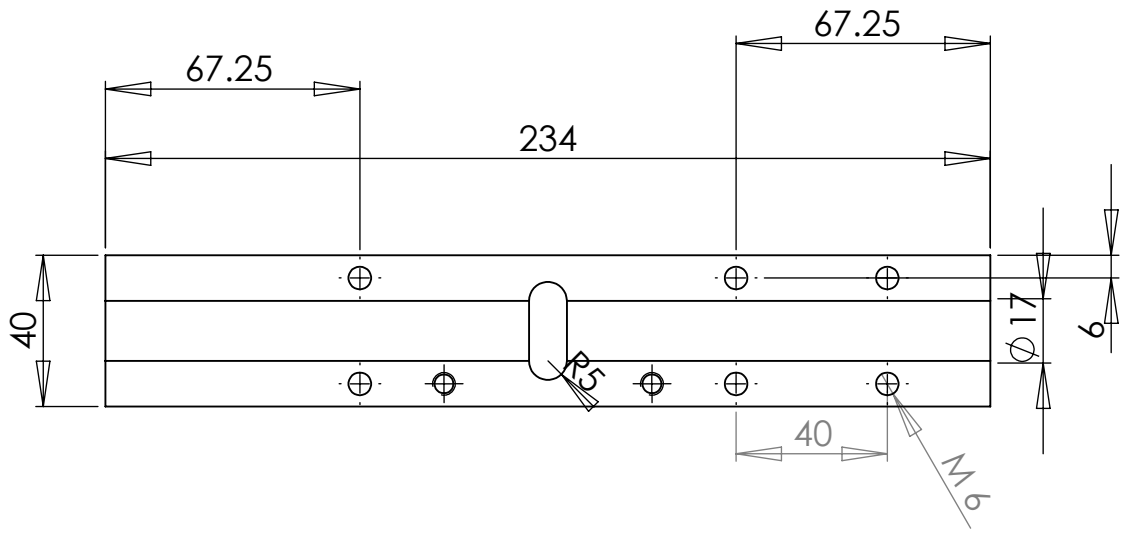

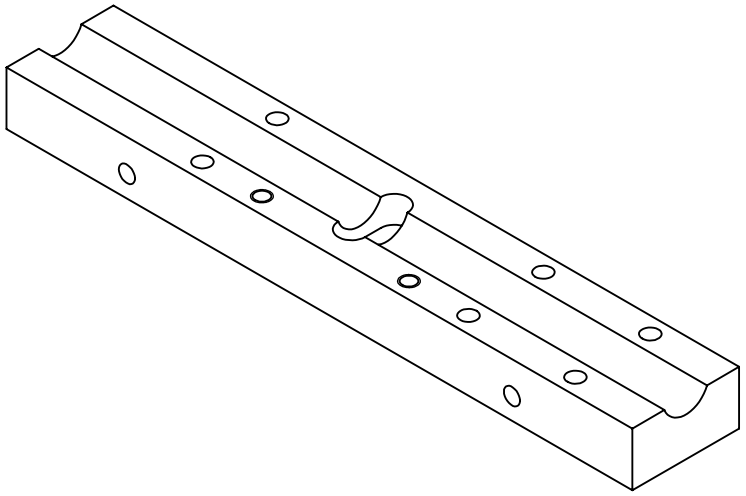

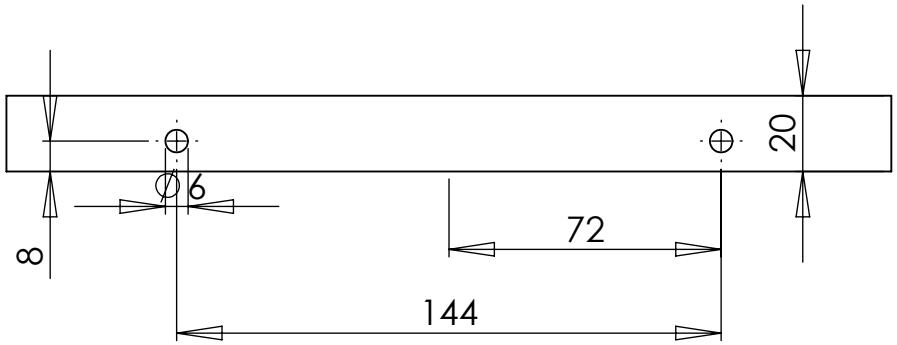

MRE Breast Coil Actuator **DRG. TITLE**		**UNIVERSITY OF CANTERBURY** **MECHANICAL ENGINEERING DEPT.** CH.CH. N.Z.	
Assembly name: Washer Material: Plexiglass	Grant: E5155 Grade:	DRAWN : Quazi Linda	DATE : 30/8/2010
		CHECKED :	DRG. No : 037
SCALE : 1:2	ALL DIMENSIONS IN mm	APPROVED :	Qty: 1

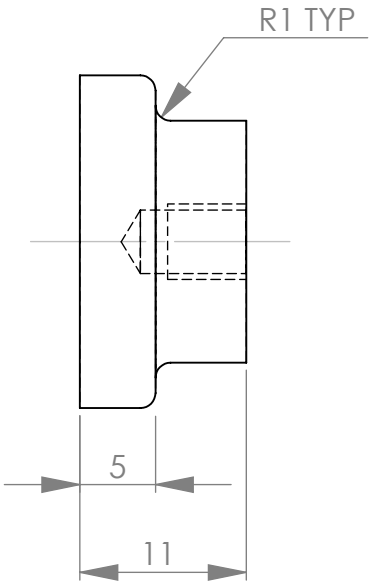

LEFT ELEVATION

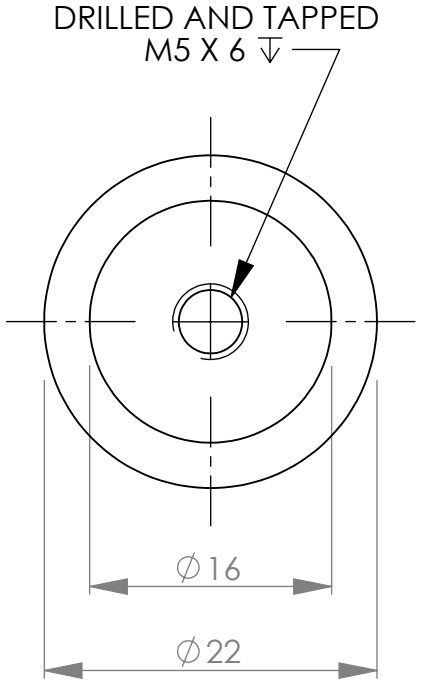

ELEVATION

QTY REQ'D : 1

MRE BREAST COIL ACTUATOR		UNIVERSITY OF CANTERBURY MECHANICAL ENGINEERING DEPT. CH.CH. N.Z.	
ACTUATOR TIP	Part No.: P 009	DRAWN : AARON HARRIS	DATE : 02-2008
	MATERIAL: BRASS	CHECKED :	DRG. No : 014
SCALE : 2:1 (A4)	ALL DIMENSIONS IN mm	APPROVED :	

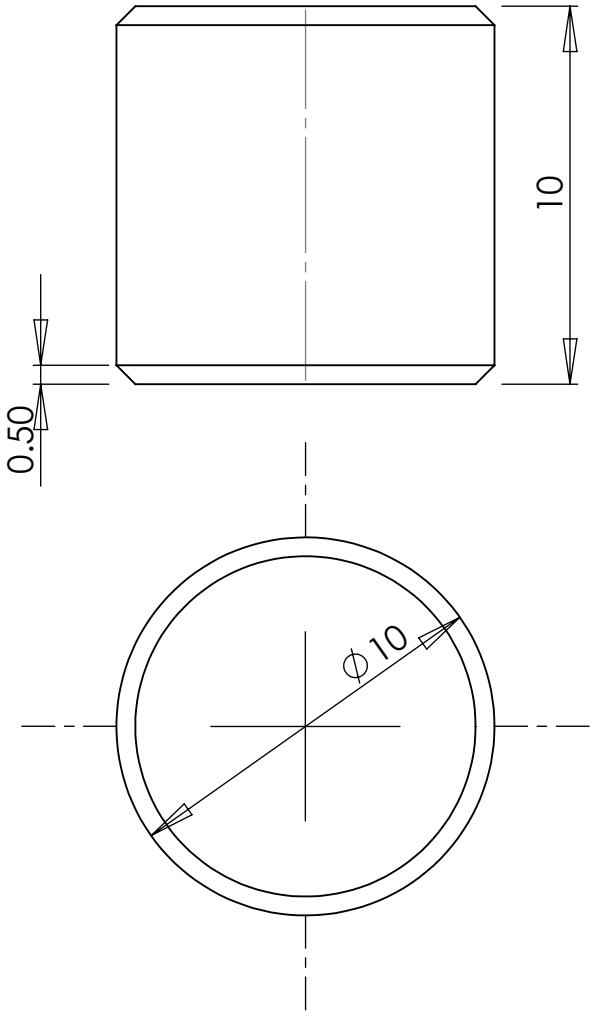

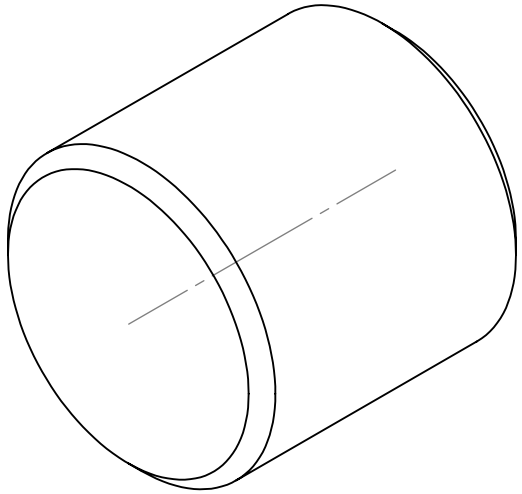

MRE Breast Coil Actuator **DRG. TITLE**		**UNIVERSITY OF CANTERBURY** **MECHANICAL ENGINEERING DEPT.** CH.CH. N.Z.	
Material: Ceramic Part name:Ceramic Insert	Grant: E 5155 Tolarence: +/-0.1	DRAWN : Quazi Linda	DATE : 16/7/2010
		CHECKED :	DRG. No : 5
SCALE : 5:1	ALL DIMENSIONS IN mm	APPROVED :	**Qty:1**

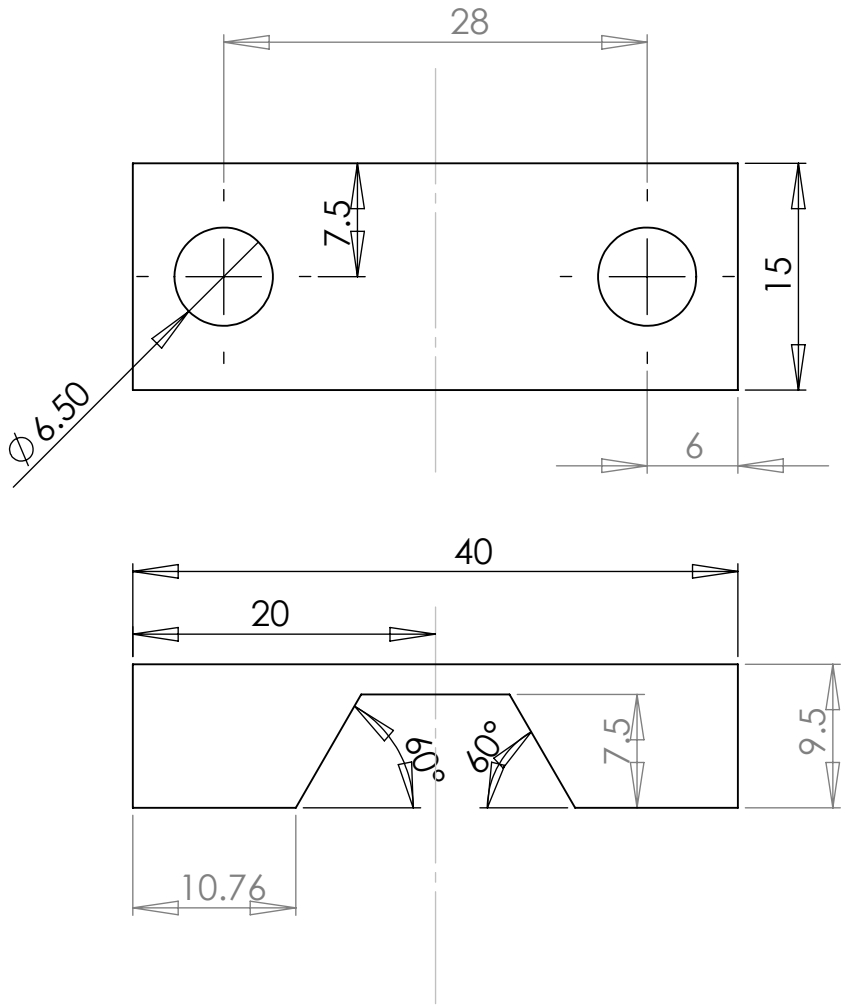

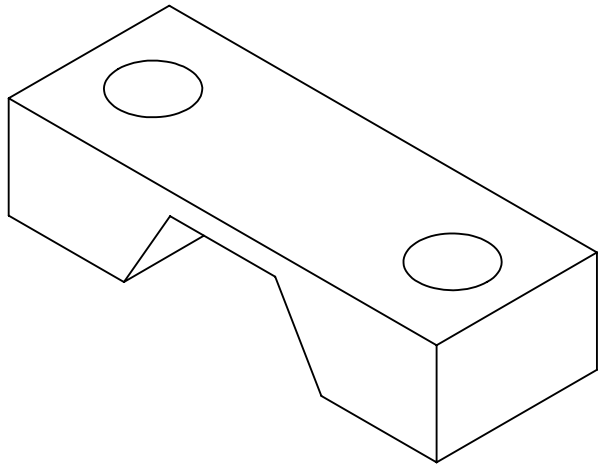

System 1

MRE Breast Coil Actuator **DRG. TITLE**		**UNIVERSITY OF CANTERBURY** **MECHANICAL ENGINEERING DEPT.** CH.CH. N.Z.	
Part name: Clamp2_bottom Material: Plexiglass	Grant: E5155 Grade:	DRAWN : Quazi Linda	DATE : 15/9/2010
		CHECKED :	DRG. No : 038
SCALE : 2:1	ALL DIMENSIONS IN mm	APPROVED :	Qty: 1

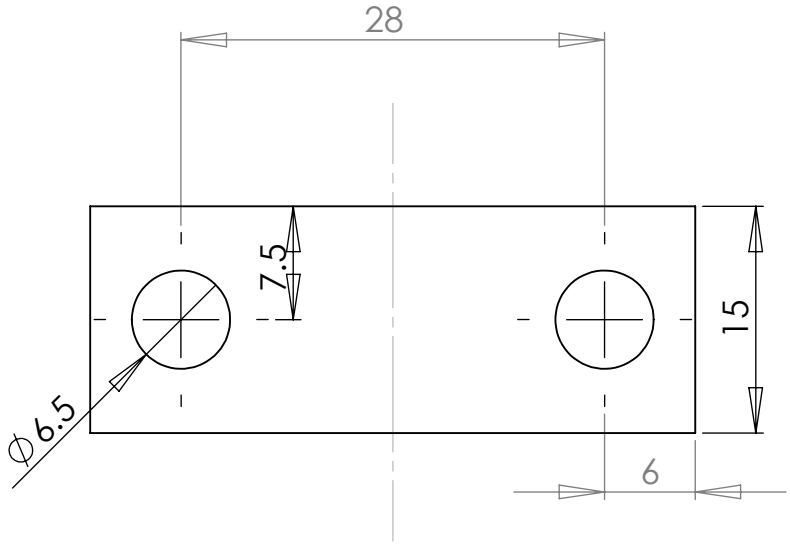

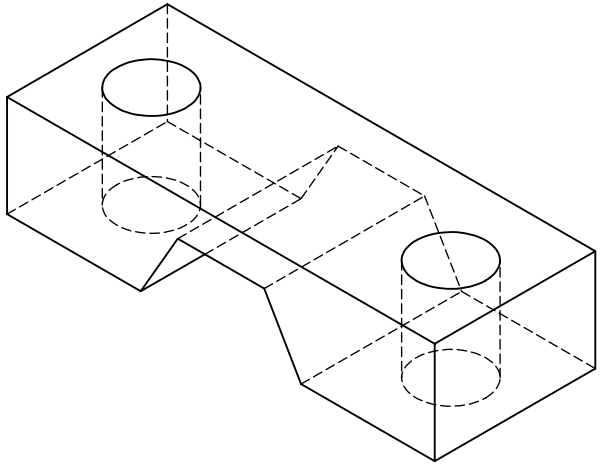

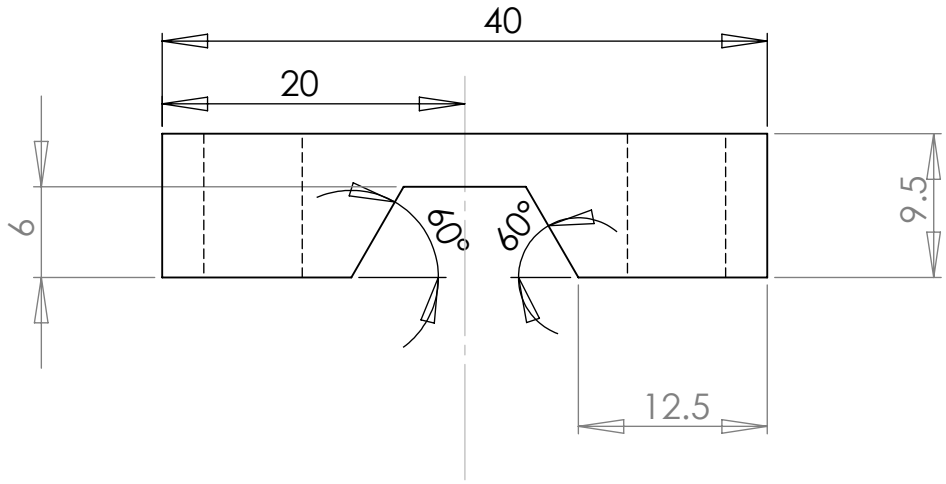

MRE Breast Coil Actuator **DRG. TITLE**		**UNIVERSITY OF CANTERBURY** **MECHANICAL ENGINEERING DEPT.** CH.CH. N.Z.	
Part name: Clamp2_bottom_thinner_actuator Material: Plexiglass	Grant: E5155 Grade:	DRAWN : Quazi Linda	DATE : 17/9/2010
		CHECKED :	DRG. No : 039
SCALE : 2:1	ALL DIMENSIONS IN mm	APPROVED :	Qty: 2

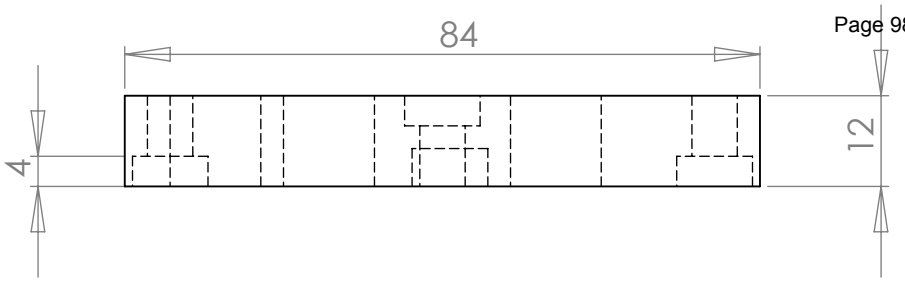

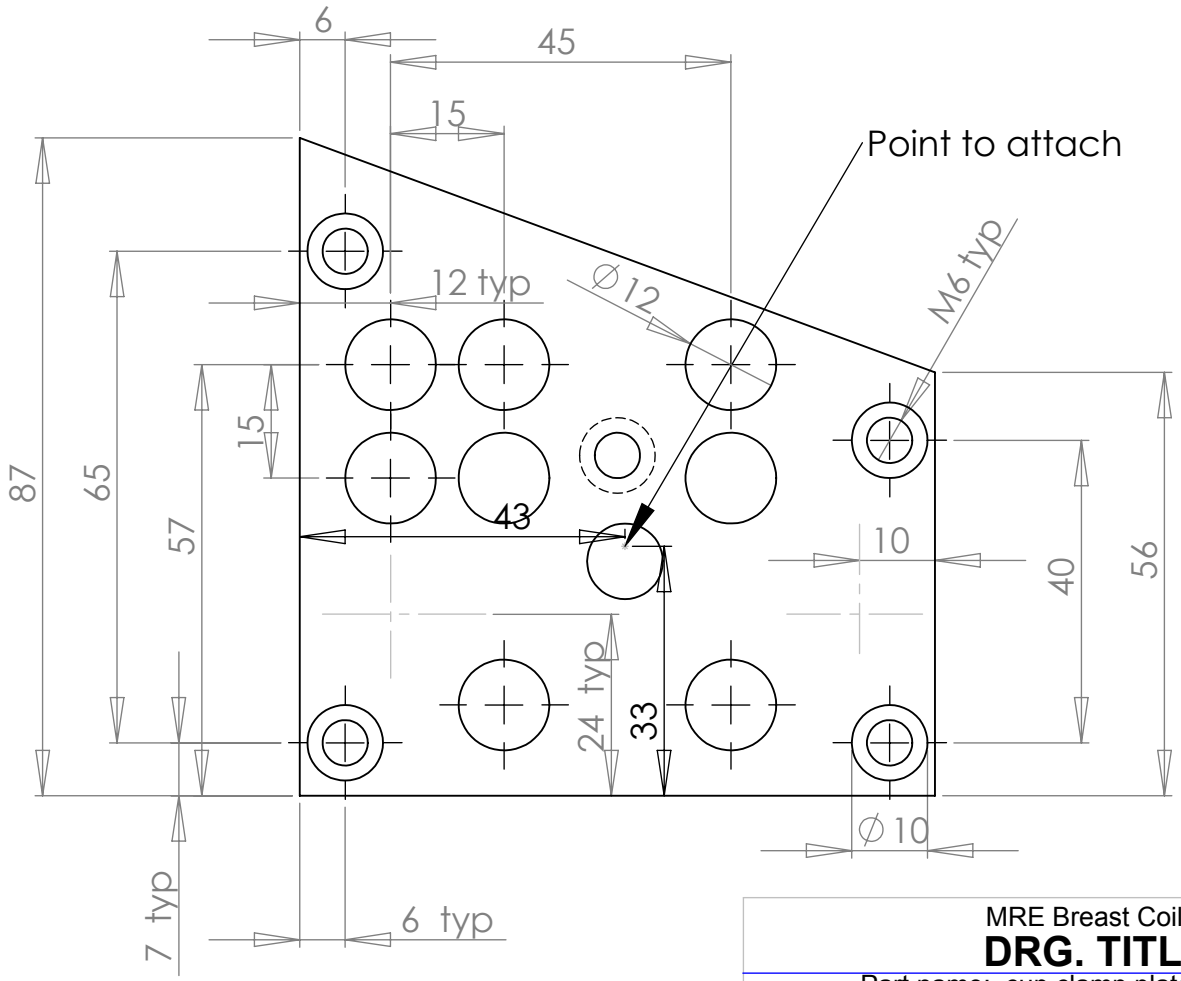

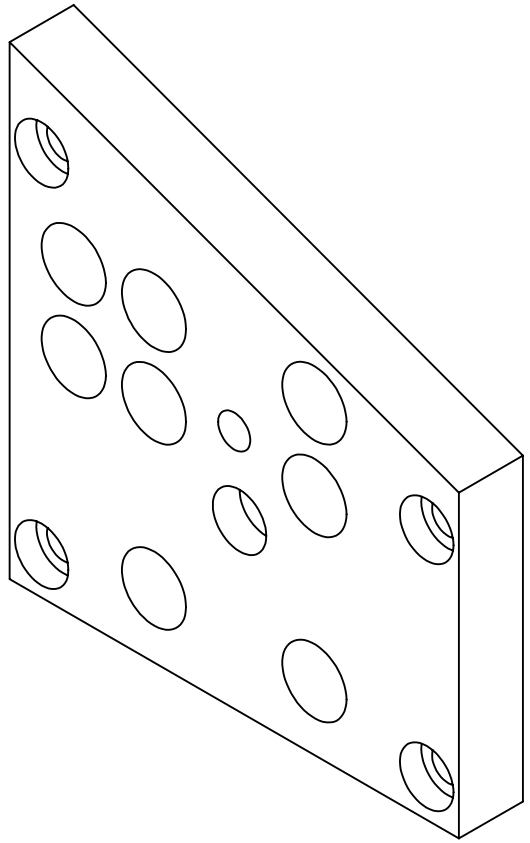

Pneumatic

MRE Breast Coil Actuator

DRG. TITLE

Part name: cup clamp plate

Material: wood/plastic

Grant: E5155

Grade:

SCALE : 2:1

ALL DIMENSIONS IN mm

UNIVERSITY OF CANTERBURY
MECHANICAL ENGINEERING DEPT. CH.CH. N.Z.

DRAWN : Quazi Linda	DATE : 15/9/2010
CHECKED :	DRG. No : 049
APPROVED :	Qty: 1

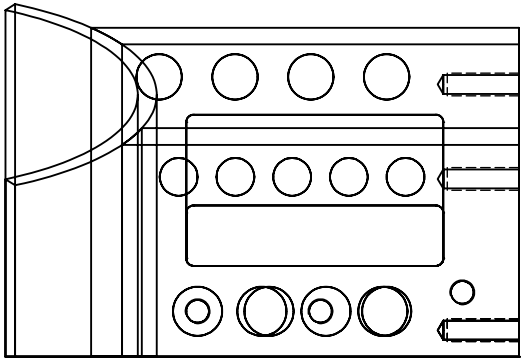

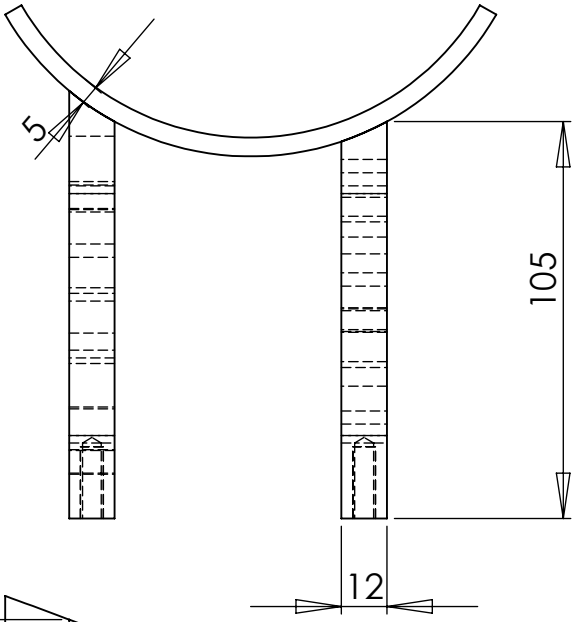

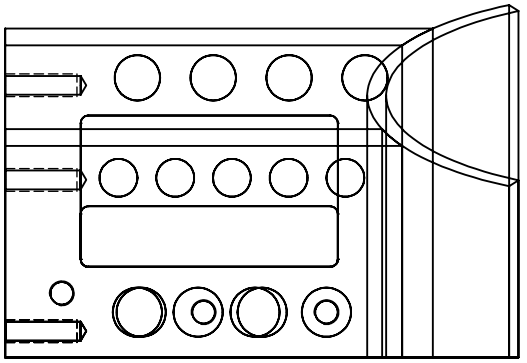

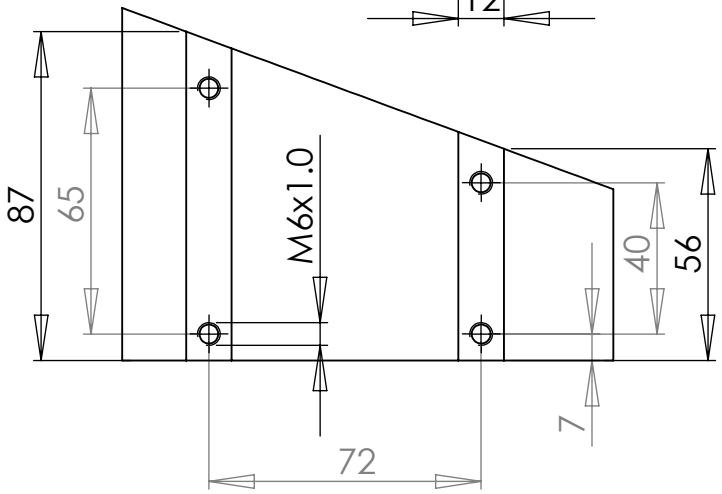

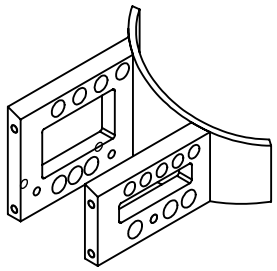

DRG. TITLE		UNIVERSITY OF CANTERBURY MECHANICAL ENGINEERING DEPT. CH.CH. N.Z.	
	Grant: E 5155 Tolarence:+/-0.1	DRAWN : Quazi Linda	DATE : 16/7/2010
		CHECKED :	DRG. No : 1a
SCALE : 1:2	ALL DIMENSIONS IN mm	APPROVED :	**Qty:1**

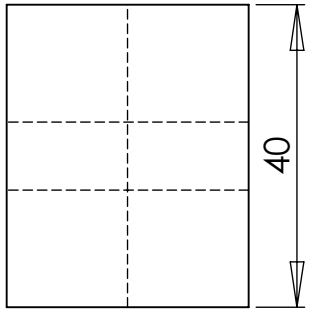

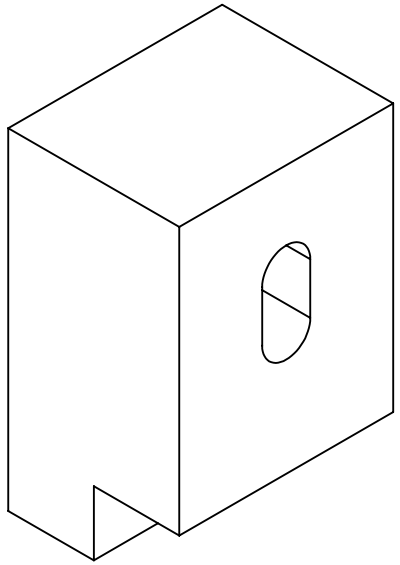

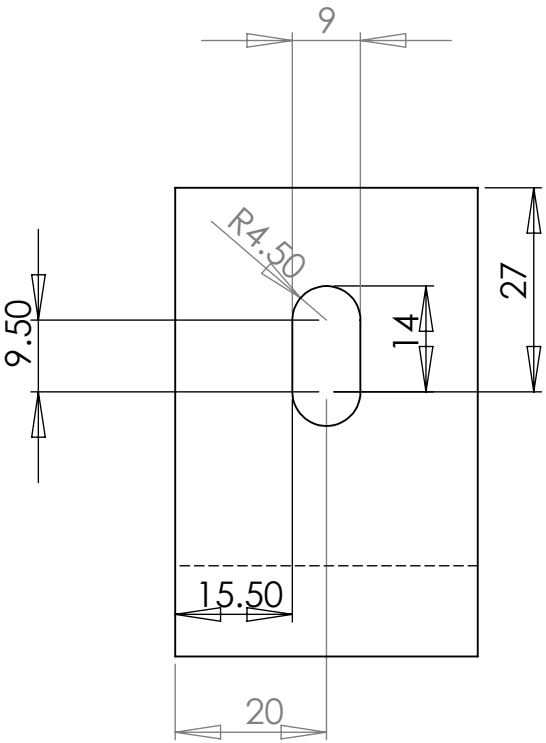

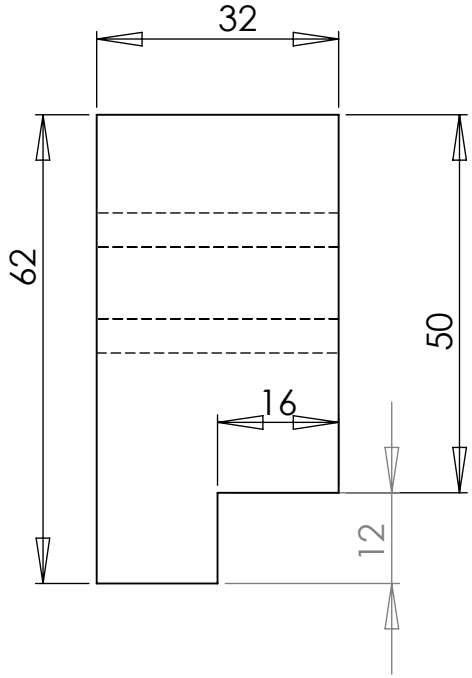

MRE Breast Coil Actuator **DRG. TITLE**		**UNIVERSITY OF CANTERBURY** **MECHANICAL ENGINEERING DEPT.** CH.CH. N.Z.	
Material: Part name:end plate	Grant: E 5155 Tolarence:	DRAWN : Quazi Linda	DATE : 16/7/2010
		CHECKED :	DRG. No :
SCALE : 1:1	ALL DIMENSIONS IN mm	APPROVED :	**Qty:1**

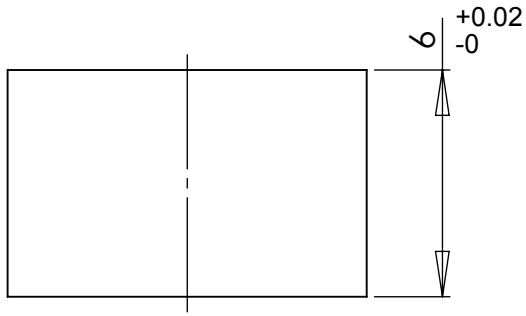

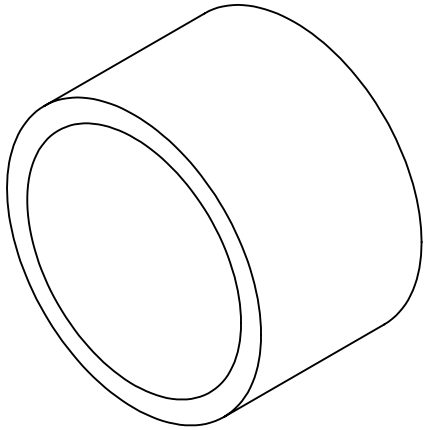

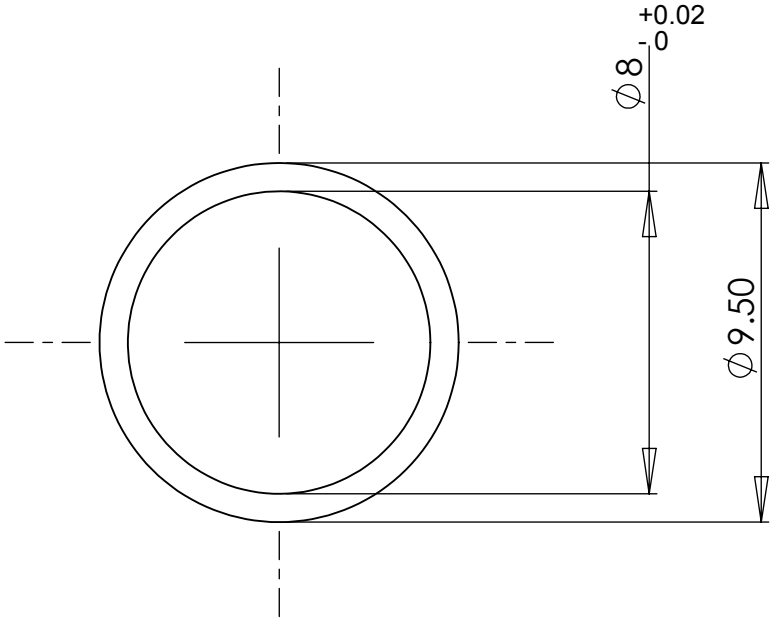

System 1

MRE Breast Coil Actuator **DRG. TITLE**		**UNIVERSITY OF CANTERBURY** **MECHANICAL ENGINEERING DEPT.** CH.CH. N.Z.	
Material: Acetal Part name:Lower tube	Grant: E 5155 Tolarence: +/-0.1	DRAWN : Quazi Linda	DATE : 16/7/2010
		CHECKED :	DRG. No : 5
SCALE : 5:1	ALL DIMENSIONS IN mm	APPROVED :	**Qty:1**

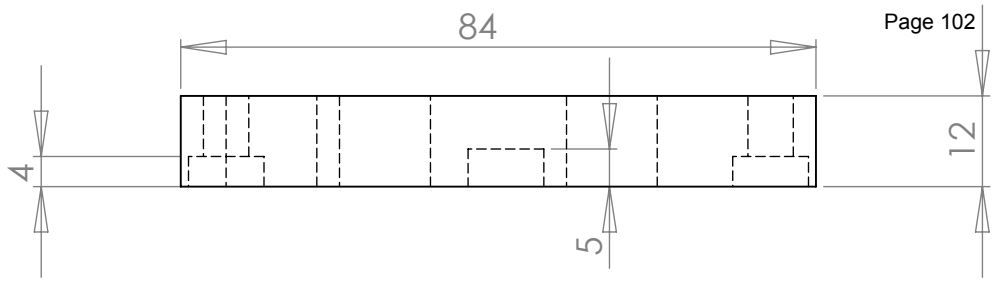

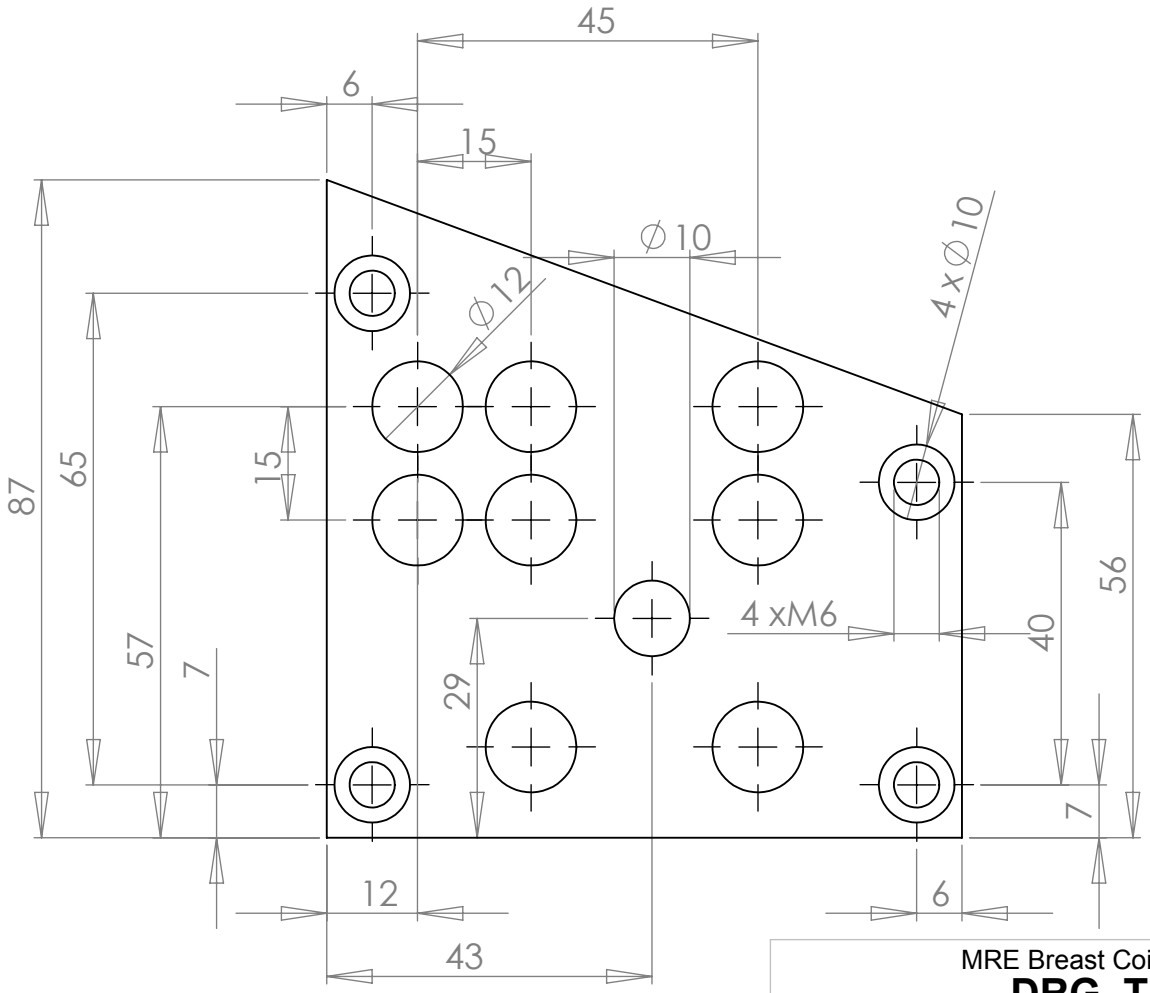

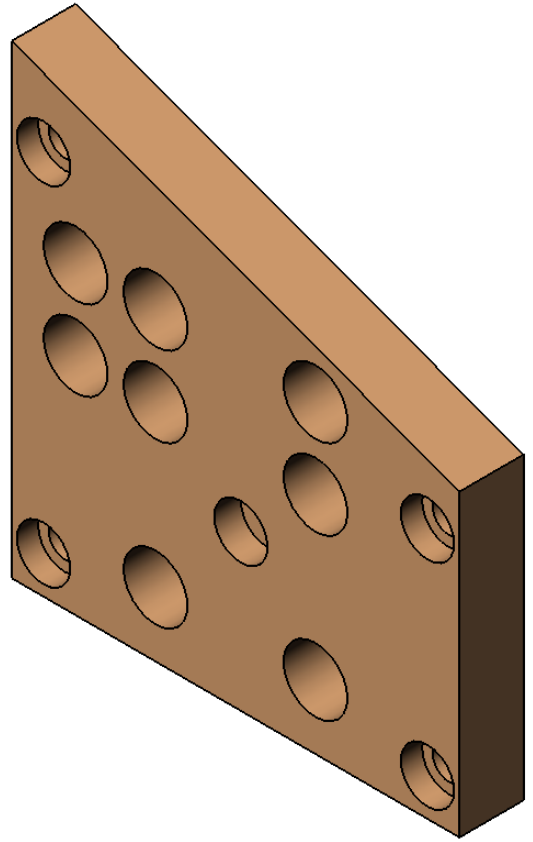

System 1

MRE Breast Coil Actuator

DRG. TITLE

Material: Plexiglass	Grant: E 5155	DRAWN : Quazi Linda	DATE : 16/7/2010
Part name:Post clamp plate	Tolarence:	CHECKED :	DRG. No :
SCALE : 1:1	ALL DIMENSIONS IN mm	APPROVED :	**Qty:1**

UNIVERSITY OF CANTERBURY
MECHANICAL ENGINEERING DEPT. CH.CH. N.Z.

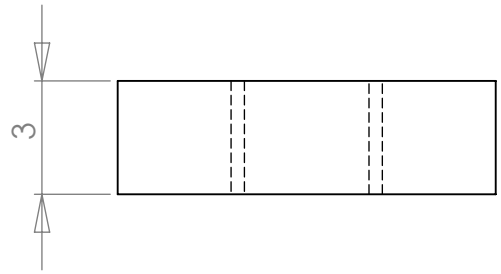

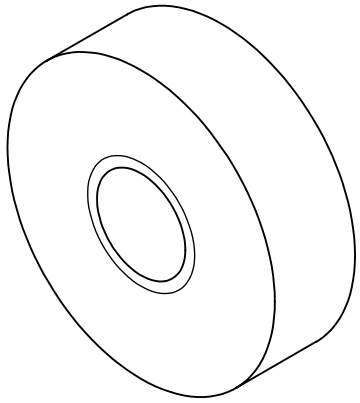

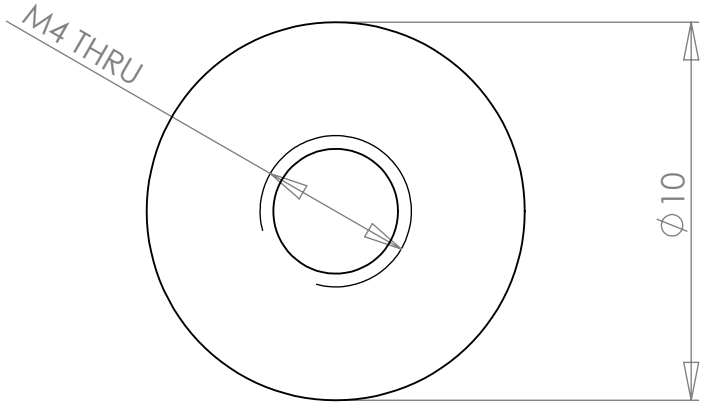

QTY REQ'D : 1

MRE BREAST COIL ACTUATOR		UNIVERSITY OF CANTERBURY MECHANICAL ENGINEERING DEPT. CH.CH. N.Z.	
ACTUATOR TIP	Part No.: P 009	DRAWN : AARON HARRIS	DATE : 02-2008
	MATERIAL: BRASS	CHECKED :	DRG. No : 014
SCALE : 2:1 (A4)	ALL DIMENSIONS IN mm	APPROVED :	

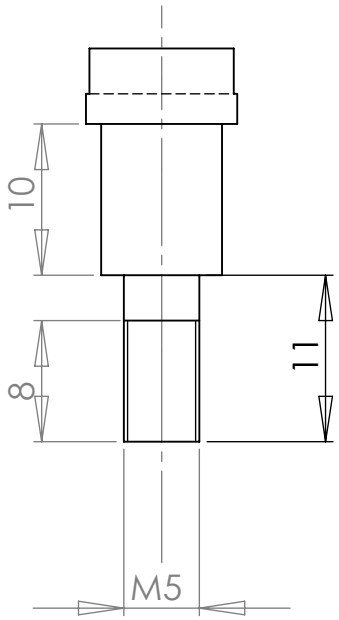

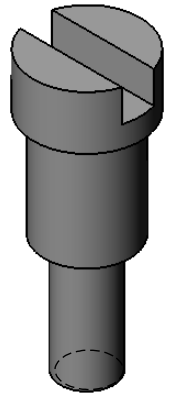

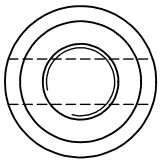

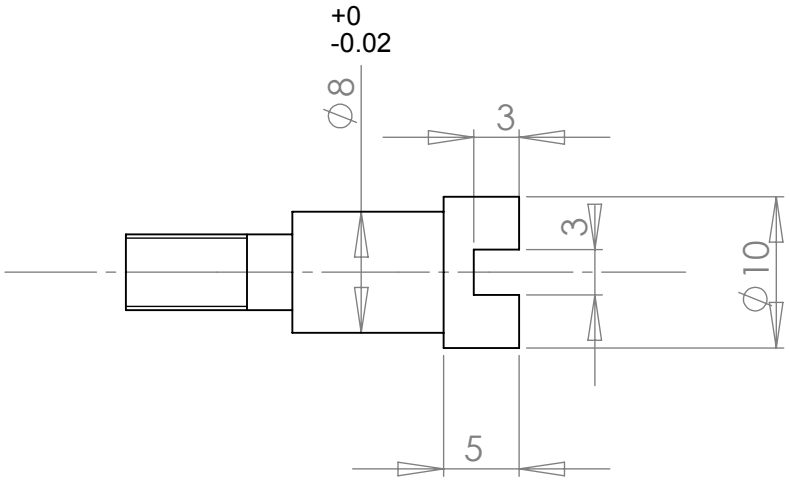

System 1

MRE Breast Coil Actuator **DRG. TITLE**		**UNIVERSITY OF CANTERBURY** **MECHANICAL ENGINEERING DEPT.** CH.CH. N.Z.	
Material: Titanium bronze Part name:Bolt	Grant: E 5155 Tolarence:+/-0.1	DRAWN : Quazi Linda	DATE : 16/7/2010
		CHECKED :	DRG. No :
SCALE : 2:1	ALL DIMENSIONS IN mm	APPROVED :	**Qty:1**

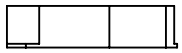

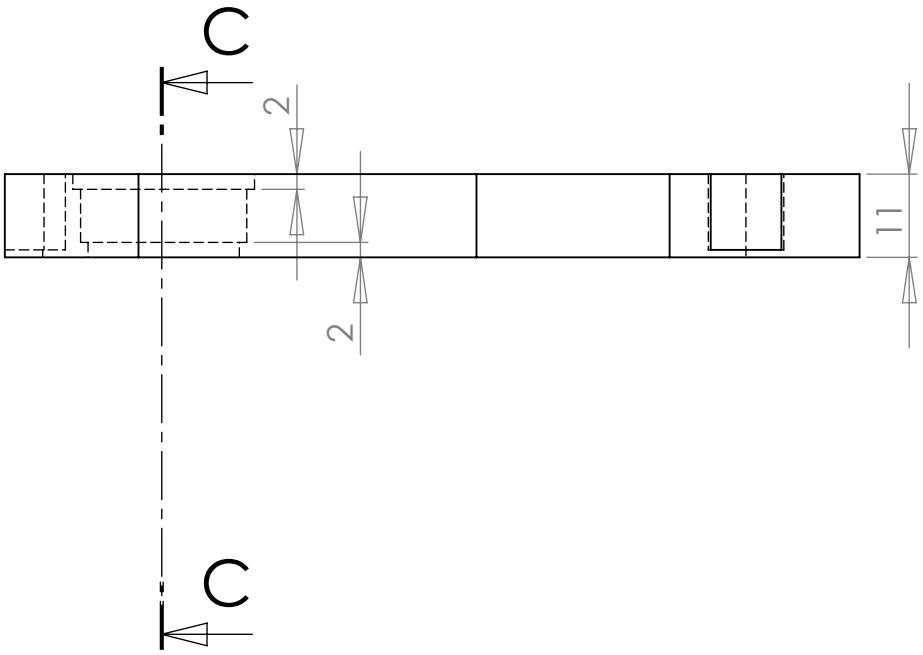

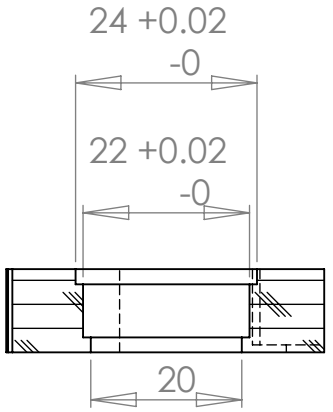

SECTION C-C

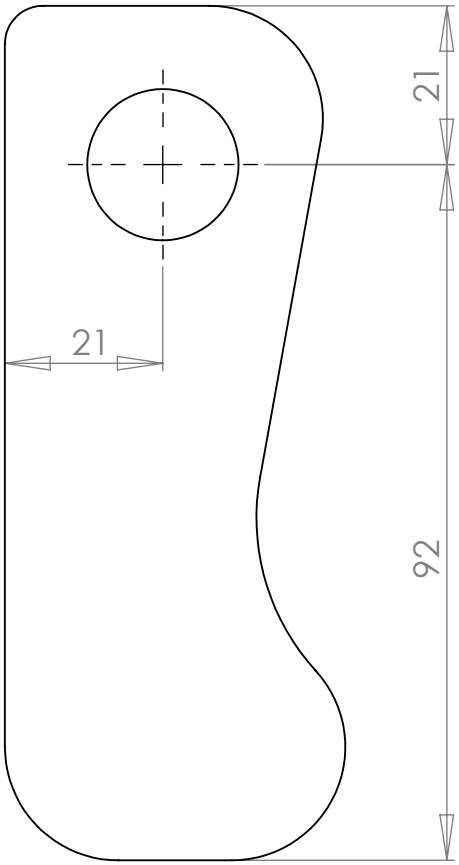

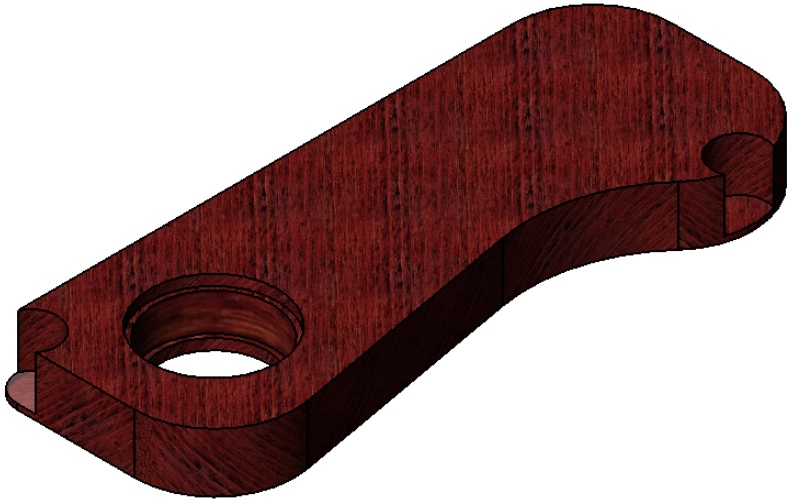

System 1

MRE Breast Coil Actuator **DRG. TITLE**		**UNIVERSITY OF CANTERBURY** **MECHANICAL ENGINEERING DEPT.** CH.CH. N.Z.
Part name: semi final woodenlever Material: Jarrah wood	Grant: E5155 Grade:	DRAWN : Quazi Linda CHECKED :
SCALE : 1:1 ALL DIMENSIONS IN mm		APPROVED :
		DATE : 15/9/2010 DRG. No : 038 Qty: 1

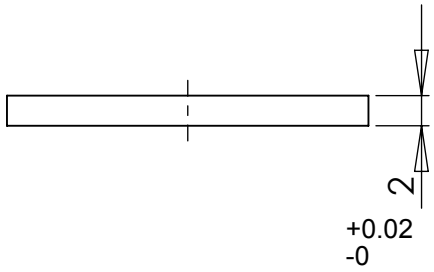

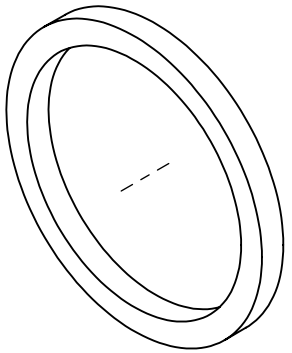

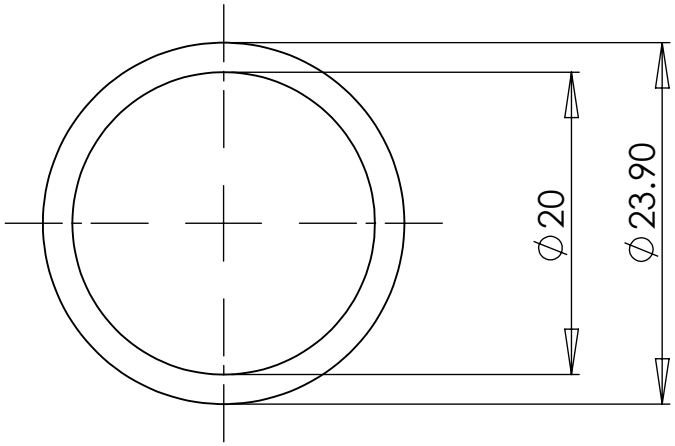

System 1

MRE Breast Coil Actuator **DRG. TITLE**		**UNIVERSITY OF CANTERBURY** **MECHANICAL ENGINEERING DEPT.** CH.CH. N.Z.	
Material: Acetal Part name:Upper tube	Grant: E 5155 Tolarence:	DRAWN : Quazi Linda	DATE : 16/7/2010
		CHECKED :	DRG. No : 3
SCALE : 2:1	ALL DIMENSIONS IN mm	APPROVED :	**Qty:1**

ITEM NO.	PART NUMBER	DESCRIPTION	Default
1	ISO 7379 - 8 x 25 --- N		1
2	ISO 4762 M6 x 60 --- 24N		1
3	ISO 4762 M8 x 20 --- 20N		1
4	ISO 4762 M6 x 45 --- 24N		2
5	ISO 4762 M5 x 35 --- 22N		4
6	ISO 4762 M5 x 16 --- 16N		4
7	ISO 4762 M5 x 20 --- 20N		2
8	ISO 4762 M5 x 25 --- 25N		2
9	QL-LA01	Lever Arm	1
10	QL-LA02	Contact Pad Adjustment Mount	1
11	QL-LA03	Lever Arm Pivot Mount	1
12	QL-LA04	Lever Arm Pivot Bush	1
13	16 dia x 45	Tension Spring	1
14	QL-BF01	Side Mount Frame	1
15	QL-BF02	Back Mount Frame	1
16	QL-BF03	Spring Mount/ Adjustment	1
17	QL-AC01	Actuator Clamp Base	2
18	QL-AC02	Actuator Clamp	2
19	P-842.6	Piezo Actuator	1
20	QL-AP01	Actuator Pad	1
21	QL-CP01	Contact Pad	1

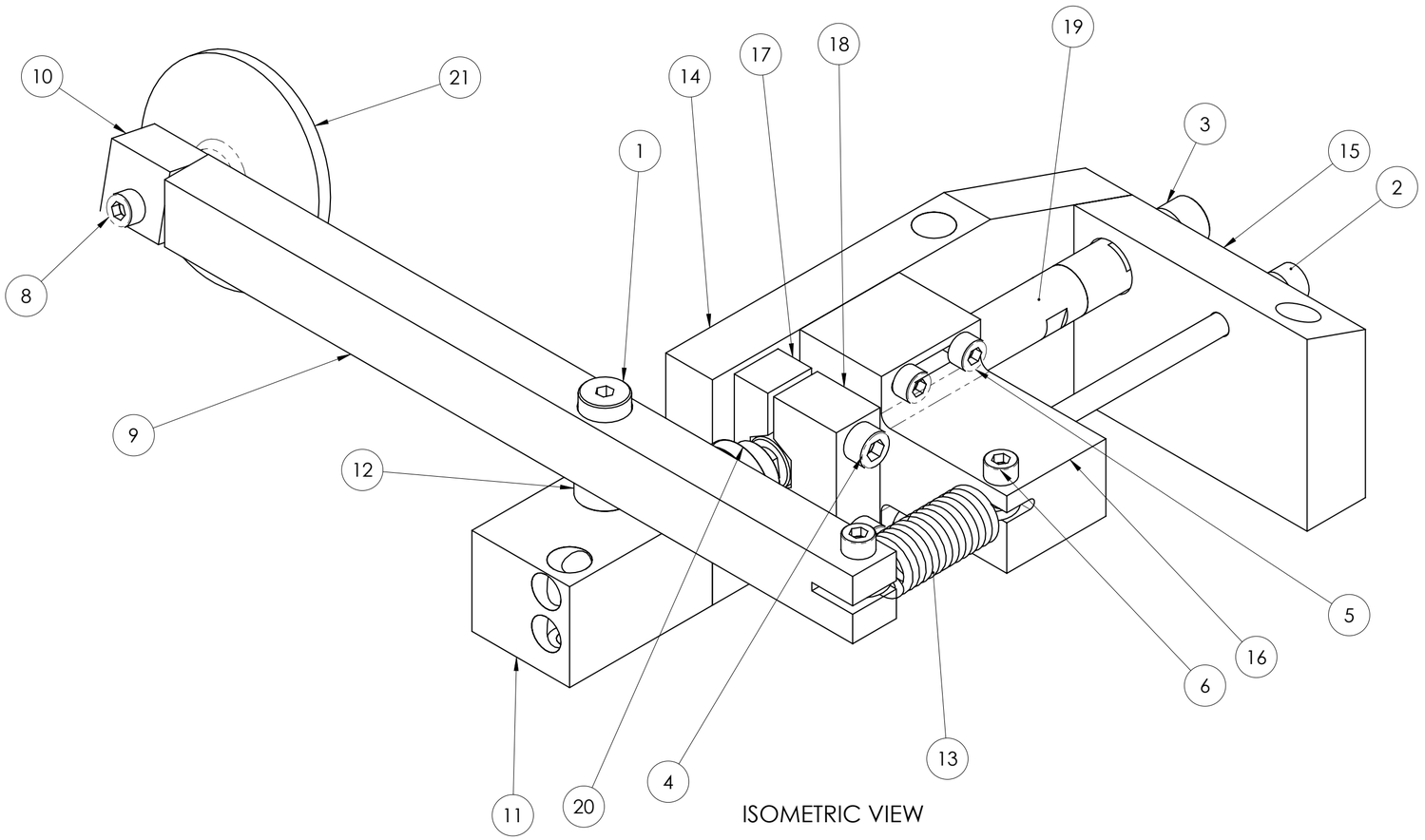

ISOMETRIC VIEW

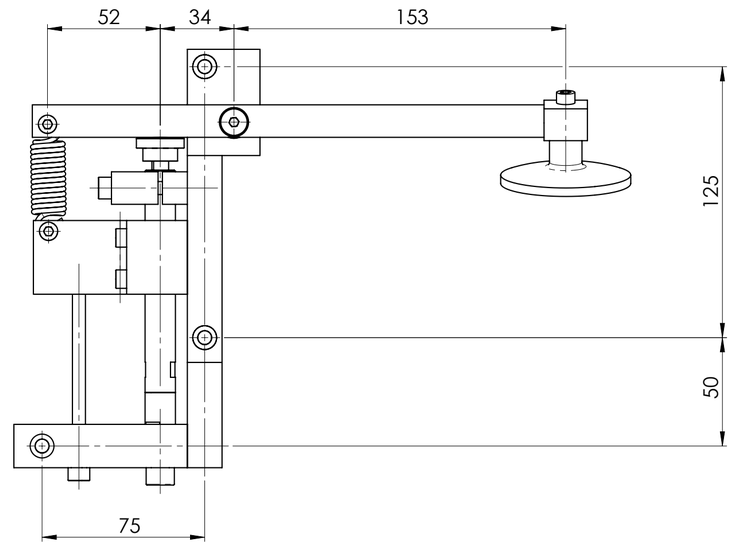

PLAN
SCALE: 1:2

DARTMOUTH COIL ACTUATOR ASSEMBLY

DARTMOUTH COIL ACTUATOR		UNIVERSITY of CANTERBURY PRODUCT INNOVATION CENTRE CHCH N.Z.	
GENERAL ASSEMBLY	PART No.: 00	DRAWN: D. Kirk	DATE: DEC 11
	No. REQ'D: 1	CHECKED:	DRG No.: 001211-QL-DC
SCALE: 1:1 1:2 (A2)	ALL DIMENSIONS IN mm	APPROVED:	

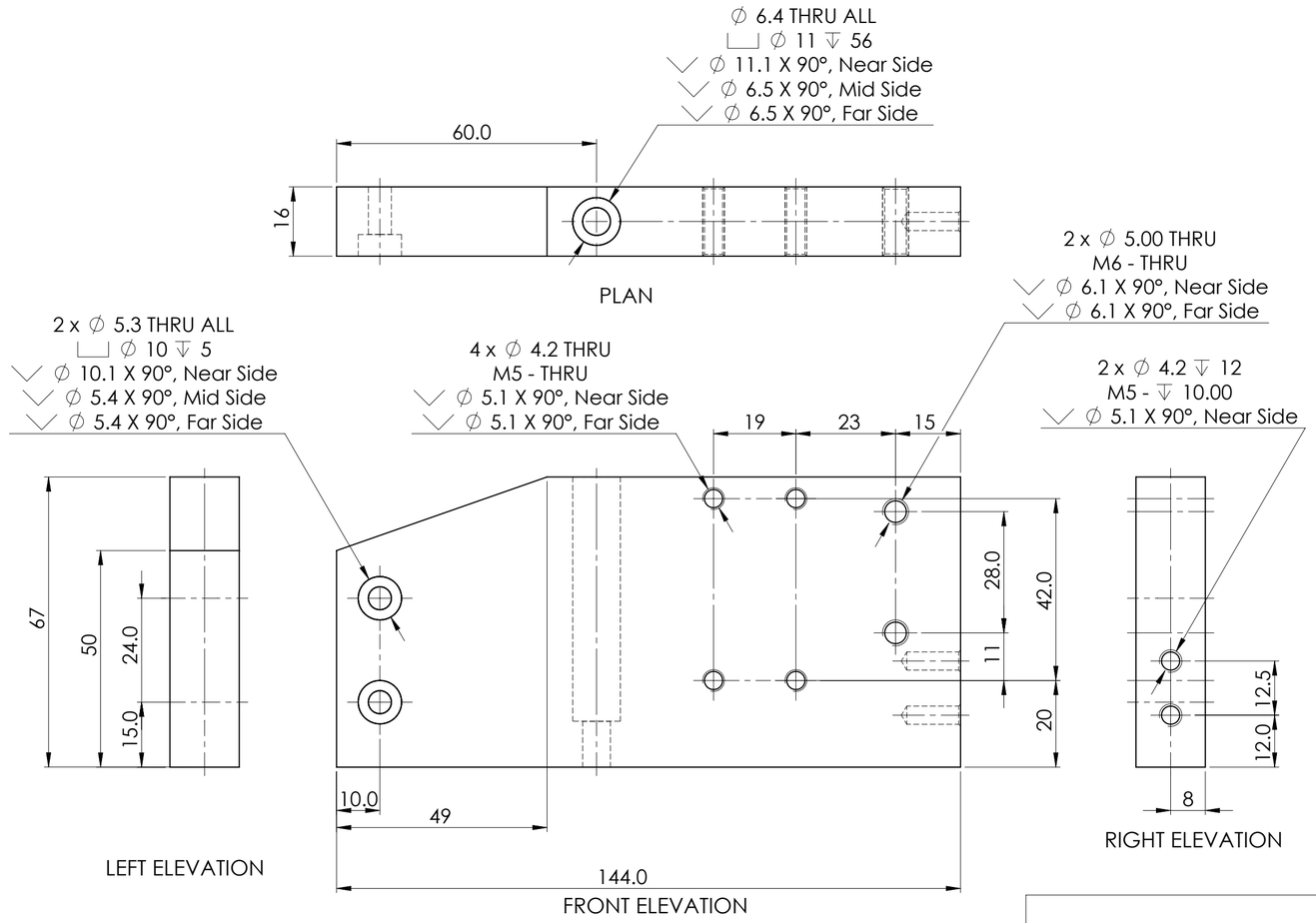

SIDE FRAME MOUNT
QTY: 1 No.
MAT'L: 6 or 7000 Series Aluminium Alloy

QL-BF01

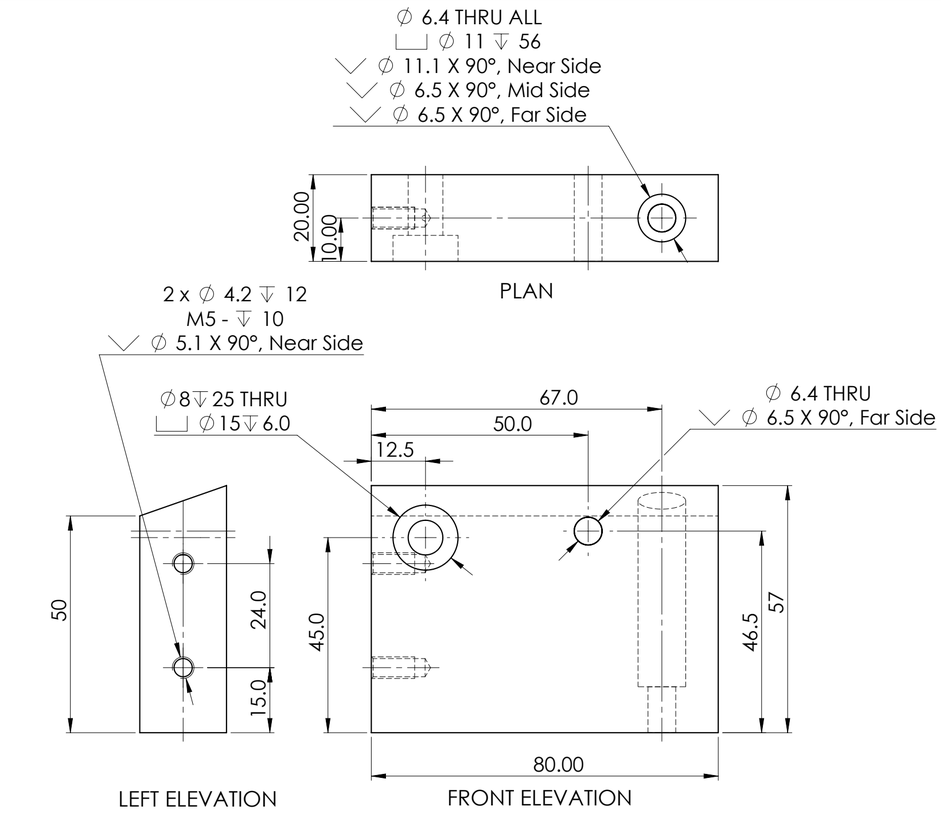

BACK FRAME MOUNT
QTY: 1 No.
MAT'L: 6 or 7000 Series Aluminium Alloy

QL-BF02

TOLERANCE VALUES

#.00 = ±0.05
#.0 = ±0.1
= ±0.15

UNLESS OTHERWISE STATED

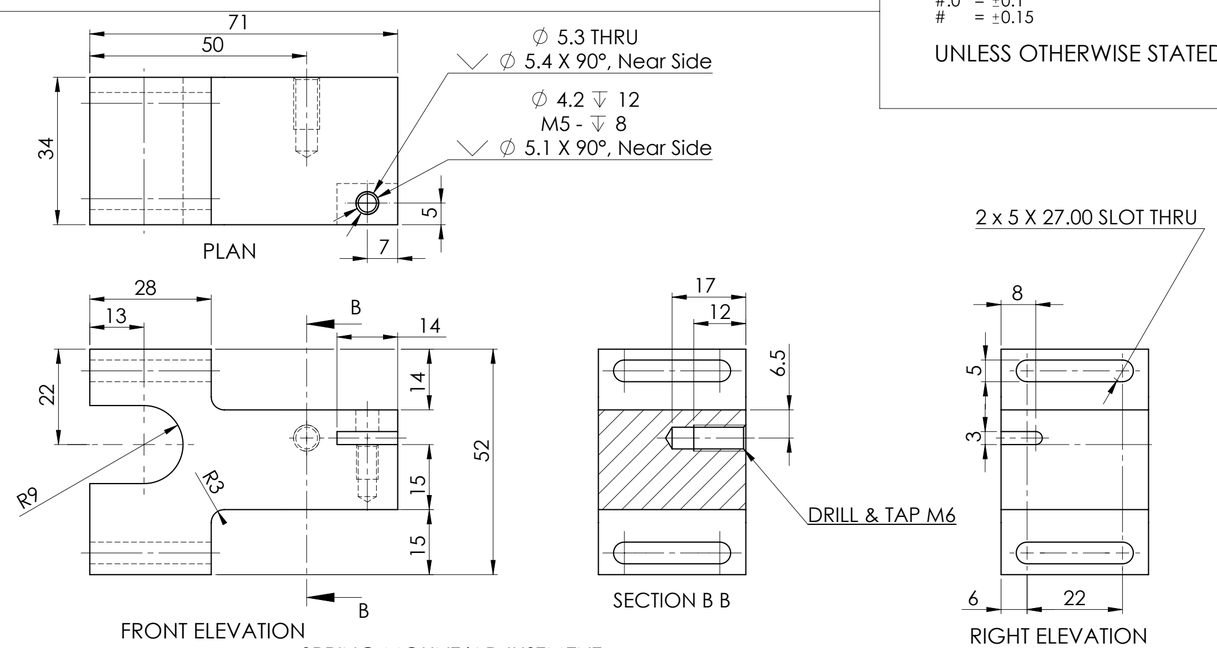

SPRING MOUNT/ADJUSTMENT
QTY: 1 No.
MAT'L: 6 or 7000 Series Aluminium Alloy

QL-BF03

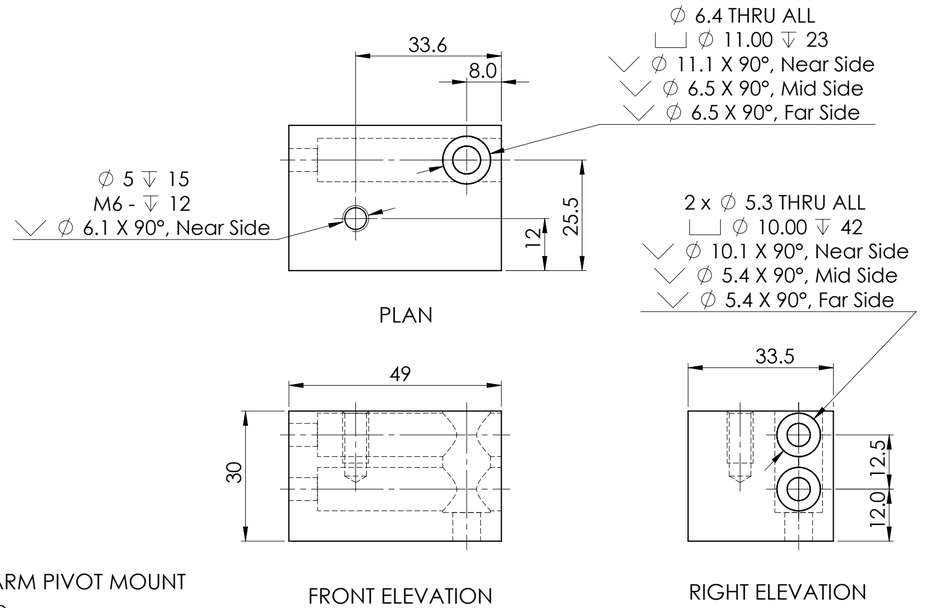

LEVER ARM PIVOT MOUNT
QTY: 1 No.
MAT'L: 6 or 7000 Series Aluminium Alloy

QL-LA03

DARTMOUTH COIL ACTUATOR		UNIVERSITY of CANTERBURY PRODUCT INNOVATION CENTRE CHCH N.Z.	
FRAME COMPONENTS	PART No.: 00	DRAWN: D. Kirk	DATE: Dec 11
	No. REQ'D: 1	CHECKED:	DRG No.: 011211-QL-DC
SCALE: 1:1 (A2)	ALL DIMENSIONS IN mm	APPROVED:	

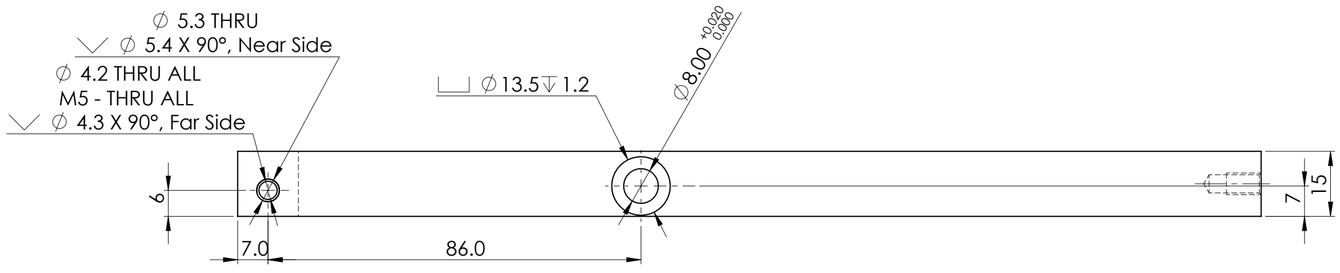

PLAN

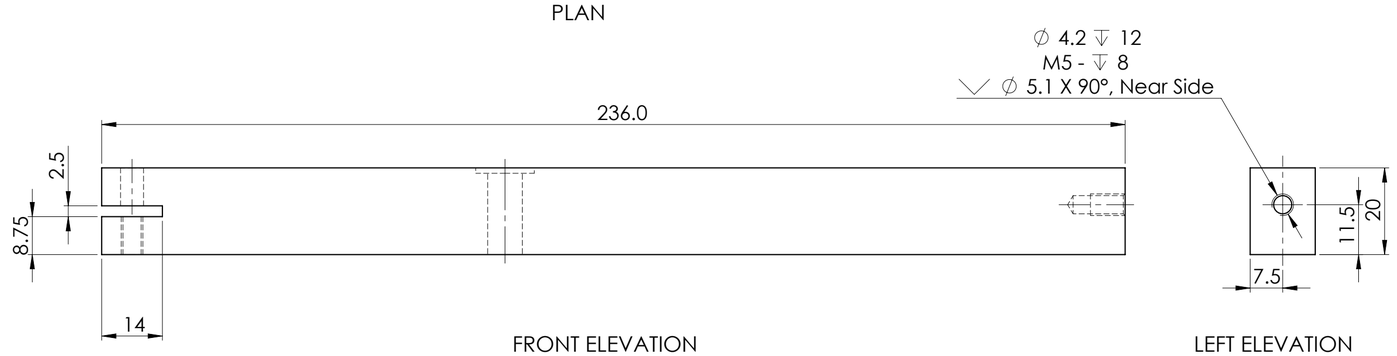

FRONT ELEVATION

LEFT ELEVATION

LEVER ARM

QTY: 1 No.
MAT'L: 6 or 7000 Series Aluminium Alloy

QL-LA01

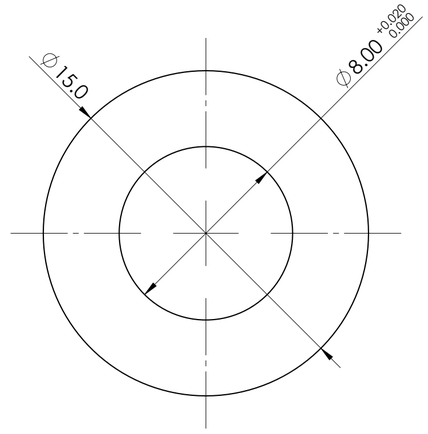

FRONT ELEVATION

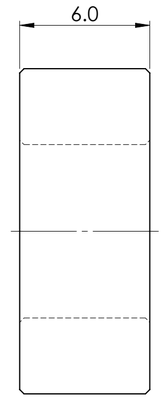

LEFT ELEVATION

LEVER ARM PIVOT BUSH

QTY: 1 No.
MAT'L: 6 or 7000 Series Aluminium Alloy

QL-LA04

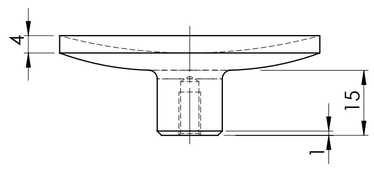

PLAN

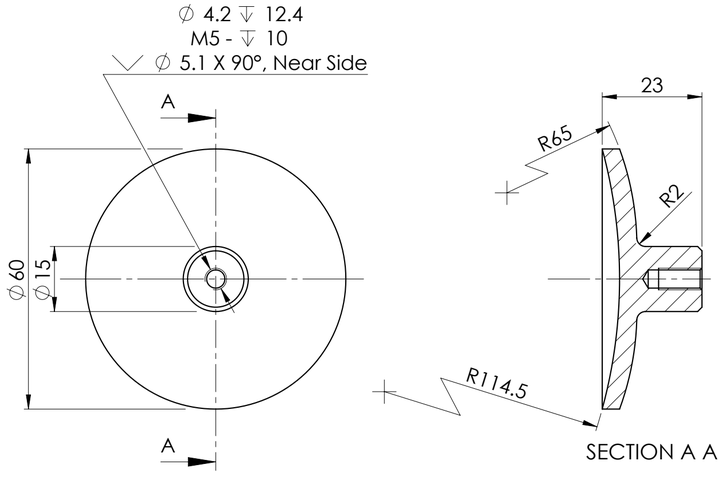

FRONT ELEVATION

SECTION A A

CONTACT PAD

QTY: 1 No.
MAT'L: Nylon 0r Polypropolene

TOLERANCE VALUES

#.00 = ±0.05
#.0 = ±0.1
= ±0.15

UNLESS OTHERWISE STATED

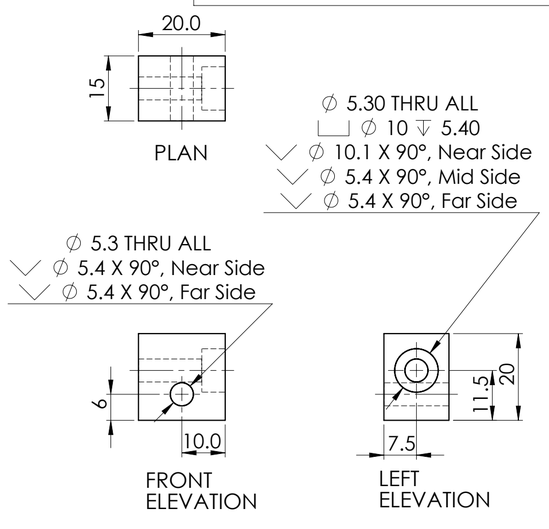

PLAN

FRONT ELEVATION

LEFT ELEVATION

CONTACT PAD ADJUSTMENT MOUNT

QTY: 1 No.
MAT'L: 6 or 7000 Series Aluminium Alloy

QL-LA02

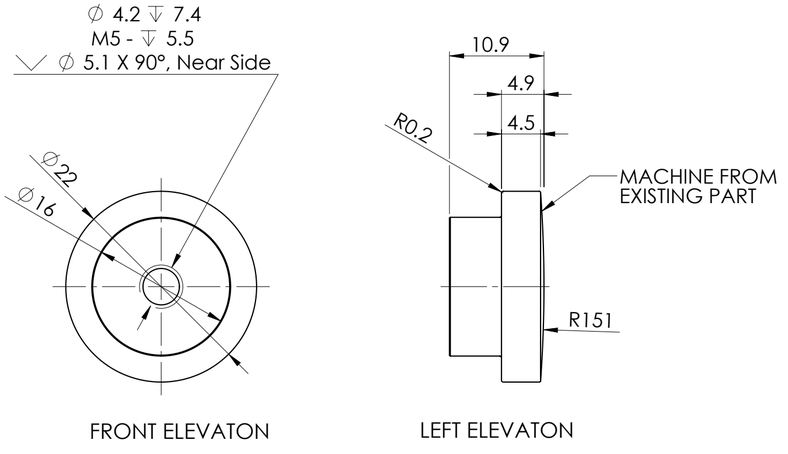

FRONT ELEVATON

LEFT ELEVATON

ACTUATOR PAD

QTY: 1 No.
MAT'L: BRONZE - MACHINE FROM EXISTING PART SUPPLIED

QL-AP01

DARTMOUTH COIL ACTUATOR		UNIVERSITY of CANTERBURY PRODUCT INNOVATION CENTRE CHCH N.Z.	
MECHANICAL COMPONENTS	PART No.: 00	DRAWN: D. Kirk	DATE: Dec 11
	No. REQ'D: 1	CHECKED:	DRG No.: 021211-QL-DC
SCALE: 5:1 2:1 1:1 (A2)	ALL DIMENSIONS IN mm	APPROVED:	

Reference

[1] Breast Cancer screening Report to Ministers of England, Wales, Scotland and Northern Ireland by a working group chaired by Professor Sir Patrick Forrest.

[2] Anderson W. (2003), Pathology, St. Louis, MO: Mosby

[3] L. Keith," Are mammography and palpation sufficient for breast cancer screening? A dissenting opinion.' *Journal of Women's Health & Gender-Based Medicine*, 11(1), 2002, pp.17-25

[4] O. Olsen and P.C. Gøtzsche. Cochrane review on screening for breast cancer with mammography. The Lancet, 358(9290):1340–1342, 2001.

[5] D.B. Kopans. Breast Imaging. Lippincott-Ravens, 1998.

[6] A. Asghari and M.K. Nicholas. Pain during mammography: the role of coping strategies. Pain, 108:170–179, 2004.

[7] R. Sapir, M. Patlas, S.D. Strano, I. Hadas-Halpern, and N.I. Cherny. Does Mammography Hurt? Journal of Pain and Symptom Management, 25(1):53–63, 2003.

[8] S. Kashikar-Zuck, F.J. Keefe, P. Kornguth, P. Beaupre, A. Holzberg, and D. De-long. Pain coping and the pain experience during mammography: a preliminary study. Pain, 73:165–172, 1997.

[9] Digital Image Elasto-Tomography: Mechanical Property Reconstruction from Surface Measured Displacement Data, A thesis submitted by Ashton Peters.

[10] P.J. Kornguth, F.J. Keefe, and M.R. Conaway. Pain during mammography: characteristics and relationship to demographic and medical variables. Pain, 66:187–194, 1996.

[11] S.K. Moore. Better breast cancer detection. IEEE Spectrum, 38:50–54, 2001.

[12] Determining the feasibility of reconstructing mechanical properties of living brain tissue using Magnetic Resonance Elastography, A Thesis Submitted to the Faculty In partial

fulfillment of the requirements for the Degree of Master of Science By PHILLIP R. PERRINEZ

[13] Elastographic Imaging, J Ophir, B. Garra, F. Kallei, E. Konofagou, T. Krouskop, R. Righetti, T. Varghese, Ultrasound in Med. & Biol, vol 26, supplement 1, pp. s23-s29, 2000

[14] L. Huwart,, B. E. van Beers, MR elastography, Gastroenterol Clic Bio 32, 68-72, 2008

[15] A. Manduca, T. E. Oliphant, M. A. Dresner, J. L. Mahowald, S. A. Kruse, E. Amromin, J. P. Felmlee, J. F. Greenleaf, and R. L. Ehman, "Magnetic resonance elastography: non-invasive mapping of tissue elasticity," Medical Image Analysis, vol. 5, pp. 237-54, 2001.

[16] J. B. Weaver, E. E. Van Houten, M. I. Miga, F. E. Kennedy, and K. D. Paulsen, "Magnetic resonance elastography using 3D gradient echo measurements of steady-state motion," Medical Physics, vol. 28, pp. 1620-8, 2001.

[17] S. A. Kruse, J. A. Smith, A. J. Lawrence, M. A. Dresner, A. Manduca, J. F. Greenleaf, and R. L. Ehman, "Tissue characterization using magnetic resonance elastography: preliminary results," Physics in Medicine & Biology, vol. 45, pp. 1579-90, 2000.

[18] K. D. Paulsen, M. I. Miga, F. E. Kennedy, P. J. Hoopes, A. Hartov, and D. W. Roberts, "A computational model for tracking subsurface tissue deformation during stereotactic neurosurgery," IEEE Transactions on Biomedical Engineering, vol. 46, pp. 213-25, 1999.

[19] R. Muthupillai and R. L. Ehman, "Magnetic resonance elastography," Nature Medicine, vol. 2, pp. 601-3, 1996.

[20] R. Muthupillai, D. J. Lomas, P. J. Rossman, J. F. Greenleaf, A. Manduca, and R. L. Ehman, "Magnetic resonance elastography by direct visualization of propagating acoustic strain waves," Science, vol. 269, pp. 1854-7, 1995.

[21] R. Muthupillai, P. J. Rossman, D. J. Lomas, J. F. Greenleaf, S. J. Riederer, and R. L. Ehman, "Magnetic resonance imaging of transverse acoustic strain waves," Magnetic Resonance in Medicine, vol. 36, pp. 266-74, 1996.

[22] A. Manduca, T. E. Oliphant, M. A. Dresner, J. L. Mahowald, S. A. Kruse, E. Amromin, J. P. Felmlee, J. F. Greenleaf, and R. L. Ehman, "Magnetic resonance elastography: non-invasive mapping of tissue elasticity," Medical Image Analysis, vol. 5, pp. 237-54, 2001.

[23] Marco L.H. Gruwel, Peter Latta, Brendon Matwiy, UtaSboto-Frankentein, Patricia Gervai, Boguslaw Tomanek, Measurement of Viscoelastic properties of condensed matter using Magnetic Resonance Elastography. *Measurement science review, 10* (5), 147-152, 2010

[24] Clayton E.H., Genin G.M., Bayly P.V., Wave propagation in the human brain and skull imaged in vivo by MR elastography, *IFMBE proceedings 32*, Maryland, USA, 31-33, 2010

[25] Talwalker, J.A., Yin M., Fidler J.L., Sanderson S.O., Kamath P.S. and Ehman R.L., Magnetic resonance imaging of hepatic fibrosis: emerging clinical applications. *Hepatology*, *47*, 332-342, 2008

[26] Alexia L. McKnight, Jennifer L. Kugel, Phillip J. Rossman, Armando Manduca, Lynn C., Richard L. Ehman, MR Elastography of Breast Cancer: Preliminary Results. *American Roentgen Ray Society*, 178:1411–1417, 2002

[27] J. T. Bushberg, Seibert, J.A., Leidholdt, Jr., Edwin M., Boone, John M., The Essential Physics of Medical Imaging, Second ed. New York: Lippincott Williams and Wilkins, 2002.

[28] Paulsen K.D. , Meaney M. Paul, Gilman C. Larry, Alternative breast imaging: four model-based approaches, Chapter 7.

[16] Weaver J.B., Houten E.E.W.,Miga, M.I. Kennedy F. E. ,Paulsen Keith D., Magnetic resonance elastography using 3D gradient echo measurements of steady-state motion, *Med. Phys*. 28(8), (2001).

[29] R. Sinkus, J Lorenzen, D Schrader, M Lorenzen, M Dargatz and D Holz., High-resolution tensor MR elastography for breast tumour detection, Phys. Med. Biol., Vol 45(6), 1649-1664, 2000

[30] R. Muthupillai, Dutt V, Grimm RC, Greenleaf JF, Riederer SJ, Ehman RL, Interleaved spiral acquisition for MR elastography, Radiology, vol 201, p 361, 1996

[31] Doyley Marvin, Weaver J.B., Houten E.E.W.,Miga, M.I. Kennedy F. E. ,Paulsen Keith D., Threshold for detecting and characterizing focal lesions using steady state MR elastography, *Med. Phys*. 30(4), 2003

[32] Houten, E.E.W., McGarry M.D.J.,Miga, M.I., Kennedy F. E., Weaver J.B., An overlapping subzone technique for MR- based elastic property reconstruction, *Magnetic resonance in medicine* 42:779-786, 1999

[33] Houten E.E.W. Miga, M.I. Kennedy F. E. Paulsen, Keith D., Three-Dimensional subzone-based reconstruction algorithm for MR elastography, *Magnetic resonance in Medicine* 45:827:837, 2001

[34] Huifang Wang, John B weaver, Irina I perreard, Marvin M Doyley and Keith Paulsen, A three dimensional quality-guided phase unwrapping method for MR elastography, *Physics in Medicine and Biology*. 56, 3935-3952, 2011

[35] McGarry M D J, Houten Elijah, Perrinez P R, Pattison A J, Weaver J B, Paulsen K D, An Octaheadral shear strain-based measure of SNR for 3D MR elastography, *Phys. Med. Biol. 56, ,* 153-164,2011

[36] Initial in-vivo results considering Rayleigh damping in Magnetic Resonance Elastography, Proceedings of the ASME 2009 International Mechanical Engineering Congress & Exposition IMECE2009, November 13-19, Lake Buena Vista, Florida, USA, D. Viviers , E.E.W. Van Houten , M.D.J. McGarry , J.B. Weaver, K.D. Paulsen

[37] McGarry M.D., Houten Elijah, Use of a Rayleigh damping model in elastography , Med. Biol. Eng. Comput. 46 (8),759-766, 2008

[38] J.F. Semblat, Rheological interpretation of Rayleigh damping, J. Sound Vib 206(5), 741-744 ,1997

[38] Sarvazyan A, Skovoroda A, Emelianov S, et al. Biophysical bases of elasticity imaging. Acoust Imaging ,21:223–240, 1995